

Strength of Materials

BY

JOHN SYMONDS *Fellow Engineer (Retired), Oceanic Division, Westinghouse Electric Corporation.*

J. P. VIDOSIC *Regents' Professor Emeritus of Mechanical Engineering, Georgia Institute of Technology.*

HAROLD V. HAWKINS *Late Manager, Product Standards and Services, Columbus McKinnon Corporation, Tonawanda, N.Y.*

DONALD D. DODGE *Supervisor (Retired), Product Quality and Inspection Technology, Manufacturing Development, Ford Motor Company.*

5.1 MECHANICAL PROPERTIES OF MATERIALS by John Symonds, Expanded by Staff

Stress-Strain Diagrams	5-2
Fracture at Low Stresses	5-7
Fatigue	5-8
Creep	5-10
Hardness	5-12
Testing of Materials	5-13

5.2 MECHANICS OF MATERIALS by J. P. Vidosic

Simple Stresses and Strains	5-15
Combined Stresses	5-18
Plastic Design	5-19
Design Stresses	5-20
Beams	5-20
Torsion	5-36
Columns	5-38
Eccentric Loads	5-40
Curved Beams	5-41
Impact	5-43
Theory of Elasticity	5-44
Cylinders and Spheres	5-45
Pressure between Bodies with Curved Surfaces	5-47

Flat Plates	5-47
Theories of Failure	5-48
Plasticity	5-49
Rotating Disks	5-50
Experimental Stress Analysis	5-51

5.3 PIPELINE FLEXURE STRESSES by Harold V. Hawkins

Pipeline Flexure Stresses	5-55
---------------------------------	------

5.4 NONDESTRUCTIVE TESTING by Donald D. Dodge

Nondestructive Testing	5-61
Magnetic Particle Methods	5-61
Penetrant Methods	5-61
Radiographic Methods	5-65
Ultrasonic Methods	5-66
Eddy Current Methods	5-66
Microwave Methods	5-67
Infrared Methods	5-67
Acoustic Signature Analysis	5-67

5.1 MECHANICAL PROPERTIES OF MATERIALS

by John Symonds, Expanded by Staff

REFERENCES: Davis et al., "Testing and Inspection of Engineering Materials," McGraw-Hill. Timoshenko, "Strength of Materials," pt. II, Van Nostrand. Richards, "Engineering Materials Science," Wadsworth. Nadai, "Plasticity," McGraw-Hill. Tetelman and McEvily, "Fracture of Structural Materials," Wiley. "Fracture Mechanics," ASTM STP-833. McClintock and Argon (eds.), "Mechanical Behavior of Materials," Addison-Wesley. Dieter, "Mechanical Metallurgy," McGraw-Hill. "Creep Data," ASME. ASTM Standards, ASTM. Blazynski (ed.), "Plasticity and Modern Metal Forming Technology," Elsevier Science.

STRESS-STRAIN DIAGRAMS

The Stress-Strain Curve The engineering tensile stress-strain curve is obtained by **static loading** of a standard specimen, that is, by applying the load slowly enough that all parts of the specimen are in equilibrium at any instant. The curve is usually obtained by controlling the loading rate in the tensile machine. ASTM Standards require a loading rate not exceeding 100,000 lb/in² (70 kgf/mm²)/min. An alternate method of obtaining the curve is to specify the strain rate as the independent variable, in which case the loading rate is continuously adjusted to maintain the required strain rate. A strain rate of 0.05 in/in/(min) is commonly used. It is measured usually by an extensometer attached to the gage length of the specimen. Figure 5.1.1 shows several stress-strain curves.

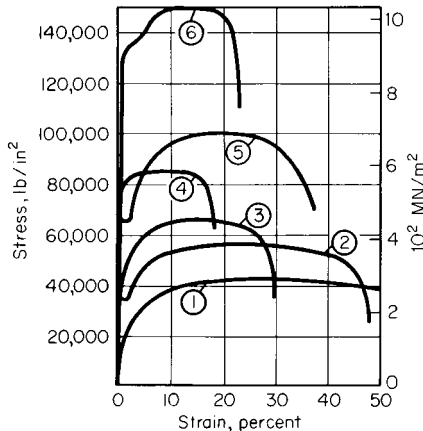


Fig. 5.1.1. Comparative stress-strain diagrams. (1) Soft brass; (2) low carbon steel; (3) hard bronze; (4) cold rolled steel; (5) medium carbon steel, annealed; (6) medium carbon steel, heat treated.

For most engineering materials, the curve will have an initial linear elastic region (Fig. 5.1.2) in which deformation is reversible and time-independent. The slope in this region is **Young's modulus E** . The **proportional elastic limit (PEL)** is the point where the curve starts to deviate from a straight line. The **elastic limit** (frequently indistinguishable from PEL) is the point on the curve beyond which plastic deformation is present after release of the load. If the stress is increased further, the stress-strain curve departs more and more from the straight line. Unloading the specimen at point X (Fig. 5.1.2), the portion XX' is linear and is essentially parallel to the original line OX'' . The horizontal distance OX' is called the **permanent set** corresponding to the stress at X . This is the basis for the construction of the arbitrary **yield strength**. To determine the yield strength, a straight line XX' is drawn parallel to the initial elastic line OX'' but displaced from it by an arbitrary value of

permanent strain. The permanent strain commonly used is 0.20 percent of the original gage length. The intersection of this line with the curve determines the stress value called the yield strength. In reporting the yield strength, the amount of permanent set should be specified. The arbitrary yield strength is used especially for those materials not exhibiting a natural yield point such as nonferrous metals; but it is not limited to these. Plastic behavior is somewhat time-dependent, particularly at high temperatures. Also at high temperatures, a small amount of time-dependent reversible strain may be detectable, indicative of **anelastic** behavior.

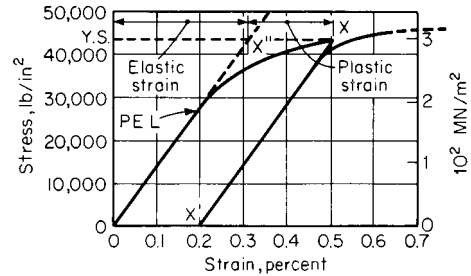


Fig. 5.1.2. General stress-strain diagram.

The **ultimate tensile strength (UTS)** is the maximum load sustained by the specimen divided by the original specimen cross-sectional area. The **percent elongation at failure** is the plastic extension of the specimen at failure expressed as (the change in original gage length \times 100) divided by the original gage length. This extension is the sum of the **uniform** and **nonuniform** elongations. The uniform elongation is that which occurs prior to the UTS. It has an unequivocal significance, being associated with uniaxial stress, whereas the nonuniform elongation which occurs during localized extension (necking) is associated with triaxial stress. The nonuniform elongation will depend on geometry, particularly the ratio of specimen gage length L_0 to diameter D or square root of cross-sectional area A . ASTM Standards specify test-specimen geometry for a number of specimen sizes. The ratio L_0/\sqrt{A} is maintained at 4.5 for flat- and round-cross-section specimens. The original gage length should always be stated in reporting elongation values.

The specimen percent **reduction in area (RA)** is the contraction in cross-sectional area at the fracture expressed as a percentage of the original area. It is obtained by measurement of the cross section of the broken specimen at the fracture location. The RA along with the load at fracture can be used to obtain the **fracture stress**, that is, fracture load divided by cross-sectional area at the fracture. See Table 5.1.1.

The type of fracture in tension gives some indications of the quality of the material, but this is considerably affected by the testing temperature, speed of testing, the shape and size of the test piece, and other conditions. Contraction is greatest in tough and ductile materials and least in brittle materials. In general, fractures are either of the **shear** or of the **separation** (loss of cohesion) type. Flat tensile specimens of ductile metals often show shear failures if the ratio of width to thickness is greater than 6:1. A completely shear-type failure may terminate in a chisel edge, for a flat specimen, or a point rupture, for a round specimen. Separation failures occur in brittle materials, such as certain cast irons. Combinations of both shear and separation failures are common on round specimens of ductile metal. Failure often starts at the axis in a necked region and produces a relatively flat area which grows until the material shears along a cone-shaped surface at the outside of the speci-

Table 5.1.1 Typical Mechanical Properties at Room Temperature
(Based on ordinary stress-strain values)

Metal	Tensile strength, 1,000 lb/in ²	Yield strength, 1,000 lb/in ²	Ultimate elongation, %	Reduction of area, %	Brinell no.
Cast iron	18-60	8-40	0	0	100-300
Wrought iron	45-55	25-35	35-25	55-30	100
Commercially pure iron, annealed	42	19	48	85	70
Hot-rolled	48	30	30	75	90
Cold-rolled	100	95			200
Structural steel, ordinary	50-65	30-40	40-30		120
Low-alloy, high-strength	65-90	40-80	30-15	70-40	150
Steel, SAE 1300, annealed	70	40	26	70	150
Quenched, drawn 1,300°F	100	80	24	65	200
Drawn 1,000°F	130	110	20	60	260
Drawn 700°F	200	180	14	45	400
Drawn 400°F	240	210	10	30	480
Steel, SAE 4340, annealed	80	45	25	70	170
Quenched, drawn 1,300°F	130	110	20	60	270
Drawn 1,000°F	190	170	14	50	395
Drawn 700°F	240	215	12	48	480
Drawn 400°F	290	260	10	44	580
Cold-rolled steel, SAE 1112	84	76	18	45	160
Stainless steel, 18-S	85-95	30-35	60-55	75-65	145-160
Steel castings, heat-treated	60-125	30-90	33-14	65-20	120-250
Aluminum, pure, rolled	13-24	5-21	35-5		23-44
Aluminum-copper alloys, cast	19-23	12-16	4-0		50-80
Wrought, heat-treated	30-60	10-50	33-15		50-120
Aluminum die castings	30		2		
Aluminum alloy 17ST	56	34	26	39	100
Aluminum alloy 51ST	48	40	20	35	105
Copper, annealed	32	5	58	73	45
Copper, hard-drawn	68	60	4	55	100
Brasses, various	40-120	8-80	60-3		50-170
Phosphor bronze	40-130		55-5		50-200
Tobin bronze, rolled	63	41	40	52	120
Magnesium alloys, various	21-45	11-30	17-0.5		47-78
Monel 400, Ni-Cu alloy	79	30	48	75	125
Molybdenum, rolled	100	75	30		250
Silver, cast, annealed	18	8	54		27
Titanium 6-4 alloy, annealed	130	120	10	25	352
Ductile iron, grade 80-55-06	80	55	6		225-255

NOTE: Compressive strength of cast iron, 80,000 to 150,000 lb/in².

Compressive yield strength of all metals, except those cold-worked = tensile yield strength.

Stress 1,000 lb/in² × 6.894 = stress, MN/m².

men, resulting in what is known as the cup-and-cone fracture. Double cup-and-cone and rosette fractures sometimes occur. Several types of tensile fractures are shown in Fig. 5.1.3.

Annealed or hot-rolled mild steels generally exhibit a **yield point** (see Fig. 5.1.4). Here, in a constant strain-rate test, a large increment of extension occurs under constant load at the elastic limit or at a stress just below the elastic limit. In the latter event the stress drops suddenly from the **upper yield point** to the **lower yield point**. Subsequent to the drop, the yield-point extension occurs at constant stress, followed by a rise to the UTS. Plastic flow during the yield-point extension is discontinuous;



Fig. 5.1.3. Typical metal fractures in tension.

successive zones of plastic deformation, known as **Luder's bands** or **stretcher strains**, appear until the entire specimen gage length has been uniformly deformed at the end of the yield-point extension. This behavior causes a banded or stepped appearance on the metal surface. The exact form of the stress-strain curve for this class of material is sensitive

to test temperature, test strain rate, and the characteristics of the tensile machine employed.

The plastic behavior in a uniaxial tensile test can be represented as the **true stress-strain curve**. The **true stress** σ is based on the instantaneous

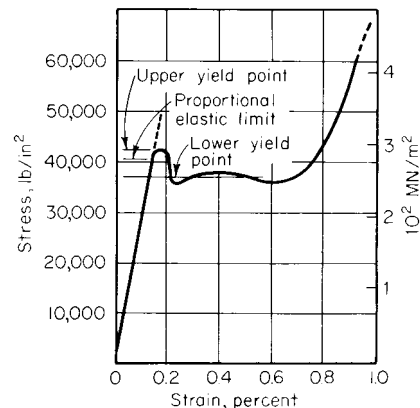


Fig. 5.1.4. Yielding of annealed steel.

5-4 MECHANICAL PROPERTIES OF MATERIALS

cross section A , so that $\sigma = \text{load}/A$. The instantaneous true strain increment is $-dA/A$, or dL/L prior to necking. Total true strain ϵ is

$$\int_{A_0}^A -\frac{dA}{A} = \ln\left(\frac{A_0}{A}\right)$$

or $\ln(L/L_0)$ prior to necking. The true stress-strain curve or flow curve obtained has the typical form shown in Fig. 5.1.5. In the part of the test subsequent to the maximum load point (UTS), when necking occurs, the true strain of interest is that which occurs in an infinitesimal length at the region of minimum cross section. True strain for this element can still be expressed as $\ln(A_0/A)$, where A refers to the minimum cross

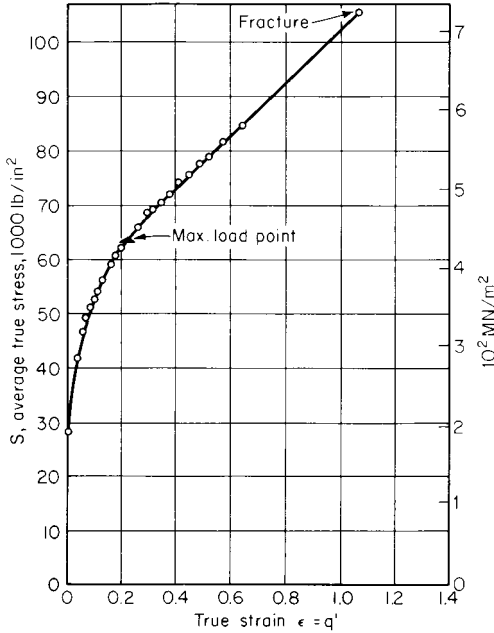


Fig. 5.1.5. True stress-strain curve for 20°C annealed mild steel.

section. Methods of constructing the true stress-strain curve are described in the technical literature. In the range between initial yielding and the neighborhood of the maximum load point the relationship between plastic strain ϵ_p and true stress often approximates

$$\sigma = k\epsilon_p^n$$

where k is the strength coefficient and n is the work-hardening exponent. For a material which shows a yield point the relationship applies only to the rising part of the curve beyond the lower yield. It can be shown that at the maximum load point the slope of the true stress-strain curve equals the true stress, from which it can be deduced that for a material obeying the above exponential relationship between ϵ_p and n , $\epsilon_p = n$ at the maximum load point. The exponent strongly influences the spread between YS and UTS on the engineering stress-strain curve. Values of n and k for some materials are shown in Table 5.1.2. A point on the flow curve identifies the flow stress corresponding to a certain strain, that is, the stress required to bring about this amount of plastic deformation. The concept of true strain is useful for accurately describing large amounts of plastic deformation. The linear strain definition $(L - L_0)/L_0$ fails to correct for the continuously changing gage length, which leads to an increasing error as deformation proceeds.

During extension of a specimen under tension, the change in the specimen cross-sectional area is related to the elongation by Poisson's ratio μ , which is the ratio of strain in a transverse direction to that in the longitudinal direction. Values of μ for the elastic region are shown in Table 5.1.3. For plastic strain it is approximately 0.5.

Table 5.1.2 Room-Temperature Plastic-Flow Constants for a Number of Metals

Material	Condition	k , 1,000 in ² (MN/m ²)	n
0.40% C steel	Quenched and tempered at 400°F (478K)	416 (2,860)	0.088
0.05% C steel	Annealed and temper-rolled	72 (49.6)	0.235
2024 aluminum	Precipitation-hardened	100 (689)	0.16
2024 aluminum	Annealed	49 (338)	0.21
Copper	Annealed	46.4 (319)	0.54
70-30 brass	Annealed	130 (895)	0.49

SOURCE: Reproduced by permission from "Properties of Metals in Materials Engineering," ASM, 1949.

Table 5.1.3 Elastic Constants of Metals (Mostly from tests of R. W. Vose)

Metal	E	G	K	μ
	Modulus of elasticity (Young's modulus), 1,000,000 lb/in ²	Modulus of rigidity (shearing modulus), 1,000,000 lb/in ²	Bulk modulus, 1,000,000 lb/in ²	Poisson's ratio
Cast steel	28.5	11.3	20.2	0.265
Cold-rolled steel	29.5	11.5	23.1	0.287
Stainless steel 18-8	27.6	10.6	23.6	0.305
All other steels, including high-carbon, heat-treated	28.6-30.0	11.0-11.9	22.6-24.0	0.283-0.292
Cast iron	13.5-21.0	5.2-8.2	8.4-15.5	0.211-0.299
Malleable iron	23.6	9.3	17.2	0.271
Copper	15.6	5.8	17.9	0.355
Brass, 70-30	15.9	6.0	15.7	0.331
Cast brass	14.5	5.3	16.8	0.357
Tobin bronze	13.8	5.1	16.3	0.359
Phosphor bronze	15.9	5.9	17.8	0.350
Aluminum alloys, various	9.9-10.3	3.7-3.9	9.9-10.2	0.330-0.334
Monel metal	25.0	9.5	22.5	0.315
Inconel	31	11		0.27-0.38
Z-nickel	30	11		± 0.36
Beryllium copper	17	7		± 0.21
Elektron (magnesium alloy)	6.3	2.5	4.8	0.281
Titanium (99.0 Ti), annealed bar	15-16	6.5		0.34
Zirconium, crystal bar	11-14			
Molybdenum, arc-cast	48-52			

The general effect of increased strain rate is to increase the resistance to plastic deformation and thus to raise the flow curve. Decreasing test temperature also raises the flow curve. The effect of strain rate is expressed as **strain-rate sensitivity** m . Its value can be measured in the tension test if the strain rate is suddenly increased by a small increment during the plastic extension. The flow stress will then jump to a higher value. The strain-rate sensitivity is the ratio of incremental changes of $\log \sigma$ and $\log \dot{\epsilon}$

$$m = \left(\frac{\delta \log \sigma}{\delta \log \dot{\epsilon}} \right)_\epsilon$$

For most engineering materials at room temperature the strain rate sensitivity is of the order of 0.01. The effect becomes more significant at elevated temperatures, with values ranging to 0.2 and sometimes higher.

Compression Testing The compressive stress-strain curve is similar to the tensile stress-strain curve up to the yield strength. Thereafter, the progressively increasing specimen cross section causes the compressive stress-strain curve to diverge from the tensile curve. Some ductile metals will not fail in the compression test. Complex behavior occurs when the direction of stressing is changed, because of the **Bauschinger effect**, which can be described as follows: If a specimen is first plastically strained in tension, its yield stress in compression is reduced and vice versa.

Combined Stresses This refers to the situation in which stresses are present on each of the faces of a cubic element of the material. For a given cube orientation the applied stresses may include shear stresses over the cube faces as well as stresses normal to them. By a suitable rotation of axes the problem can be simplified: applied stresses on the new cubic element are equivalent to three mutually orthogonal **principal stresses** $\sigma_1, \sigma_2, \sigma_3$ alone, each acting normal to a cube face. Combined stress behavior in the elastic range is described in Sec. 5.2, Mechanics of Materials.

Prediction of the conditions under which plastic yielding will occur under combined stresses can be made with the help of several empirical theories. In the **maximum-shear-stress theory** the criterion for yielding is that yielding will occur when

$$\sigma_1 - \sigma_3 = \sigma_{ys}$$

in which σ_1 and σ_3 are the largest and smallest principal stresses, respectively, and σ_{ys} is the uniaxial tensile yield strength. This is the simplest theory for predicting yielding under combined stresses. A more accurate prediction can be made by the **distortion-energy theory**, according to which the criterion is

$$(\sigma_1 - \sigma_2)^2 + (\sigma_2 - \sigma_3)^2 + (\sigma_3 - \sigma_1)^2 = 2(\sigma_{ys})^2$$

Stress-strain curves in the plastic region for combined stress loading can be constructed. However, a particular stress state does not determine a unique strain value. The latter will depend on the stress-state path which is followed.

Plane strain is a condition where strain is confined to two dimensions. There is generally stress in the third direction, but because of mechanical constraints, strain in this dimension is prevented. Plane strain occurs in certain metalworking operations. It can also occur in the neighborhood of a crack tip in a tensile loaded member if the member is sufficiently thick. The material at the crack tip is then in triaxial tension, which condition promotes brittle fracture. On the other hand, ductility is enhanced and fracture is suppressed by triaxial compression.

Stress Concentration In a structure or machine part having a notch or any abrupt change in cross section, the maximum stress will occur at this location and will be greater than the stress calculated by elementary formulas based upon simplified assumptions as to the stress distribution. The ratio of this maximum stress to the nominal stress (calculated by the elementary formulas) is the stress-concentration factor K_t . This is a constant for the particular geometry and is independent of the material, provided it is isotropic. The stress-concentration factor may be determined experimentally or, in some cases, theoretically from the mathematical theory of elasticity. The factors shown in Figs. 5.1.6 to 5.1.13 were determined from both photoelastic tests and the theory of elasticity. Stress concentration will cause failure of brittle materials if

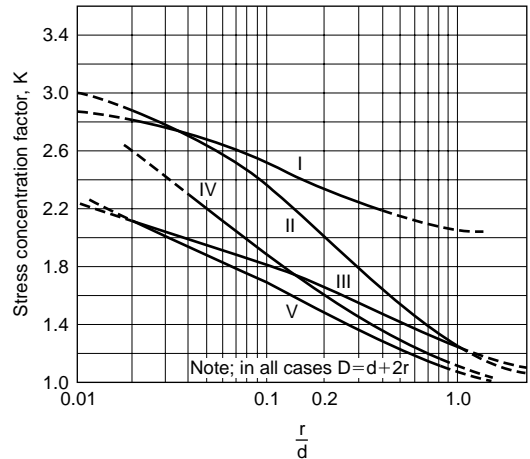
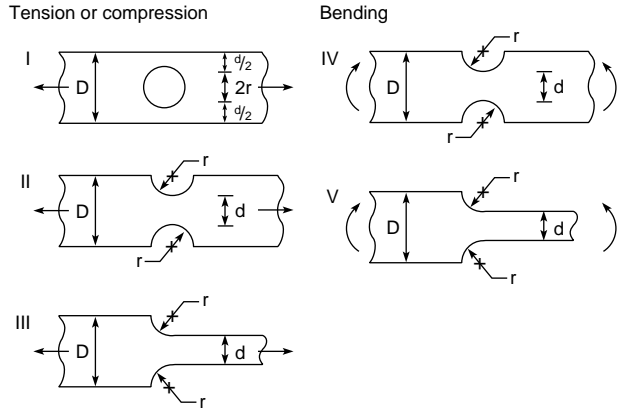


Fig. 5.1.6. Flat plate with semicircular fillets and grooves or with holes. I, II, and III are in tension or compression; IV and V are in bending.

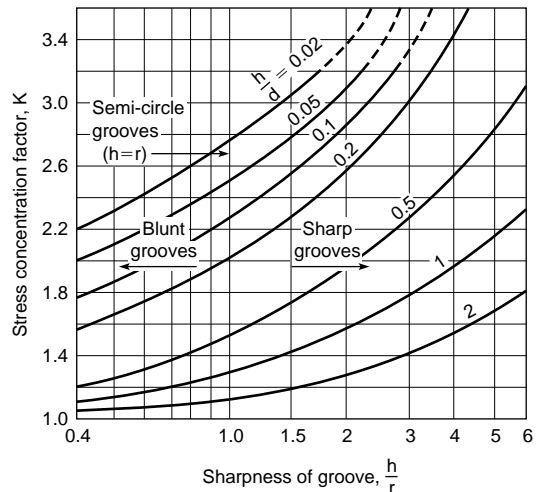
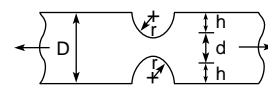


Fig. 5.1.7. Flat plate with grooves, in tension.

the concentrated stress is larger than the ultimate strength of the material. In ductile materials, concentrated stresses higher than the yield strength will generally cause local plastic deformation and redistribution of stresses (rendering them more uniform). On the other hand, even with ductile materials areas of stress concentration are possible sites for fatigue if the component is cyclically loaded.

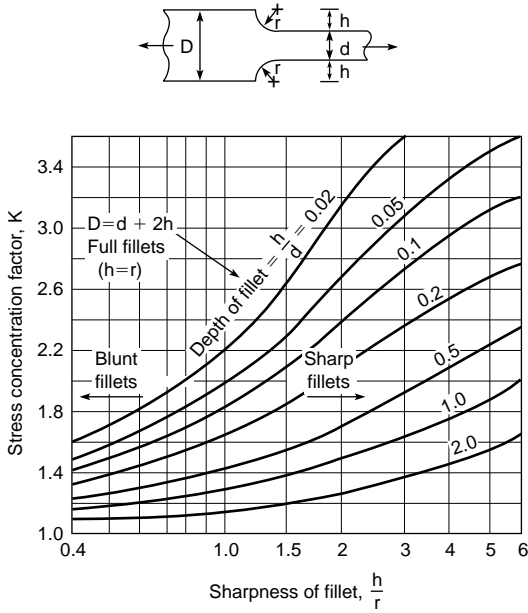


Fig. 5.1.8. Flat plate with fillets, in tension.

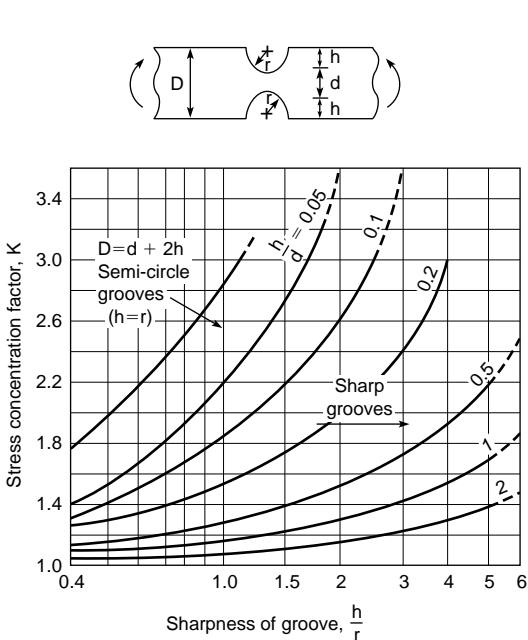


Fig. 5.1.9. Flat plate with grooves, in bending.

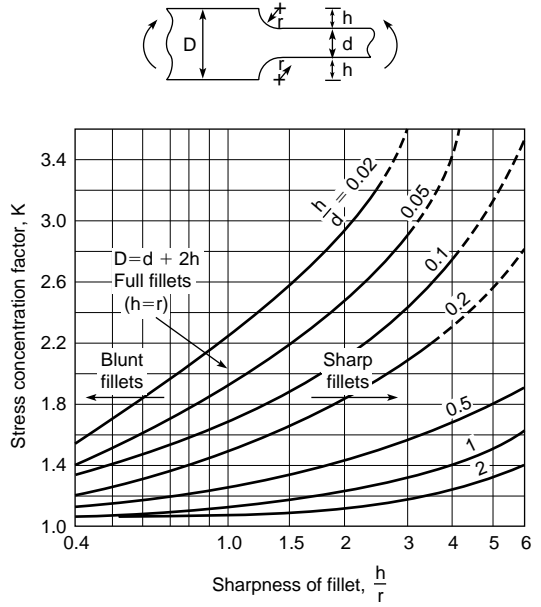


Fig. 5.1.10. Flat plate with fillets, in bending.

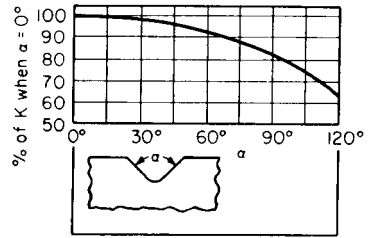


Fig. 5.1.11. Flat plate with angular notch, in tension or bending.

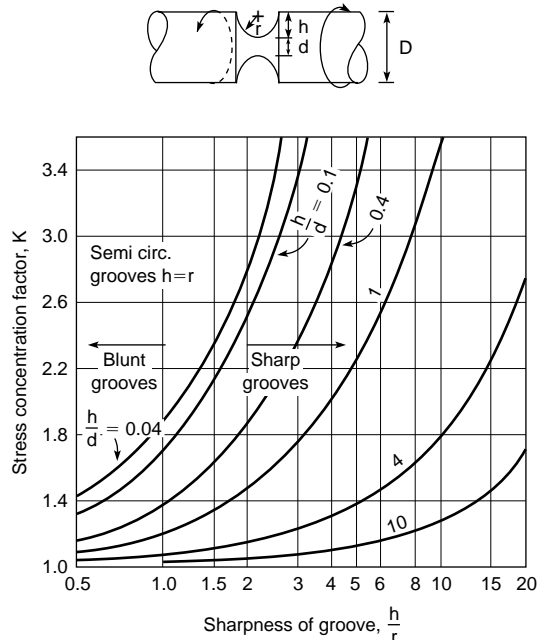


Fig. 5.1.12. Grooved shaft in torsion.

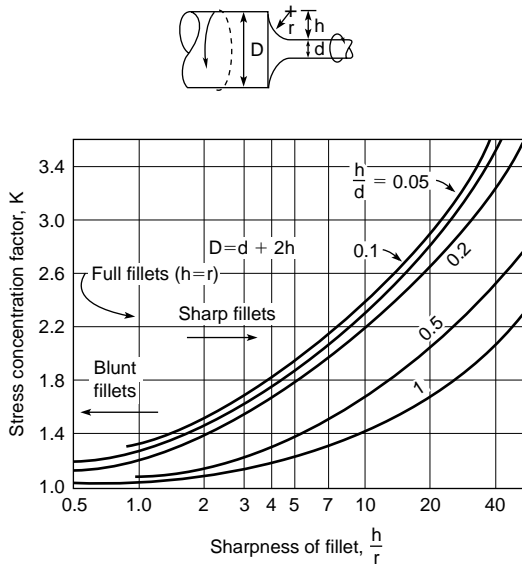


Fig. 5.1.13. Filleted shaft in torsion.

FRACTURE AT LOW STRESSES

Materials under tension sometimes fail by rapid fracture at stresses much below their strength level as determined in tests on carefully prepared specimens. These **brittle, unstable, or catastrophic failures** originate at preexisting stress-concentrating flaws which may be inherent in a material.

The **transition-temperature approach** is often used to ensure fracture-safe design in structural-grade steels. These materials exhibit a characteristic temperature, known as the **ductile brittle transition (DBT)** temperature, below which they are susceptible to brittle fracture. The transition-temperature approach to fracture-safe design ensures that the

transition temperature of a material selected for a particular application is suitably matched to its intended use temperature. The DBT can be detected by plotting certain measurements from tensile or impact tests against temperature. Usually the transition to brittle behavior is complex, being neither fully ductile nor fully brittle. The range may extend over 200°F (110 K) interval. The **nil-ductility temperature (NDT)**, determined by the **drop weight test** (see ASTM Standards), is an important reference point in the transition range. When NDT for a particular steel is known, temperature-stress combinations can be specified which define the limiting conditions under which catastrophic fracture can occur.

In the **Charpy V-notch (CVN)** impact test, a notched-bar specimen (Fig. 5.1.26) is used which is loaded in bending (see ASTM Standards). The energy absorbed from a swinging pendulum in fracturing the specimen is measured. The pendulum strikes the specimen at 16 to 19 ft (4.88 to 5.80 m/s) so that the specimen deformation associated with fracture occurs at a rapid strain rate. This ensures a conservative measure of toughness, since in some materials, toughness is reduced by high strain rates. A CVN impact energy vs. temperature curve is shown in Fig. 5.1.14, which also shows the transitions as given by percent brittle fracture and by percent lateral expansion. The CVN energy has no analytical significance. The test is useful mainly as a guide to the fracture behavior of a material for which an empirical correlation has been established between impact energy and some rigorous fracture criterion. For a particular grade of steel the CVN curve can be correlated with NDT. (See ASME Boiler and Pressure Vessel Code.)

Fracture Mechanics This analytical method is used for ultra-high-strength alloys, transition-temperature materials below the DBT temperature, and some low-strength materials in heavy section thickness.

Fracture mechanics theory deals with crack extension where plastic effects are negligible or confined to a small region around the crack tip. The present discussion is concerned with a through-thickness crack in a tension-loaded plate (Fig. 5.1.15) which is large enough so that the crack-tip stress field is not affected by the plate edges. Fracture mechanics theory states that unstable crack extension occurs when the work required for an increment of crack extension, namely, surface energy and energy consumed in local plastic deformation, is exceeded by the elastic-strain energy released at the crack tip. The elastic-stress

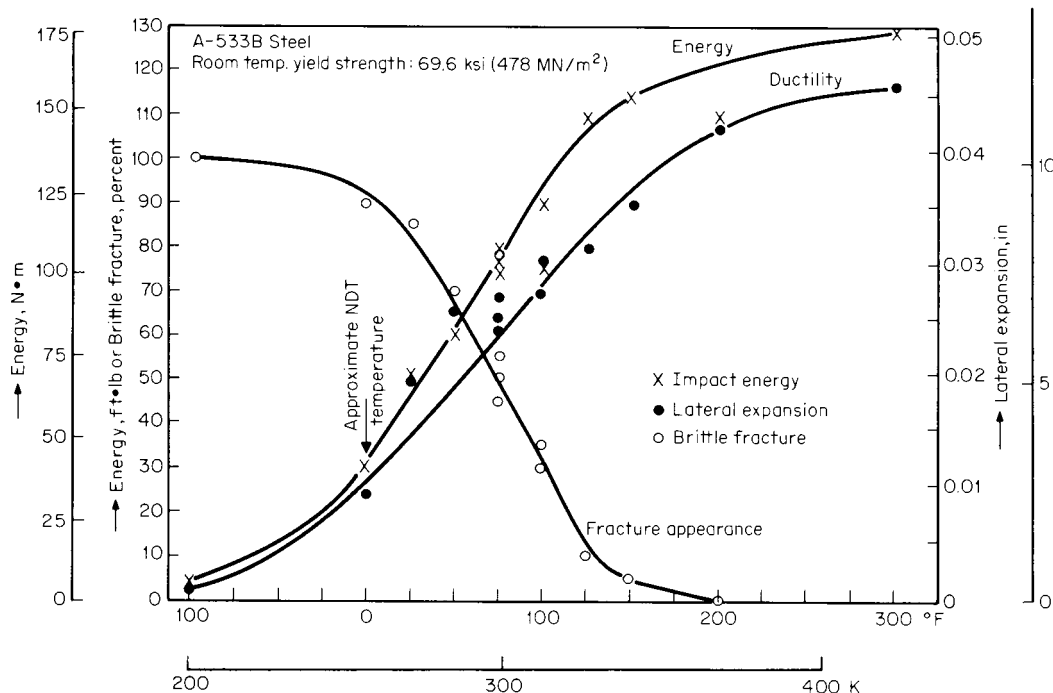


Fig. 5.1.14. CVN transition curves. (Data from Westinghouse R & D Lab.)

field surrounding one of the crack tips in Fig. 5.1.15 is characterized by the stress intensity K_I , which has units of $(\text{lb} \sqrt{\text{in}}) / \text{in}^2$ or $(\text{N}\sqrt{\text{m}}) / \text{m}^2$. It is a function of applied nominal stress σ , crack half-length a , and a geometry factor Q :

$$K_I^2 = Q\sigma^2\pi a \quad (5.1.1)$$

for the situation of Fig. 5.1.15. For a particular material it is found that as K_I is increased, a value K_{Ic} is reached at which unstable crack propa-

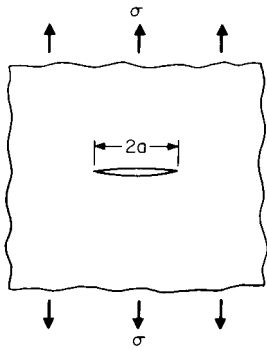


Fig. 5.1.15. Through-thickness crack geometry.

gation occurs. K_{Ic} depends on plate thickness B , as shown in Fig. 5.1.16. It attains a constant value when B is great enough to provide plane-strain conditions at the crack tip. The low plateau value of K_{Ic} is an important material property known as the **plane-strain critical stress intensity** or **fracture toughness** K_{Ic} . Values for a number of materials are shown in Table 5.1.4. They are influenced strongly by processing and small changes in composition, so that the values shown are not necessarily typical. K_{Ic} can be used in the critical form of Eq. (5.1.1):

$$(K_{Ic})^2 = Q\sigma^2\pi a_{cr} \quad (5.1.2)$$

to predict failure stress when a maximum flaw size in the material is known or to determine maximum allowable flaw size when the stress is set. The predictions will be accurate so long as plate thickness B satisfies the **plane-strain criterion**: $B \geq 2.5(K_{Ic}/\sigma_{ys})^2$. They will be conservative if a plane-strain condition does not exist. A big advantage of the fracture mechanics approach is that stress intensity can be calculated by equations analogous to (5.1.1) for a wide variety of geometries, types of

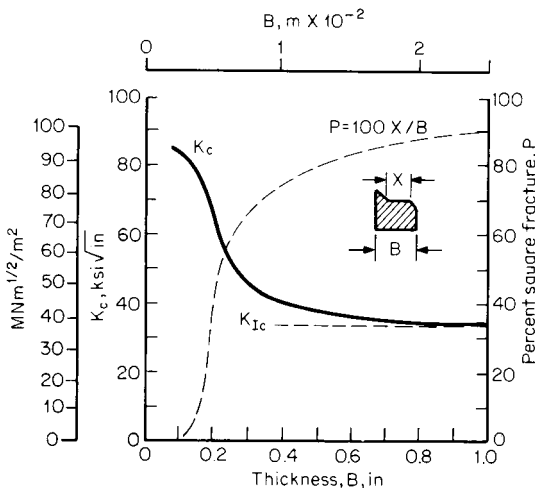


Fig. 5.1.16. Dependence of K_{Ic} and fracture appearance (in terms of percentage of square fracture) on thickness of plate specimens. Based on data for aluminum 7075-T6. (From Scrawly and Brown, STP-381, ASTM.)

Table 5.1.4 Room-Temperature K_{Ic} Values on High-Strength Materials*

Material	0.2% YS, 1,000 in ² (MN/m ²)	K_{Ic} , 1,000 in ² $\sqrt{\text{in}}$ (MN m ^{1/2} /m ²)
18% Ni maraging steel	300 (2,060)	46 (50.7)
18% Ni maraging steel	270 (1,850)	71 (78)
18% Ni maraging steel	198 (1,360)	87 (96)
Titanium 6-4 alloy	152 (1,022)	39 (43)
Titanium 6-4 alloy	140 (960)	75 (82.5)
Aluminum alloy 7075-T6	75 (516)	26 (28.6)
Aluminum alloy 7075-T6	64 (440)	30 (33)

* Determined at Westinghouse Research Laboratories.

crack, and loadings (Paris and Sih, "Stress Analysis of Cracks," STP-381, ASTM, 1965). Failure occurs in all cases when K_I reaches K_{Ic} . Fracture mechanics also provides a framework for predicting the occurrence of **stress-corrosion cracking** by using Eq. (5.1.2) with K_{Ic} replaced by K_{Isc} , which is the material parameter denoting resistance to stress-corrosion-crack propagation in a particular medium.

Two standard test specimens for K_{Ic} determination are specified in ASTM standards, which also detail specimen preparation and test procedure. Recent developments in fracture mechanics permit treatment of crack propagation in the ductile regime. (See "Elastic-Plastic Fracture," ASTM.)

FATIGUE

Fatigue is generally understood as the gradual deterioration of a material which is subjected to repeated loads. In fatigue testing, a specimen is subjected to periodically varying constant-amplitude stresses by means of mechanical or magnetic devices. The applied stresses may alternate between equal positive and negative values, from zero to maximum positive or negative values, or between unequal positive and negative values. The most common loading is alternate tension and compression of equal numerical values obtained by rotating a smooth cylindrical specimen while under a bending load. A series of fatigue tests are made on a number of specimens of the material at different stress levels. The stress endured is then plotted against the number of cycles sustained. By choosing lower and lower stresses, a value may be found which will not produce failure, regardless of the number of applied cycles. This stress value is called the **fatigue limit**. The diagram is called the stress-cycle diagram or **S-N diagram**. Instead of recording the data on cartesian coordinates, either stress is plotted vs. the logarithm of the number of cycles (Fig. 5.1.17) or both stress and cycles are plotted to logarithmic scales. Both diagrams show a relatively sharp bend in the curve near the fatigue limit for ferrous metals. The fatigue limit may be established for most steels between 2 and 10 million cycles. Nonferrous metals usually show no clearly defined fatigue limit. The S-N curves in these cases indicate a continuous decrease in stress values to several hundred million cycles, and both the stress value and the number of cycles sustained should be reported. See Table 5.1.5.

The mean stress (the average of the maximum and minimum stress values for a cycle) has a pronounced influence on the stress range (the algebraic difference between the maximum and minimum stress values). Several empirical formulas and graphical methods such as the "modified Goodman diagram" have been developed to show the influence of the mean stress on the stress range for failure. A simple but conservative approach (see Soderberg, Working Stresses, *Jour. Appl. Mech.*, 2, Sept. 1935) is to plot the variable stress S_v (one-half the stress range) as ordinate vs. the mean stress S_m as abscissa (Fig. 5.1.18). At zero mean stress, the ordinate is the fatigue limit under completely reversed stress. Yielding will occur if the mean stress exceeds the yield stress S_y , and this establishes the extreme right-hand point of the diagram. A straight line is drawn between these two points. The coordinates of any other point along this line are values of S_m and S_v which may produce failure.

Surface defects, such as roughness or scratches, and notches or

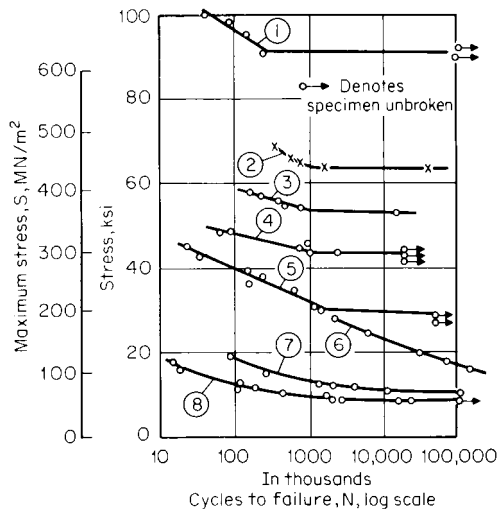


Fig. 5.1.17. The *S-N* diagrams from fatigue tests. (1) 1.20% C steel, quenched and drawn at 860°F (460°C); (2) alloy structural steel; (3) SAE 1050, quenched and drawn at 1,200°F (649°C); (4) SAE 4130, normalized and annealed; (5) ordinary structural steel; (6) Duralumin; (7) copper, annealed; (8) cast iron (reversed bending).

shoulders all reduce the fatigue strength of a part. With a notch of prescribed geometric form and known concentration factor, the reduction in strength is appreciably less than would be called for by the concentration factor itself, but the various metals differ widely in their susceptibility to the effect of roughness and concentrations, or **notch sensitivity**.

For a given material subjected to a prescribed state of stress and type of loading, notch sensitivity can be viewed as the ability of that material to resist the concentration of stress incidental to the presence of a notch. Alternately, notch sensitivity can be taken as a measure of the degree to which the geometric stress concentration factor is reduced. An attempt is made to rationalize notch sensitivity through the equation $q = (K_f - 1)/(K - 1)$, where q is the notch sensitivity, K is the geometric stress concentration factor (from data similar to those in Figs. 5.1.5 to 5.1.13 and the like), and K_f is defined as the ratio of the strength of unnotched material to the strength of notched material. Ratio K_f is obtained from laboratory tests, and K is deduced either theoretically or from laboratory tests, but both must reflect the same state of stress and type of loading. The value of q lies between 0 and 1, so that (1) if $q = 0$, $K_f = 1$ and the material is not notch-sensitive (soft metals such as copper, aluminum, and annealed low-strength steel); (2) if $q = 1$, $K_f = K$, the material is fully notch-sensitive and the full value of the geometric stress concentration factor is not diminished (hard, high-strength steel). In practice, q will lie somewhere between 0 and 1, but it may be hard to quantify.

Accordingly, the pragmatic approach to arrive at a solution to a design problem often takes a conservative route and sets $q = 1$. The exact material properties at play which are responsible for notch sensitivity are not clear.

Further, notch sensitivity seems to be higher, and ordinary fatigue strength lower in large specimens, necessitating full-scale tests in many cases (see Peterson, *Stress Concentration Phenomena in Fatigue of*

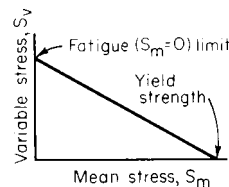


Fig. 5.1.18. Effect of mean stress on the variable stress for failure.

Metals, *Trans. ASME*, **55**, 1933, p. 157, and Buckwalter and Horgor, *Investigation of Fatigue Strength of Axles, Press Fits, Surface Rolling and Effect of Size*, *Trans. ASM*, **25**, Mar. 1937, p. 229). **Corrosion** and **galling** (due to rubbing of mating surfaces) cause great reduction of fatigue strengths, sometimes amounting to as much as 90 percent of the original endurance limit. Although any corroding agent will promote severe corrosion fatigue, there is so much difference between the effects of “sea water” or “tap water” from different localities that numerical values are not quoted here.

Overstressing specimens above the fatigue limit for periods shorter than necessary to produce failure at that stress reduces the fatigue limit in a subsequent test. Similarly, **understressing** below the fatigue limit may increase it. Shot peening, nitriding, and cold work usually improve fatigue properties.

No very good overall correlation exists between fatigue properties and any other mechanical property of a material. The best correlation is between the fatigue limit under completely reversed bending stress and the ordinary tensile strength. For many ferrous metals, the fatigue limit is approximately 0.40 to 0.60 times the tensile strength if the latter is below 200,000 lb/in². Low-alloy high-yield-strength steels often show higher values than this. The fatigue limit for nonferrous metals is approximately 0.20 to 0.50 times the tensile strength. The fatigue limit in reversed shear is approximately 0.57 times that in reversed bending.

In some very important engineering situations components are cyclically stressed into the plastic range. Examples are thermal strains resulting from temperature oscillations and notched regions subjected to secondary stresses. Fatigue life in the plastic or “**low-cycle**” fatigue range has been found to be a function of plastic strain, and low-cycle fatigue testing is done with strain as the controlled variable rather than stress. Fatigue life N and cyclic plastic strain ϵ_p tend to follow the relationship

$$N\epsilon_p^2 = C$$

where C is a constant for a material when $N < 10^5$. (See Coffin, *A Study*

Table 5.1.5 Typical Approximate Fatigue Limits for Reversed Bending

Metal	Tensile strength, 1,000 lb/in ²	Fatigue limit, 1,000 lb/in ²	Metal	Tensile strength, 1,000 lb/in ²	Fatigue limit, 1,000 lb/in ²
Cast iron	20–50	6–18	Copper	32–50	12–17
Malleable iron	50	24	Monel	70–120	20–50
Cast steel	60–80	24–32	Phosphor bronze	55	12
Armco iron	44	24	Tobin bronze, hard	65	21
Plain carbon steels	60–150	25–75	Cast aluminum alloys	18–40	6–11
SAE 6150, heat-treated	200	80	Wrought aluminum alloys	25–70	8–18
Nitralloy	125	80	Magnesium alloys	20–45	7–17
Brasses, various	25–75	7–20	Molybdenum, as cast	98	45
Zirconium crystal bar	52	16–18	Titanium (Ti-75A)	91	45

NOTE: Stress, 1,000 lb/in² × 6.894 = stress, MN/m².

of Cyclic-Thermal Stresses in a Ductile Material, *Trans. ASME*, **76**, 1954, p. 947.)

The type of physical change occurring inside a material as it is repeatedly loaded to failure varies as the life is consumed, and a number of stages in fatigue can be distinguished on this basis. The early stages comprise the events causing nucleation of a crack or flaw. This is most likely to appear on the surface of the material; fatigue failures generally originate at a surface. Following nucleation of the crack, it grows during the crack-propagation stage. Eventually the crack becomes large enough for some rapid terminal mode of failure to take over such as ductile rupture or brittle fracture. The rate of crack growth in the crack-propagation stage can be accurately quantified by fracture mechanics methods. Assuming an initial flaw and a loading situation as shown in Fig. 5.1.15, the rate of crack growth per cycle can generally be expressed as

$$da/dN = C_0(\Delta K_I)^n \quad (5.1.3)$$

where C_0 and n are constants for a particular material and ΔK_I is the range of stress intensity per cycle. K_I is given by (5.1.1). Using (5.1.3), it is possible to predict the number of cycles for the crack to grow to a size at which some other mode of failure can take over. Values of the constants C_0 and n are determined from specimens of the same type as those used for determination of K_{Ic} but are instrumented for accurate measurement of slow crack growth.

Constant-amplitude fatigue-test data are relevant to many rotary-machinery situations where constant cyclic loads are encountered. There are important situations where the component undergoes variable loads and where it may be advisable to use **random-load testing**. In this method, the load spectrum which the component will experience in service is determined and is applied to the test specimen artificially.

CREEP

Experience has shown that, for the design of equipment subjected to sustained loading at elevated temperatures, little reliance can be placed on the usual short-time tensile properties of metals at those temperatures. Under the application of a constant load it has been found that materials, both metallic and nonmetallic, show a gradual flow or **creep** even for stresses below the proportional limit at elevated temperatures. Similar effects are present in low-melting metals such as lead at room temperature. The deformation which can be permitted in the satisfactory operation of most high-temperature equipment is limited.

In metals, creep is a plastic deformation caused by slip occurring along crystallographic directions in the individual crystals, together with some flow of the grain-boundary material. After complete release of load, a small fraction of this plastic deformation is recovered with time. Most of the flow is nonrecoverable for metals.

Since the early creep experiments, many different types of tests have come into use. The most common are the **long-time creep test** under constant tensile load and the **stress-rupture test**. Other special forms are the **stress-relaxation test** and the **constant-strain-rate test**.

The **long-time creep test** is conducted by applying a dead weight to one end of a lever system, the other end being attached to the specimen surrounded by a furnace and held at constant temperature. The axial deformation is read periodically throughout the test and a curve is plotted of the strain ϵ_0 as a function of time t (Fig. 5.1.19). This is repeated for various loads at the same testing temperature. The portion of the

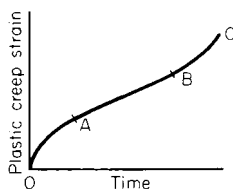


Fig. 5.1.19. Typical creep curve.

curve *OA* in Fig. 5.1.19 is the region of **primary creep**, *AB* the region of **secondary creep**, and *BC* that of **tertiary creep**. The strain rates, or the slopes of the curve, are decreasing, constant, and increasing, respectively, in these three regions. Since the period of the creep test is usually much shorter than the duration of the part in service, various extrapolation procedures are followed (see Gittus, "Creep, Viscoelasticity and Creep Fracture in Solids," Wiley, 1975). See Table 5.1.6.

In practical applications the region of constant-strain rate (secondary creep) is often used to estimate the probable deformation throughout the life of the part. It is thus assumed that this rate will remain constant during periods beyond the range of the test-data. The working stress is chosen so that this total deformation will not be excessive. An **arbitrary creep strength**, which is defined as the stress which at a given temperature will result in 1 percent deformation in 100,000 h, has received a certain amount of recognition, but it is advisable to determine the proper stress for each individual case from diagrams of stress vs. creep rate (Fig. 5.1.20) (see "Creep Data," ASTM and ASME).

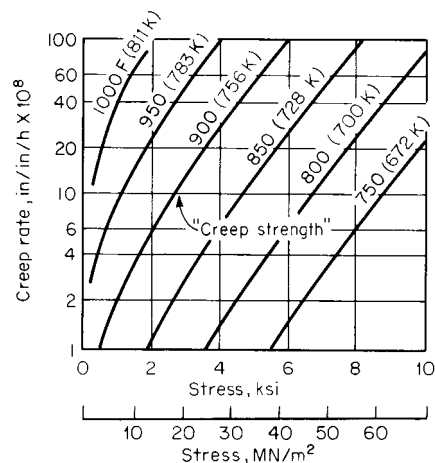


Fig. 5.1.20. Creep rates for 0.35% C steel.

Additional temperatures ($^{\circ}\text{F}$) and stresses (in 1,000 lb/in 2) for stated creep rates (percent per 1,000 h) for wrought nonferrous metals are as follows:

60-40 Brass: Rate 0.1, temp. 350 (400), stress 8 (2); rate 0.01, temp 300 (350) [400], stress 10 (3) [1].

Phosphor bronze: Rate 0.1, temp 400 (550) [700] [800], stress 15 (6) [4] [4]; rate 0.01, temp 400 (550) [700], stress 8 (4) [2].

Nickel: Rate 0.1, temp 800 (1000), stress 20 (10).
70 CU, 30 NI. Rate 0.1, temp 600 (750), stress 28 (13-18); rate 0.01, temp 600 (750), stress 14 (8-9).

Aluminum alloy 17 S (Duralumin): Rate 0.1, temp 300 (500) [600], stress 22 (5) [1.5].

Lead pure (commercial) (0.03 percent Ca): At 110 $^{\circ}\text{F}$, for rate 0.1 percent the stress range, lb/in 2 , is 150-180 (60-140) [200-220]; for rate of 0.01 percent, 50-90 (10-50) [110-150].

Stress, 1,000 lb/in $^2 \times 6.894 =$ stress, MN/m 2 , $t_k = \frac{1}{2}(t_r + 459.67)$.

Structural changes may occur during a creep test, thus altering the metallurgical condition of the metal. In some cases, premature rupture appears at a low fracture strain in a normally ductile metal, indicating that the material has become embrittled. This is a very insidious condition and difficult to predict. The **stress-rupture test** is well adapted to study this effect. It is conducted by applying a constant load to the specimen in the same manner as for the long-time creep test. The nominal stress is then plotted vs. the time for fracture at constant temperature on a log-log scale (Fig. 5.1.21).

Table 5.1.6 Stresses for Given Creep Rates and Temperatures*

Material Temp, °F	Creep rate 0.1% per 1,000 h					Creep rate 0.01% per 1,000 h				
	800	900	1,000	1,100	1,200	800	900	1,000	1,100	1,200
Wrought steels:										
SAE 1015	17-27	11-18	3-12	2-7	1	10-18	6-14	3-8	1	
0.20 C, 0.50 Mo	26-33	18-25	9-16	2-6	1-2	16-24	11-22	4-12	2	1
0.10-0.25 C, 4-6 Cr + Mo	22	15-18	9-11	3-6	2-3	14-17	11-15	4-7	2-3	1-2
SAE 4140	27-33	20-25	7-15	4-7	1-2	19-28	12-19	3-8	2-4	1
SAE 1030-1045	8-25	5-15	5	2	1	5-15	3-7	2-4	1	
Commercially pure iron	7		4		3	5		2		
0.15 C, 1-2.5 Cr, 0.50 Mo	25-35	18-28	8-20	6-8	3-4	20-30	12-18	3-12	2-5	1-2
SAE 4340	20-40	15-30	2-12	1-3		8-20		1-6		
SAE X3140	7-10		5-4			3-8		1-2		
0.20 C, 4-6 Cr	30	10-20	7-10	1				3-5		
0.25 C, 4-6 Cr + W	30	10-15	4-10	2-8			6-11	2-7		
0.16 C, 1.2 Cu		18	10-15	3	1		10-18	7-12		
0.20 C, 1 Mo	35	27	12			25	12	6		
0.10-0.40 C, 0.2-0.5 Mo, 1-2 Mn	30-40	12-20	4-14			25-28	8-15	2-8		0.5
SAE 2340	7-12	5	2							
SAE 6140	30	12	4			7	6	1		
SAE 7240	30	21	6-15	2		30	11	3-9	1	
Cr + Va + W, various	20-70	14-30	5-15			18-50	8-18	2-13		
Temp, °F	1,100	1,200	1,300	1,400	1,500	1,000	1,100	1,200	1,300	1,400
Wrought chrome-nickel steels:										
18-8†	10-18	5-11	3-10	2-5	2.5	11-16	5-12	2-10		1-2
10-25 Cr, 10-30 Ni‡	10-20	5-15	3-10	2-5			6-15	3-10	2-8	1-3
Temp, °F	800	900	1,000	1,100	1,200	800	900	1,000	1,100	1,200
Cast steels:										
0.20-0.40 C	10-20	5-10	3			8-15		1		
0.10-0.30 C, 0.5-1 Mo	28	20-30	6-12	2		20	10-15	2-5		
0.15-0.30 C, 4-6 Cr + Mo	25-30	15-25	8-15	8		20-25	9-15	2-7	2	
18-8§			20-25	15	10			20	15	8
Cast iron	20	8	4			10		2		
Cr Ni cast iron			9					3		

* Based on 1,000-h tests. Stresses in 1,000 lb/in².

† Additional data. At creep rate 0.1 percent and 1,000 (1,600)°F the stress is 18-25 (1); at creep rate 0.01 percent at 1,500°F, the stress is 0.5.

‡ Additional data. At creep rate 0.1 percent and 1,000 (1,600)°F the stress is 10-30 (1).

§ Additional data. At creep rate 0.1 percent and 1,600°F the stress is 3; at creep rate 0.01 and 1,500°F, the stress is 2-3.

The stress reaction is measured in the **constant-strain-rate test** while the specimen is deformed at a constant strain rate. In the **relaxation test**, the decrease of stress with time is measured while the total strain (elastic + plastic) is maintained constant. The latter test has direct application to the loosening of turbine bolts and to similar problems. Although some correlation has been indicated between the results of these various types of tests, no general correlation is yet available, and it has been found necessary to make tests under each of these special conditions to obtain satisfactory results.

The interrelationship between strain rate and temperature in the form

of a velocity-modified temperature (see MacGregor and Fisher, *A Velocity-modified Temperature for the Plastic Flow of Metals, Jour. Appl. Mech.*, Mar. 1945) simplifies the creep problem in reducing the number of variables.

Superplasticity Superplasticity is the property of some metals and alloys which permits extremely large, uniform deformation at elevated temperature, in contrast to conventional metals which neck down and subsequently fracture after relatively small amounts of plastic deformation. Superplastic behavior requires a metal with small equiaxed grains, a slow and steady rate of deformation (strain

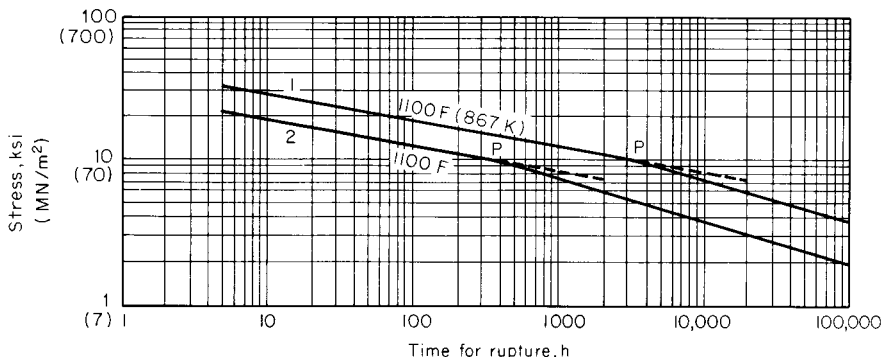


Fig. 5.1.21 Relation between time to failure and stress for a 3% chromium steel. (1) Heat treated 2 h at 1,740°F (950°C) and furnace cooled; (2) hot rolled and annealed 1,580°F (860°C).

rate), and a temperature elevated to somewhat more than half the melting point. With such metals, large plastic deformation can be brought about with lower external loads; ultimately, that allows the use of lighter fabricating equipment and facilitates production of finished parts to near-net shape.

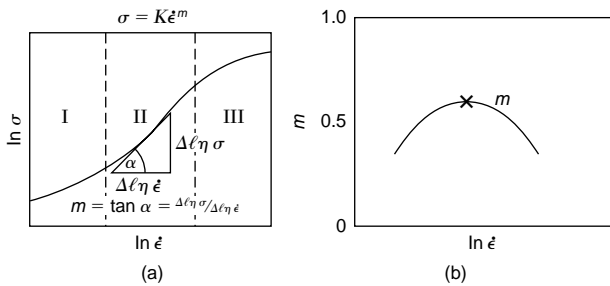


Fig. 5.1.22. Stress and strain rate relations for superplastic alloys. (a) Log-log plot of $\sigma = K\dot{\epsilon}^m$; (b) m as a function of strain rate.

Stress and strain rates are related for a metal exhibiting superplasticity. A factor in this behavior stems from the relationship between the applied stress and strain rates. This factor m —the strain rate sensitivity index—is evaluated from the equation $\sigma = K\dot{\epsilon}^m$, where σ is the applied stress, K is a constant, and $\dot{\epsilon}$ is the strain rate. Figure 5.1.22a plots a stress/strain rate curve for a superplastic alloy on log-log coordinates. The slope of the curve defines m , which is maximum at the point of inflection. Figure 5.1.22b shows the variation of m versus $\ln \dot{\epsilon}$. Ordinary metals exhibit low values of m —0.2 or less; for those behaving superplastically, $m = 0.6$ to 0.8 +. As m approaches 1, the behavior of the metal will be quite similar to that of a newtonian viscous solid, which elongates plastically without necking down.

In Fig. 5.1.22a, in region I, the stress and strain rates are low and creep is predominantly a result of diffusion. In region III, the stress and strain rates are highest and creep is mainly the result of dislocation and slip mechanisms. In region II, where superplasticity is observed, creep is governed predominantly by grain boundary sliding.

HARDNESS

Hardness has been variously defined as resistance to local penetration, to scratching, to machining, to wear or abrasion, and to yielding. The multiplicity of definitions, and corresponding multiplicity of hardness-measuring instruments, together with the lack of a fundamental definition, indicates that hardness may not be a fundamental property of a material but rather a composite one including yield strength, work hardening, true tensile strength, modulus of elasticity, and others.

Scratch hardness is measured by **Mohs scale** of minerals (Sec. 1.2) which is so arranged that each mineral will scratch the mineral of the next lower number. In recent mineralogical work and in certain microscopic metallurgical work, jeweled scratching points either with a set load or else loaded to give a set width of scratch have been used. Hardness in its relation to machinability and to wear and abrasion is generally dealt with in direct machining or wear tests, and little attempt is made to separate hardness itself, as a numerically expressed quantity, from the results of such tests.

The resistance to localized penetration, or **indentation hardness**, is widely used industrially as a measure of hardness, and indirectly as an indicator of other desired properties in a manufactured product. The indentation tests described below are essentially nondestructive, and in most applications may be considered nonmarring, so that they may be applied to each piece produced; and through the empirical relationships of hardness to such properties as tensile strength, fatigue strength, and impact strength, pieces likely to be deficient in the latter properties may be detected and rejected.

Brinell hardness is determined by forcing a hardened sphere under a

known load into the surface of a material and measuring the diameter of the indentation left after the test. The **Brinell hardness number**, or simply the **Brinell number**, is obtained by dividing the load used, in kilograms, by the actual surface area of the indentation, in square millimeters. The result is a pressure, but the units are rarely stated.

$$\text{BHN} = P / \left[\frac{\pi D}{2} (D - \sqrt{D^2 - d^2}) \right]$$

where BHN is the Brinell hardness number; P the imposed load, kg; D the diameter of the spherical indenter, mm; and d the diameter of the resulting impression, mm.

Hardened-steel bearing balls may be used for hardness up to 450, but beyond this hardness specially treated steel balls or jewels should be used to avoid flattening the indenter. The standard-size ball is 10 mm and the standard loads 3,000, 1,500, and 500 kg, with 100, 125, and 250 kg sometimes used for softer materials. If for special reasons any other size of ball is used, the load should be adjusted approximately as follows: for iron and steel, $P = 30D^2$; for brass, bronze, and other soft metals, $P = 5D^2$; for extremely soft metals, $P = D^2$ (see "Methods of Brinell Hardness Testing," ASTM). Readings obtained with other than the standard ball and loadings should have the load and ball size appended, as such readings are only approximately equal to those obtained under standard conditions.

The size of the specimen should be sufficient to ensure that no part of the plastic flow around the impression reaches a free surface, and in no case should the thickness be less than 10 times the depth of the impression. The load should be applied steadily and should remain on for at least 15 s in the case of ferrous materials and 30 s in the case of most nonferrous materials. Longer periods may be necessary on certain soft materials that exhibit creep at room temperature. In testing thin materials, it is not permissible to pile up several thicknesses of material under the indenter, as the readings so obtained will invariably be lower than the true readings. With such materials, smaller indenters and loads, or different methods of hardness testing, are necessary.

In the standard Brinell test, the diameter of the impression is measured with a low-power hand microscope, but for production work several testing machines are available which automatically measure the depth of the impression and from this give readings of hardness. Such machines should be calibrated frequently on test blocks of known hardness.

In the **Rockwell method** of hardness testing, the depth of penetration of an indenter under certain arbitrary conditions of test is determined. The indenter may be either a steel ball of some specified diameter or a spherical-tipped conical diamond of 120° angle and 0.2-mm tip radius, called a "Brale." A *minor load* of 10 kg is first applied which causes an initial penetration and holds the indenter in place. Under this condition, the dial is set to zero and the major load applied. The values of the latter are 60, 100, or 150 kg. Upon removal of the major load, the reading is taken while the minor load is still on. The hardness number may then be read directly from the scale which measures penetration, and this scale is so arranged that soft materials with deep penetration give low hardness numbers.

A variety of combinations of indenter and major load are possible; the most commonly used are R_B using as indenter a $1/16$ -in ball and a major load of 100 kg and R_C using a Brale as indenter and a major load of 150 kg (see "Rockwell Hardness and Rockwell Superficial Hardness of Metallic Materials," ASTM).

Compared with the Brinell test, the Rockwell method makes a smaller indentation, may be used on thinner material, and is more rapid, since hardness numbers are read directly and need not be calculated. However, the Brinell test may be made without special apparatus and is somewhat more widely recognized for laboratory use. There is also a **Rockwell superficial hardness test** similar to the regular Rockwell, except that the indentation is much shallower.

The **Vickers method** of hardness testing is similar in principle to the Brinell in that it expresses the result in terms of the pressure under the indenter and uses the same units, kilograms per square millimeter. The indenter is a diamond in the form of a square pyramid with an apical

angle of 136° , the loads are much lighter, varying between 1 and 120 kg, and the impression is measured by means of a medium-power compound microscope.

$$V = P/(0.5393d^2)$$

where V is the Vickers hardness number, sometimes called the **diamond-pyramid hardness** (DPH); P the imposed load, kg; and d the diagonal of indentation, mm. The Vickers method is more flexible and is considered to be more accurate than either the Brinell or the Rockwell, but the equipment is more expensive than either of the others and the Rockwell is somewhat faster in production work.

Among the other hardness methods may be mentioned the **Scleroscope**, in which a diamond-tipped "hammer" is dropped on the surface and the rebound taken as an index of hardness. This type of apparatus is seriously affected by the resilience as well as the hardness of the material and has largely been superseded by other methods. In the **Monotron** method, a penetrator is forced into the material to a predetermined depth and the load required is taken as the indirect measure of the hardness. This is the reverse of the Rockwell method in principle, but the loads and indentations are smaller than those of the latter. In the **Herbert pendulum**, a 1-mm steel or jewel ball resting on the surface to be tested acts as the fulcrum for a 4-kg compound pendulum of 10-s period. The swinging of the pendulum causes a rolling indentation in the material, and from the behavior of the pendulum several factors in hardness, such as **work hardenability**, may be determined which are not revealed by other methods. Although the Herbert results are of considerable significance, the instrument is suitable for laboratory use only (see Herbert, *The Pendulum Hardness Tester, and Some Recent Developments in Hardness Testing, Engineer, 135, 1923, pp. 390, 686*). In the **Herbert cloudburst** test, a shower of steel balls, dropped from a predetermined height, dulls the surface of a hardened part in proportion to its softness and thus reveals defective areas. A variety of **mutual indentation methods**, in which crossed cylinders or prisms of the material to be tested are forced together, give results comparable with the Brinell test. These are particularly useful on wires and on materials at high temperatures.

The relation among the scales of the various hardness methods is not exact, since no two measure exactly the same sort of hardness, and a relationship determined on steels of different hardnesses will be found only approximately true with other materials. The **Vickers-Brinell relation** is nearly linear up to at least 400, with the Vickers approximately 5 percent higher than the Brinell (actual values run from +2 to +11 percent) and nearly independent of the material. Beyond 500, the values become more widely divergent owing to the flattening of the Brinell ball. The **Brinell-Rockwell relation** is fairly satisfactory and is shown in Fig. 5.1.23. Approximate relations for the **Shore Scleroscope** are also given on the same plot.

The **hardness of wood** is defined by the ASTM as the load in pounds required to force a ball 0.444 in in diameter into the wood to a depth of 0.222 in, the speed of penetration being $\frac{1}{4}$ in/min. For a summary

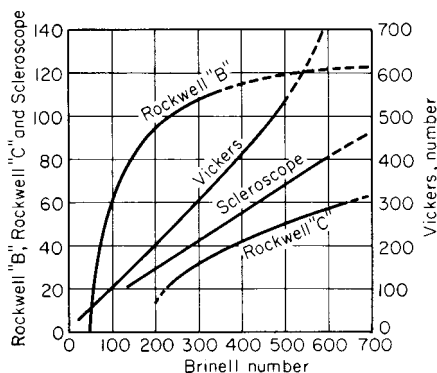


Fig. 5.1.23. Hardness scales.

of the work in hardness see Williams, "Hardness and Hardness Measurements," ASM.

TESTING OF MATERIALS

Testing Machines Machines for the mechanical testing of materials usually contain elements (1) for gripping the specimen, (2) for deforming it, and (3) for measuring the load required in performing the deformation. Some machines (ductility testers) omit the measurement of load and substitute a measurement of deformation, whereas other machines include the measurement of both load and deformation through apparatus either integral with the testing machine (stress-strain recorders) or auxiliary to it (strain gages). In most general-purpose testing machines, the deformation is controlled as the independent variable and the resulting load measured, and in many special-purpose machines, particularly those for light loads, the load is controlled and the resulting deformation is measured. Special features may include those for constant rate of loading (pacing disks), for constant rate of straining, for constant load maintenance, and for cyclical load variation (fatigue).

In modern testing systems, the load and deformation measurements are made with load-and-deformation-sensitive transducers which generate electrical outputs. These outputs are converted to load and deformation readings by means of appropriate electronic circuitry. The readings are commonly displayed automatically on a recorder chart or digital meter, or they are read into a computer. The transducer outputs are typically used also as feedback signals to control the test mode (constant loading, constant extension, or constant strain rate). The load transducer is usually a load cell attached to the test machine frame, with electrical output to a bridge circuit and amplifier. The load cell operation depends on change of electrical resistivity with deformation (and load) in the transducer element. The deformation transducer is generally an extensometer clipped on to the test specimen gage length, and operates on the same principle as the load cell transducer: the change in electrical resistance in the specimen gage length is sensed as the specimen deforms. Optical extensometers are also available which do not make physical contact with the specimen. Verification and classification of extensometers is controlled by ASTM Standards. The application of load and deformation to the specimen is usually by means of a screw-driven mechanism, but it may also be applied by means of hydraulic and servohydraulic systems. In each case the load application system responds to control inputs from the load and deformation transducers. Important features in test machine design are the methods used for reducing friction, wear, and backlash. In older testing machines, test loads were determined from the machine itself (e.g., a pressure reading from the machine hydraulic pressure) so that machine friction made an important contribution to inaccuracy. The use of machine-independent transducers in modern testing has eliminated much of this source of error.

Grips should not only hold the test specimen against slippage but should also apply the load in the desired manner. Centering of the load is of great importance in compression testing, and should not be neglected in tension testing if the material is brittle. Figure 5.1.24 shows the theoretical errors due to off-center loading; the results are directly applicable to compression tests using swivel loading blocks. Swivel (ball-and-socket) holders or compression blocks should be used with all except the most ductile materials, and in compression testing of brittle materials (concrete, stone, brick), any rough faces should be smoothly capped with plaster of paris and one-third portland cement. Serrated grips may be used to hold ductile materials or the shanks of other holders in tension; a taper of 1 in 6 on the wedge faces gives a self-tightening action without excessive jamming. Ropes are ordinarily held by wet eye splices, but braided ropes or small cords may be given several turns over a fixed pin and then clamped. Wire ropes should be zined into forged sockets (solder and lead have insufficient strength). Grip selection for tensile testing is described in ASTM standards.

Accuracy and Calibration ASTM standards require that commercial machines have errors of less than 1 percent within the "loading range" when checked against acceptable standards of comparison at at least five suitably spaced loads. The "loading range" may be any range

through which the preceding requirements for accuracy are satisfied, except that it shall not extend below 100 times the least load to which the machine will respond or which can be read on the indicator. The use of calibration plots or tables to correct the results of an otherwise inaccurate machine is not permitted under any circumstances. Machines with errors less than 0.1 percent are commercially available (Tate-Emery and others), and somewhat greater accuracy is possible in the most refined research apparatus.

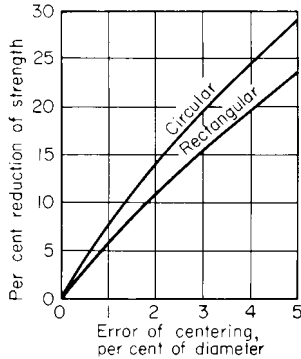


Fig. 5.1.24. Effect of centering errors on brittle test specimens.

Dead loads may be used to check machines of low capacity; accurately calibrated proving levers may be used to extend the range of available weights. Various elastic devices (such as the Morehouse proving ring) made of specially treated steel, with sensitive distortion-measuring devices, and calibrated by dead weights at the NIST (formerly Bureau of Standards) are among the most satisfactory means of checking the higher loads.

Two standard forms of test specimens (ASTM) are shown in Figs. 5.1.25 and 5.1.26. In wrought materials, and particularly in those which

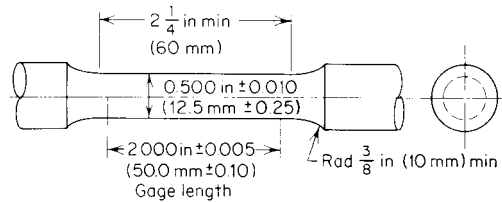


Fig. 5.1.25. Test specimen, 2-in (50-mm) gage length, 1/2-in (12.5-mm) diameter. Others available for 0.35-in (8.75-mm) and 0.25-in (6.25-mm) diameters. (ASTM).

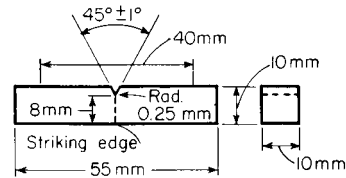


Fig. 5.1.26. Charpy V-notch impact specimens. (ASTM.)

have been cold-worked, different properties may be expected in different directions with respect to the direction of the applied work, and the test specimen should be cut out from the parent material in such a way as to give the strength in the desired direction. With the exception of fatigue specimens and specimens of extremely brittle materials, surface finish is of little practical importance, although extreme roughness tends to decrease the ultimate elongation.

5.2 MECHANICS OF MATERIALS

by J. P. Vidotic

REFERENCES: Timoshenko and MacCullough, "Elements of Strength of Materials," Van Nostrand. Seeley, "Advanced Mechanics of Materials," Wiley. Timoshenko and Goodier, "Theory of Elasticity," McGraw-Hill. Phillips, "Introduction to Plasticity," Ronald. Van Den Broek, "Theory of Limit Design," Wiley. Hetényi, "Handbook of Experimental Stress Analysis," Wiley. Dean and Douglas, "Semi-Conductor and Conventional Strain Gages," Academic. Robertson and Harvey, "The Engineering Uses of Holography," University Printing House, London. Sellers, "Basic Training Guide to the New Metrics and SI Units," National Tool, Die and Precision Machining Association. Roark and Young, "Formulas for Stress and Strain," McGraw-Hill. Perry and Lissner, "The Strain Gage Primer," McGraw-Hill. Donnell, "Beams, Plates, and Sheets," Engineering Societies Monographs, McGraw-Hill. Griffel, "Beam Formulas" and "Plate Formulas," Ungar. Durelli et al., "Introduction to the Theoretical and Experimental Analysis of Stress and Strain," McGraw-Hill. "Stress Analysis Manual," Department of Commerce, Pub. no. AD 759 199, 1969. Blodgett, "Welded Structures," Lincoln Arc Welding Foundation. "Characteristics and Applications of Resistance Strain Gages," Department of Commerce, NBS Circ. 528, 1954.

tures," Lincoln Arc Welding Foundation. "Characteristics and Applications of Resistance Strain Gages," Department of Commerce, NBS Circ. 528, 1954.

EDITOR'S NOTE: The almost universal availability and utilization of computers in engineering practice has led to the development of many forms of software individually tailored to the solution of specific design problems in the area of mechanics of materials. Their use will permit the reader to amplify and supplement a good portion of the formulary and tabular collection in this section, as well as utilize those powerful computational tools in newer and more powerful techniques to facilitate solutions to problems. Many of the approximate methods, involving laborious iterative mathematical schemes, have been supplanted by the computer. Developments along those lines continue apace and bid fair to expand the types of problems handled, all with greater confidence in the results obtained thereby.

Main Symbols**Unit Stress**

- S = apparent stress
 S_v or S_s = pure shearing
 T = true (ideal) stress
 S_p = proportional elastic limit
 S_y = yield point
 S_M = ultimate strength, tension
 S_c = ultimate compression
 S_v = vertical shear in beams
 S_R = modulus of rupture

Moment

- M = bending
 M_t = torsion

External Action

- P = force
 G = weight of body
 W = weight of load
 V = external shear

Modulus of Elasticity

- E = longitudinal
 G = shearing
 K = bulk
 U_p = modulus of resilience
 U_R = ultimate resilience

Geometric

- l = length
 A = area
 V = volume
 v = velocity
 r = radius of gyration
 I = rectangular moment of inertia
 I_p or J = polar moment of inertia

Deformation

- e, e' = gross deformation
 ϵ, ϵ' = unit deformation; strain
 d or α = unit, angular
 s' = unit, lateral
 μ = Poisson's ratio
 n = reciprocal of Poisson's ratio
 r = radius
 f = deflection

SIMPLE STRESSES AND STRAINS

Deformations are changes in form produced by external forces or loads that act on nonrigid bodies. Deformations are **longitudinal**, e , a lengthening (+) or shortening (-) of the body; and **angular**, α , a change of angle between the faces.

Unit deformation (dimensionless number) is the deformation in unit distance. Unit longitudinal deformation (longitudinal strain), $\epsilon = e/l$ (Fig. 5.2.1). Unit angular-deformation $\tan \alpha$ equals α approx (Fig. 5.2.2).

The accompanying lateral deformation results in unit lateral deformation (lateral strain) $\epsilon' = e'/l'$ (Fig. 5.2.1). For homogeneous, isotropic material operating in the elastic region, the ratio ϵ'/ϵ is a constant and is a definite property of the material; this ratio is called **Poisson's ratio** μ .

A fundamental relation among the **three interdependent constants** $E, G,$ and μ for a given material is $E = 2G(1 + \mu)$. Note that μ cannot be larger than 0.5; thus the shearing modulus G is always smaller than the elastic modulus E . At the extremes, for example, $\mu \approx 0.5$ for rubber and

paraffin; $\mu \approx 0$ for cork. For concrete, μ varies from 0.10 to 0.20 at working stresses and can reach 0.25 at higher stresses; μ for ordinary glass is about 0.25. In the absence of definitive data, μ for most structural metals can be taken to lie between 0.25 and 0.35. Extensive listings of Poisson's ratio are found in other sections; see Tables 5.1.3 and 6.1.9.

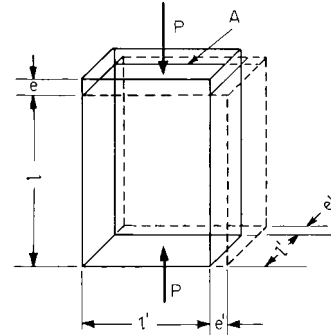


Fig. 5.2.1

Stress is an internal distributed force, or, force per unit area; it is the internal mechanical reaction of the material accompanying deformation. Stresses always occur in pairs. Stresses are **normal** [tensile stress (+) and compressive stress (-)]; and **tangential**, or **shearing**.

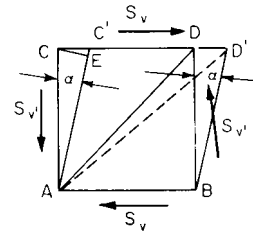


Fig. 5.2.2

Intensity of stress, or **unit stress**, S , lb/in² (kgf/cm²), is the amount of force per unit of area (Fig. 5.2.3). P is the load acting through the center of gravity of the area. The uniformly distributed normal stress is

$$S = P/A$$

When the stress is not uniformly distributed, $S = dP/dA$.

A **long rod** will stretch under its own weight G and a terminal load P (see Fig. 5.2.4). The total elongation e is that due to the terminal load plus that due to one-half the weight of the rod considered as acting at the end.

$$e = (Pl + Gl/2)/(AE)$$

The maximum stress is at the upper end.

When a load is carried by several paths to a support, the different paths take portions of the load in proportion to their stiffness, which is controlled by material (E) and by design.

EXAMPLE. Two pairs of bars rigidly connected (with the same elongation) carry a load P_0 (Fig. 5.2.5). A_1, A_2 and E_1, E_2 and P_1, P_2 and S_1, S_2 are cross sections, moduli of elasticity, loads, and stresses of the bars, respectively; e = elongation.

$$\begin{aligned}
 e &= P_1/(E_1A_1) = P_2/(E_2A_2) \\
 P_0 &= 2P_1 + 2P_2 \\
 S_2 &= P_2/A_2 = \frac{1}{2}[P_0E_2/(E_1A_1 + E_2A_2)] \\
 S_1 &= \frac{1}{2}[P_0E_1/(E_1A_1 + E_2A_2)]
 \end{aligned}$$

Temperature Stresses When the deformation arising from change of temperature is prevented, temperature stresses arise that are proportional to the amount of deformation that is prevented. Let a = coeffi-

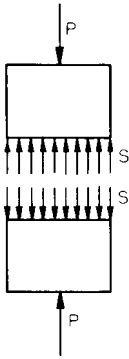


Fig. 5.2.3

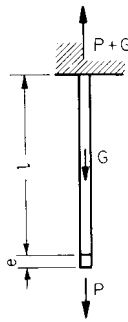


Fig. 5.2.4

cient of expansion per degree of temperature, l_1 = length of bar at temperature t_1 , and l_2 = length at temperature t_2 . Then

$$l_2 = l_1[1 + a(t_2 - t_1)]$$

If, subsequently, the bar is cooled to a temperature t_1 , the proportionate deformation is $s = a(t_2 - t_1)$ and the corresponding unit stress $S = Ea(t_2 - t_1)$. For coefficients of expansion, see Sec. 4. In the case of steel, a change of temperature of 12°F (6.7 K, 6.7°C) will cause in general a unit stress of 2,340 lb/in² (164 kgf/cm²).

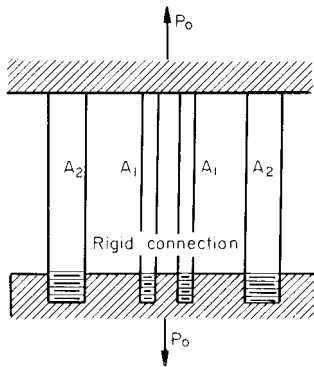


Fig. 5.2.5

Shearing stresses (Fig. 5.2.2) act tangentially to surface of contact and do not change length of sides of elementary volume; they change the angle between faces and the length of diagonal. Two pairs of shearing stresses must act together. Shearing stress intensities are of equal magnitude on all four faces of an element. $S_v = S'_v$ (Fig. 5.2.6).

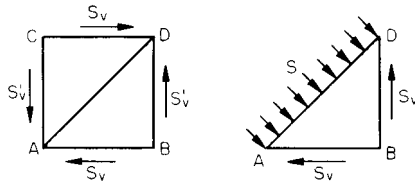


Fig. 5.2.6

In the presence of pure shear on external faces (Fig. 5.2.6), the resultant stress S on one diagonal plane at 45° is pure tension and on the other diagonal plane pure compression; $S = S_v = S'_v$. S on diagonal plane is called "diagonal tension" by writers on reinforced concrete. Failure under pure shear is difficult to produce experimentally, except under torsion and in certain special cases. Figure 5.2.7 shows an ideal case,

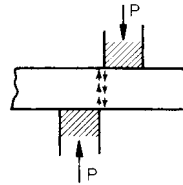


Fig. 5.2.7

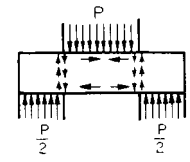


Fig. 5.2.8

and Fig. 5.2.8 a common form of test piece that introduces bending stresses.

Let Fig. 5.2.9 represent the symmetric section of area A with a shearing force V acting through its centroid. If pure shear exists, $S_v = V/A$, and this shear would be uniformly distributed over the area A . When this shear is accompanied by bending (transverse shear in beams), the unit shear

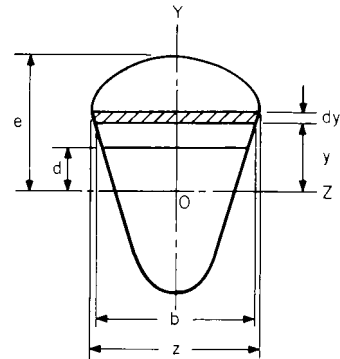


Fig. 5.2.9

S_v increases from the extreme fiber to its maximum, which may or may not be at the neutral axis OZ . The unit shear parallel to OZ at a point d distant from the neutral axis (Fig. 5.2.9) is

$$S_v = \frac{V}{Ib} \int_d^e yz \, dy$$

where z = the section width at distance y ; and I is the moment of inertia of the entire section about the neutral axis OZ . Note that $\int_d^e yz \, dy$ is the first moment of the area above d with respect to axis OZ . For a rectangular cross section (Fig. 5.2.10a),

$$S_v = \frac{3}{2} \frac{V}{bh} \left[1 - \left(\frac{2y}{h} \right)^2 \right]$$

$$S_v (\text{max}) = \frac{3}{2} \frac{V}{bh} = \frac{3}{2} \frac{V}{A} \quad \text{for } y = 0$$

For a circular cross section (Fig. 5.2.10b),

$$S_v = \frac{4}{3} \frac{V}{\pi r^2} \left[1 - \left(\frac{y}{r} \right)^2 \right]$$

$$S_v (\text{max}) = \frac{4}{3} \frac{V}{\pi r^2} = \frac{4}{3} \frac{V}{A} \quad \text{for } y = 0$$

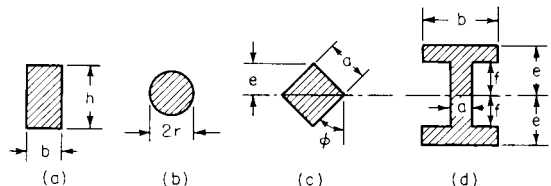


Fig. 5.2.10

Table 5.2.1 Resilience per Unit of Volume U_p $(S = \text{longitudinal stress; } S_v = \text{shearing stress; } E = \text{tension modulus of elasticity; } G = \text{shearing modulus of elasticity})$

Tension or compression	$\frac{1}{2}S^2/E$	Torsion	
Shear	$\frac{1}{2}S_v^2/G$	Solid circular	$\frac{1}{4}S^2/G$
Beams (free ends)		Hollow, radii R_1 and R_2	$\frac{R_1^2 + R_2^2}{R_1^2} \frac{1}{4} \frac{S^2}{G}$
Rectangular section, bent in arc of circle; no shear	$\frac{1}{6}S^2/E$	Springs	
Ditto, circular section	$\frac{1}{8}S^2/E$	Carriage	$\frac{1}{6}S^2/E$
Concentrated center load; rectangular cross section	$\frac{1}{18}S^2/E$	Flat spiral, rectangular section	$\frac{1}{24}S^2/E$
Ditto, circular cross section	$\frac{1}{24}S^2/E$	Helical: axial load, circular wire	$\frac{1}{4}S^2/G$
Uniform load, rectangular cross section	$\frac{5}{36}S^2/E$	Helical: axial twist	$\frac{1}{8}S^2/E$
1-beam section, concentrated center load	$\frac{3}{32}S^2/E$	Helical: axial twist, rectangular section	$\frac{1}{6}S^2/E$

For a **circular ring** (thickness small in comparison with the major diameter), $S_v(\text{max}) = 2V/A$, for $y = 0$.

For a **square cross section** (diagonal vertical, Fig. 5.2.10c),

$$S_v = \frac{V\sqrt{2}}{a^2} \left[1 + \frac{y\sqrt{2}}{a} - 4 \left(\frac{y}{a} \right)^2 \right]$$

$$S_v(\text{max}) = 1.591 \frac{V}{A} \quad \text{for } y = \frac{e}{4}$$

For an **I-shaped cross section** (Fig. 5.2.10d),

$$S_v(\text{max}) = \frac{3}{4} \frac{V}{a} \left[\frac{be^2 - (b-a)f^2}{be^3 - (b-a)f^3} \right] \quad \text{for } y = 0$$

Elasticity is the ability of a material to return to its original dimensions after the removal of stresses. The **elastic limit** S_p is the limit of stress within which the deformation completely disappears after the removal of stress; i.e., no set remains.

Hooke's law states that, within the elastic limit, deformation produced is proportional to the stress. Unless modified, the deduced formulas of mechanics apply only within the elastic limit. Beyond this, they are modified by experimental coefficients, as, for instance, the modulus of rupture.

The **modulus of elasticity**, lb/in² (kgf/cm²), is the ratio of the increment of unit stress to increment of unit deformation within the elastic limit.

The **modulus of elasticity in tension**, or **Young's modulus**,

$$E = \text{unit stress/unit deformation} = Pl/(Ae)$$

The modulus of elasticity in compression is similarly measured.

The **modulus of elasticity in shear or coefficient of rigidity**, $G = S_v/\alpha$ where α is expressed in radians (see Fig. 5.2.2).

The **bulk modulus of elasticity** K is the ratio of normal stress, applied to all six faces of a cube, to the change of volume.

Change of volume under normal stress is so small that it is rarely of significance. For example, given a body with length l , width b , thickness d , Poisson's ratio μ , and longitudinal strain ϵ , $V = lbd = \text{original volume}$. The deformed volume = $(1 + \epsilon)l(1 - \mu\epsilon)b(1 - \mu\epsilon)d$. Neglecting powers of ϵ , the deformed volume = $(1 + \epsilon - 2\mu\epsilon)V$. The change in volume is $\epsilon(1 - 2\mu)V$; the **unit volumetric strain** is $\epsilon(1 - 2\mu)$. Thus, a steel rod ($\mu = 0.3$, $E = 30 \times 10^6$ lb/in²) compressed to a stress of 30,000 lb/in² will experience $\epsilon = 0.001$ and a unit volumetric strain of 0.0004, or 1 part in 2,500.

The following relationships exist between the modulus of elasticity in tension or compression E , modulus of elasticity in shear G , bulk modulus of elasticity K , and Poisson's ratio μ :

$$\begin{aligned} E &= 2G(1 + \mu) \\ G &= E/[2(1 + \mu)] \\ \mu &= (E - 2G)/(2G) \\ K &= E/[3(1 - 2\mu)] \\ \mu &= (3K - E)/(6K) \end{aligned}$$

Resilience U (in · lb)[(cm · kgf)] is the potential energy stored up in a deformed body. The amount of resilience is equal to the work required to deform the body from zero stress to stress S . When S does not exceed

the elastic limit. For normal stress, resilience = work of deformation = average force times deformation = $\frac{1}{2}Pe = \frac{1}{2}AS \times SI/E = \frac{1}{2}S^2V/E$.

Modulus of resilience U_p (in · lb/in³) [(cm · kgf/cm³)], or **unit resilience**, is the elastic energy stored up in a cubic inch of material at the elastic limit. For normal stress,

$$U_p = \frac{1}{2}S^2_p/E$$

The unit resilience for any other kind of stress, as shearing, bending, torsion, is a constant times one-half the square of the stress divided by the appropriate modulus of elasticity. For values, see Table 5.2.1.

Unit rupture work U_R , sometimes called **ultimate resilience**, is measured by the area of the stress-deformation diagram to rupture.

$$U_R = \frac{1}{2}e_u(S_y + 2S_M) \quad \text{approx}$$

where e_u is the total deformation at rupture.

For structural steel, $U_R = \frac{1}{2} \times 27/100 \times [35,000 + (2 \times 60,000)] = 13,950$ in · lb/in³ (982 cm · kgf/cm³).

EXAMPLE 1. A load $P = 40,000$ lb compresses a wooden block of cross-sectional area $A = 10$ in² and length = 10 in, an amount $e = \frac{1}{100}$ in. Stress $S = \frac{1}{10} \times 40,000 = 4,000$ lb/in². Unit elongation $s = \frac{1}{100} \div 10 = \frac{1}{250}$. Modulus of elasticity $E = 4,000 \div \frac{1}{250} = 1,000,000$ lb/in². Unit resilience $U_p = \frac{1}{2} \times 4,000 \times 4,000/1,000,000 = 8$ in · lb/in³ (0.563 cm · kgf/cm³).

EXAMPLE 2. A weight $G = 5,000$ lb falls through a height $h = 2$ ft; $V =$ number of cubic inches required to absorb the shock without exceeding a stress of 4,000 lb/in². Neglect compression of block. Work done by falling weight = $Gh = 5,000 \times 2 \times 12$ in · lb (2,271 × 61 cm · kgf) Resilience of block = $V \times 8$ in · lb = $5,000 \times 2 \times 12$. Therefore, $V = 15,000$ in³ (245,850 cm³).

Thermal Stresses A bar will change its length when its temperature is raised (or lowered) by the amount $\Delta l_0 = \alpha l_0(t_2 - t_1)$. The linear coefficient of thermal expansion α is assumed constant at normal temperatures and l_0 is the length at 32°F (273.2 K, 0°C). If this expansion (or contraction) is prevented, a **thermal-time stress** is developed, equal to $S = E\alpha(t_2 - t_1)$, as the temperature goes from t_1 to t_2 . In thin flat plates the stress becomes $S = E\alpha(t_2 - t_1)/(1 - \mu)$; μ is Poisson's ratio. Such stresses can occur in castings containing large and small sections. Similar stresses also occur when heat flows through members because of the difference in temperature between one point and another. The heat flowing across a length b as a result of a linear drop in temperature Δt equals $Q = kA\Delta t/b$ Btu/h (cal/h). The thermal conductivity k is in Btu/(h)(ft²)(°F)/(in of thickness) [cal/(h)(m²)(k)/(m)]. The **thermal-flow stress** is then $S = E\alpha Qb/(kA)$. Note, when Q is substituted the stress becomes $S = E\alpha \Delta t$ as above, only t is now a function of distance rather than time.

EXAMPLE. A cast-iron plate 3 ft square and 2 in thick is used as a fire wall. The temperature is 330°F on the hot side and 160°F on the other. What is the thermal-flow stress developed across the plate?

$$\begin{aligned} S &= E\alpha \Delta t = 13 \times 10^6 \times 6.5 \times 10^{-6} \times 170 \\ &= 14,360 \text{ lb/in}^2 (1,010 \text{ kgf/cm}^2) \end{aligned}$$

$$\begin{aligned} \text{or} \quad Q &= 2.3 \times 9 \times 170/2 = 1,760 \text{ Btu/h} \\ \text{and} \quad S &= 13 \times 10^6 \times 6.5 \times 10^{-6} \times 1,760 \times 2/2.3 \times 9 \\ &= 14,360 \text{ lb/in}^2 (1,010 \text{ kgf/cm}^2) \end{aligned}$$

COMBINED STRESSES

In the discussion that follows, the element is subjected to stresses lying in one plane; this is the case of **plane stress**, or **two-dimensional stress**.

Simple stresses, defined as such by the flexure and torsion theories, lie in planes normal or parallel to the line of action of the forces. Normal, as well as shearing, stresses may, however, exist in other directions. A particle out of a loaded member will contain normal and shearing stresses as shown in Fig. 5.2.11. Note that the four shearing stresses must be of the same magnitude, if equilibrium is to be satisfied.

If the particle is "cut" along the plane AA, equilibrium will reveal that, in general, normal as well as shearing stresses act upon the plane AC (Fig. 5.2.12). The normal stress on plane AC is labeled S_n , and shearing S_s . The application of equilibrium yields

$$S_n = \frac{S_x + S_y}{2} + \frac{S_x - S_y}{2} \cos 2\theta + S_{xy} \sin 2\theta$$

and
$$S_s = \frac{S_x - S_y}{2} \sin 2\theta - S_{xy} \cos 2\theta$$

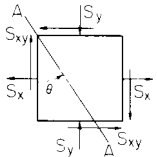


Fig. 5.2.11

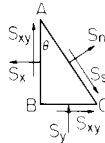


Fig. 5.2.12

A *sign convention* must be used. A tensile stress is positive while compression is negative. A shearing stress is positive when directed as on plane AB of Fig. 5.2.12; i.e., when the shearing stresses on the vertical planes form a clockwise couple, the stress is positive.

The planes defined by $\tan 2\theta = 2S_{xy}/S_x - S_y$, the *principal planes*, contain the **principal stresses**—the maximum and minimum normal stresses. These stresses are

$$S_M, S_m = \frac{S_x + S_y}{2} \pm \sqrt{\left(\frac{S_x - S_y}{2}\right)^2 + S_{xy}^2}$$

The maximum and minimum shearing stresses are represented by the quantity

$$S_{sM,m} = \pm \sqrt{\left(\frac{S_x - S_y}{2}\right)^2 + S_{xy}^2}$$

and they act on the planes defined by

$$\tan 2\theta = -\frac{S_x - S_y}{2S_{xy}}$$

EXAMPLE. The steam in a boiler subjects a particular particle on the outer surface of the boiler shell to a circumferential stress of 8,000 lb/in² and a longitudinal stress of 4,000 lb/in² as shown in Fig. 5.2.13. Find the stresses acting on the plane XX, making an angle of 60° with the direction of the 8,000 lb/in² stress. Find the principal stresses and locate the principal planes. Also find the maximum and minimum shearing stresses.

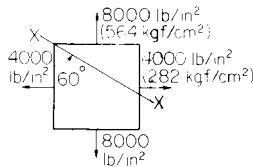


Fig. 5.2.13

$$60^\circ S_n = \frac{4,000 + 8,000}{2} + \frac{4,000 - 8,000}{2} (-0.5000) + 0 = 7,000 \text{ lb/in}^2$$

$$60^\circ S_s = \frac{4,000 - 8,000}{2} (0.8660) - 0 = -1,732 \text{ lb/in}^2$$

$$S_{M,m} = \frac{4,000 + 8,000}{2} \pm \sqrt{\left(\frac{4,000 - 8,000}{2}\right)^2 + 0} = 6,000 \pm 2,000 = 8,000 \text{ and } 4,000 \text{ lb/in}^2 \text{ (564 and 282 kgf/cm}^2\text{)}$$

$$\text{at } \tan 2\theta = \frac{2 \times 0}{4,000 - 8,000} = 0 \text{ or } \theta = 90^\circ \text{ and } 0^\circ$$

$$S_{sM,m} = \pm \sqrt{\left(\frac{4,000 - 8,000}{2}\right)^2 + 0} = \pm 2,000 \text{ lb/in}^2 \text{ (}\pm 141 \text{ kgf/cm}^2\text{)}$$

Mohr's Stress Circle The biaxial stress field with its combined stresses can be represented graphically by the Mohr stress circle. For instance, for the particle given in Fig. 5.2.11, Mohr's circle is as shown in Fig. 5.2.14. The stress *sign convention* previously defined must be adhered to. Furthermore, in order to locate the point (on Mohr's circle) that yields the stresses on a plane θ° from the vertical side of the particle (such as plane AA in Fig. 5.2.11), $2\theta^\circ$ must be laid off in the same

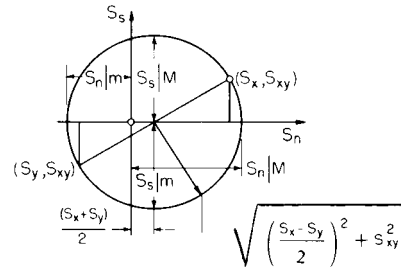


Fig. 5.2.14

direction from the radius to (S_x, S_{xy}) . For the previous example, Mohr's circle becomes Fig. 5.2.15.

Eight special stress fields are shown in Figs. 5.2.16 to 5.2.23, along with Mohr's circle for each.

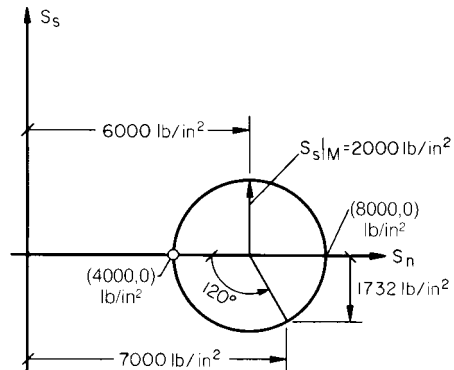


Fig. 5.2.15

Combined Loading Combined flexure and torsion arise, for instance, when a shaft twisted by a torque M , is bent by forces produced by belts or gears. An element on the surface, such as ABCD on the shaft of Fig. 5.2.24, is subjected to a flexure stress $S_x = Mc/I = 8F/(\pi d^3)$ and a

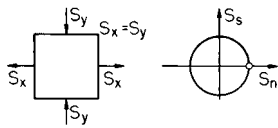


Fig. 5.2.16

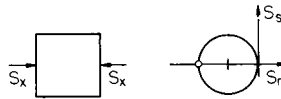


Fig. 5.2.17

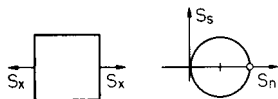


Fig. 5.2.18

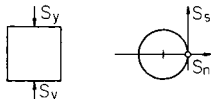


Fig. 5.2.19

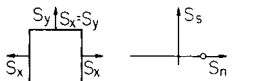


Fig. 5.2.20

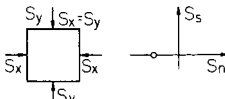


Fig. 5.2.21

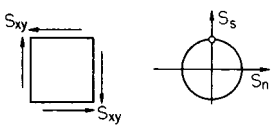


Fig. 5.2.22

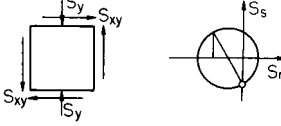


Fig. 5.2.23

torsional shearing stress $S_{xy} = M_c/J = 16M_t/(\pi d^3)$. These stresses will induce combined stresses. The maximum combined stresses will be

$$S_n = \frac{1}{2} (S_x \pm \sqrt{S_x^2 + 4S_{xy}^2})$$

and

$$S_s = \pm \frac{1}{2} \sqrt{S_x^2 + 4S_{xy}^2}$$

The above situation applies to any case of normal stress with shear, as when a bolt is under both tension and shear. A beam particle subjected to both flexure and transverse shear is another case.

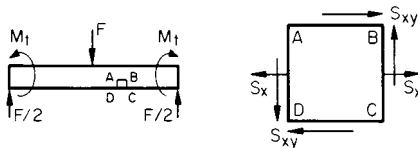


Fig. 5.2.24

Combined torsion and longitudinal loads exist on a propeller shaft. A particle on this shaft will contain a tensile stress computed using $S = F/A$ and a torsion shearing stress equal to $S_s = M_c/J$. The free body of a particle on the surface of a vertical turbine shaft is subjected to direct compression and torsion.

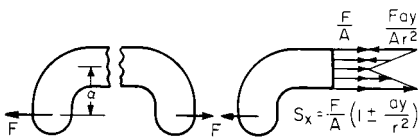


Fig. 5.2.25

When combined loading results in stresses of the same type and direction, the addition is algebraic. Such a situation exists on an offset link like that of Fig. 5.2.25.

Mohr's Strain Circle Strain equations can also be derived for plane-strain fields. Strains e_x and e_y are the extensional strains (tension or

compression) occurring at a point in two right-angle directions, and the change of the angle between them is γ_{xy} . The strain e at the point in any direction a at an angle θ with the x direction derives as

$$e_a = \frac{e_x + e_y}{2} + \frac{e_x - e_y}{2} \cos 2\theta + \frac{\gamma_{xy}}{2} \sin 2\theta$$

Similarly, the shearing strain γ_{ab} (change in the original right angle between directions a and b) is defined by

$$\gamma_{ab} = (e_x - e_y) \sin 2\theta + \gamma_{xy} \cos 2\theta$$

Inspection easily reveals that the above equations for e_a and γ_{ab} are mathematically identical to those for S_n and S_s . Thus, once a sign convention is established, a Mohr circle for strain can be constructed and used as the stress circle is used. The strain e is positive when an extension and negative when a contraction. If the direction associated with the first subscript a rotates counterclockwise during straining with respect to the direction indicated by the second subscript b , the shearing strain is positive; if clockwise, it is negative. In constructing the circle, positive extensional strains will be plotted to the right as abscissas and positive **half-shearing** strains will be plotted upward as ordinates.

For the strains shown in Fig. 5.2.26a, Mohr's strain circle becomes that shown in Fig. 5.2.26b. The extensional strain in the direction a , making an angle of θ_a with the x direction, is e_a , and the shearing strain is γ_{ab} counterclockwise. The strain 90° away is e_b . The maximum principal strain is e_M at an angle θ_M clockwise from the x direction. The other principal or minimum strain is e_m 90° away.

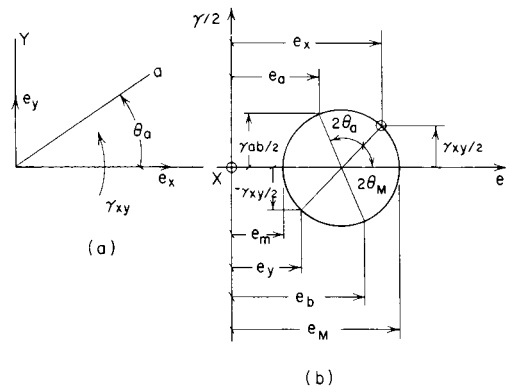


Fig. 5.2.26

PLASTIC DESIGN

Early efforts in stress analysis were based on limit loads, that is, loads which stress a member "wholly" to the yield strength. Euler's famous paper on column action ("Sur la Force des Colonnes," Academie des Sciences de Berlin, 1757) deals with the column problem this way. More recently, the concept of limit loads, referred to as **limit**, or **plastic design**, has found strong application in the design of certain structures. The theory presupposes a ductile material, absence of stress raisers, and fabrication free of embrittlement. Local load overstress is allowed, provided the structure does not deform appreciably.

To visualize the limit-load approach, consider a simple beam of uniform section subjected to a concentrated load of midspan, as depicted in Fig. 5.2.27a. According to elastic theory, the outermost fiber on each side and at midspan—the section of maximum bending moment—will first reach the yield-strength value. Across the depth of the beam, the stress distribution will, of course, follow the triangular pattern, becoming zero at the neutral axis. If the material is ductile, the stress in the outermost fibers will remain at the yield value until every other fiber reaches the same value as the load increases. Thus the stress distribution assumes the rectangular pattern before the *plastic hinge* forms and failure ensues.

The problem is that of finding the final limit load. Elastic-flexure theory gives the maximum load—triangular distribution—as

$$F_y = \frac{2S_ybh^2}{3l}$$

For the rectangular stress distribution, the limit load becomes

$$F_L = \frac{S_ybh^2}{l}$$

The ratio $F_L/F_y = 1.50$ —an increase of 50 percent in load capability. The ratio F_L/F_y has been named **shape factor** (Jenssen, *Plastic Design in Welded Structures Promises New Economy and Safety, Welding Jour.*, Mar. 1959). See Fig. 5.2.27b for shape factors for some other sections. The shape factor may also be determined by dividing the first moment of area about the neutral axis by the section modulus.

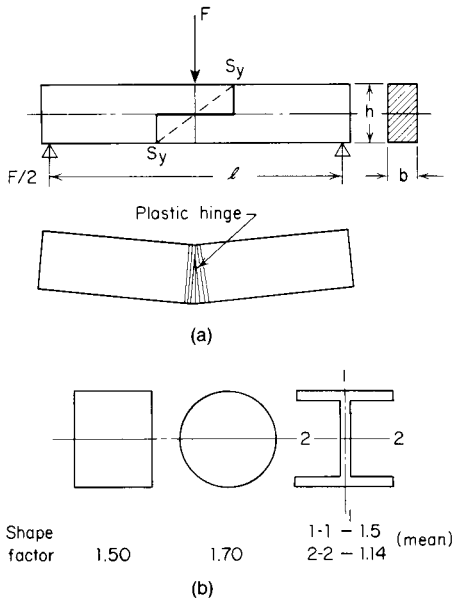


Fig. 5.2.27

A constant-section beam with both ends fixed, supporting a uniformly distributed load, illustrates another application of the plastic-load approach. The bending-moment diagram based on the elastic theory drawn in Fig. 5.2.28 (broken line) shows a moment at the center

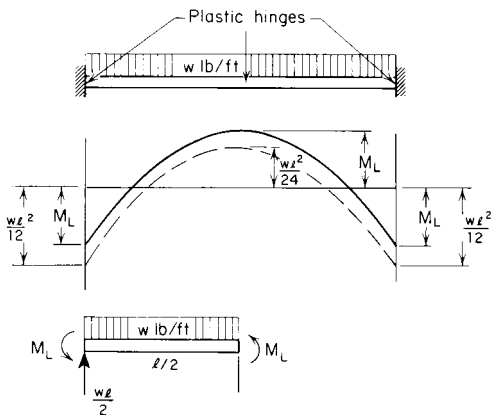


Fig. 5.2.28

equal to one-half the moment at either end. A preferable situation, it might be argued, is one in which the moments are the same at the three stations—solid line. Thus, applying equilibrium to, say, the left half of the beam yields a bending moment at each of the three plastic hinges

$$M_L = \frac{wl^2}{16}$$

DESIGN STRESSES

If a machine part is to safely transmit loads acting upon it, a permissible maximum stress must be established and used in the design. This is the allowable stress, the working stress, or preferably, the **design stress**. The design stress should not waste material, yet should be large enough to prevent failure in case loads exceed expected values, or other uncertainties react unfavorably.

The design stress is determined by dividing the applicable material property—yield strength, ultimate strength, fatigue strength—by a **factor of safety**. The factor should be selected only after all **uncertainties** have been thoroughly considered. Among these are the uncertainty with respect to the magnitude and kind of operating load, the reliability of the material from which the component is made, the assumptions involved in the theories used, the environment in which the equipment might operate, the extent to which localized and fabrication stresses might develop, the uncertainty concerning causes of possible failure, and the endangering of human life in case of failure. Factors of safety vary from industry to industry, being the result of accumulated experience with a class of machines or a kind of environment. Many codes, such as the ASME code for power shafting, recommend design stresses found safe in practice.

In general, the **ductility** of the material determines the property upon which the factor should be based. Materials having an elongation of over 5 percent are considered ductile. In such cases, the factor of safety is based upon the yield strength or the endurance limit. For materials with an elongation under 5 percent, the ultimate strength must be used because these materials are **brittle** and so fracture without yielding.

Factors of safety based on yield are often taken **between 1.5 and 4.0**. For more reliable materials or well-defined design and operating conditions, the lower factors are appropriate. In the case of untried materials or otherwise uncertain conditions, the larger factors are safer. The same values can be used when loads vary, but in such cases they are applied to the fatigue or endurance strength. When the ultimate strength determines the design stress (in the case of brittle materials), the factors of safety can be doubled.

Thus, under static loading, the design stress for, say, SAE 1020, which has a yield strength of 45,000 lb/in² (3,170 kgf/cm²) may be taken at 45,000/2, or 22,500 lb/in² (1,585 kgf/cm²), if a reasonably certain design condition exists. A Class 30 cast-iron part might be designed at 30,000/5 or 6,000 lb/in² (423 kgf/cm²). A 2017S-0 aluminum-alloy component (13,000 lb/in² endurance strength) could be computed at a design stress of 13,000/2.5 or 5,200 lb/in² (366 kgf/cm²) in the usual fatigue-load application.

BEAMS

For properties of structural steel and wooden beams, see Sec. 12.2.

Notation

- I = rectangular moment of inertia
- I_p = polar moment of inertia
- I/c = section modulus
- M = bending moment
- P, W' = concentrated load
- Q or V = total vertical shear
- R = reaction
- S = unit normal stress
- S_s or S_y = transverse shearing stress
- W = total distributed load

- f = deflection
- i = slope
- l = distance between supports
- r = radius of gyration
- r_c = radius of curvature
- w = distributed load per longitudinal unit

A **simple beam** rests on supports at its ends which permit rotation. A **cantilever beam** is fixed (no rotation) at one end. When computing reactions and moments, distributed loads may be replaced by their resultants acting at the center of gravity of the distributed-load area.

Reactions are the forces and/or couples acting at the supports and holding the beam in place. In general, the weight of the beam should be accounted for.

The **bending moment** (pound-feet or pound-inches) ($\text{kgf} \cdot \text{m}$) at any section is the algebraic sum of the external forces and moments acting on the beam on one side of the section. It is also equal to the moment of the internal-stress forces at the section, $M = \int s dA/y$. A bending moment that bends a beam convex downward (tensile stress on bottom fiber) is considered **positive**, while convex upward (compression on bottom) is **negative**.

The **vertical shear** V (lb) (kgf) effective on a section is the algebraic sum of all the forces acting parallel to and on one side of the section, $V = \Sigma F$. It is also equal to the sum of the transverse shear stresses acting on the section, $V = \int S_x dA$.

Moment and shear diagram may be constructed by plotting to scale the particular entity as the ordinate for each section of the beam. Such diagrams show in continuous form the variation along the length of the beam.

Moment-Shear Relation The shear V is the first derivative of moment with respect to distance along the beam, $V = dM/dx$. This relationship does not, however, account for any sudden changes in moment.

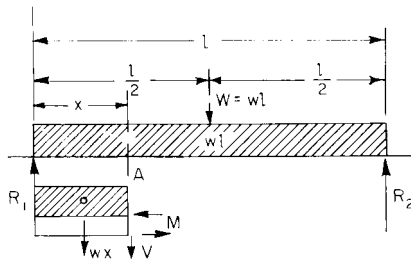


Fig. 5.2.29

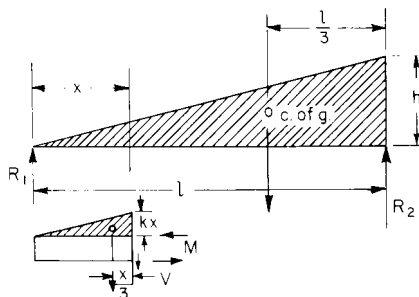


Fig. 5.2.30

EXAMPLES. Figure 5.2.29 illustrates a simple beam subjected to a uniform load. $M = R_1x - wx \times \frac{x}{2} = \frac{w}{2}x^2 - \frac{wx^2}{2}$ and $V = R_1 - wx = \frac{wl}{2} - wx$. Note also

$$\text{that } V = \frac{d}{dx} \left(\frac{wlx}{2} - \frac{wx^2}{2} \right) = \frac{wl}{2} - wx.$$

Figure 5.2.30 is a simple beam carrying a uniformly varying load; $M = R_1x -$

$$h \frac{x}{1} \times \frac{x}{2} \times \frac{x}{3} = \frac{hlx}{6} - \frac{hx^3}{6l}, \text{ if } h \text{ is in pounds per foot and weight of beam is neglected. The vertical shear } V = R_1 - \frac{hx}{l} \times \frac{x}{2} = \frac{hl}{6} - \frac{hx^2}{2l}.$$

$$\frac{d}{dx} \left(\frac{hlx}{6} - \frac{hx^3}{6l} \right) = \frac{hl}{6} - \frac{hx^2}{2l}.$$

Table 5.2.2 gives the reactions, bending-moment equations, vertical shear equations, and the deflection of some of the more common types of beams.

Maximum Safe Load on Steel Beams See Table 5.2.3 To obtain maximum safe load (or maximum deflection under maximum safe load) for any of the conditions of loading given in Table 5.2.5, multiply the corresponding coefficient in that table by the greatest safe load (or deflection) for distributed load for the particular section under consideration as given in Table 5.2.4.

The following approximate factors for reducing the load should be used when beams are long in comparison with their breadth:

Ratio of unsupported (lateral) length to flange width or breadth	20	30	40	50	60	70
Ratio of greatest safe load to calculated load	1	0.9	0.8	0.7	0.6	0.5

Theory of Flexure A bent beam is shown in Fig. 5.2.31. The concave side is in compression and the convex side in tension. These are divided by the **neutral plane** of zero stress $A'B'BA$. The intersection of the neutral plane with the face of the beam is in the **neutral line or elastic curve** AB . The intersection of the neutral plane with the cross section is the **neutral axis** NN' .

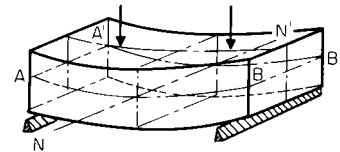


Fig. 5.2.31

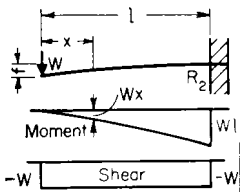
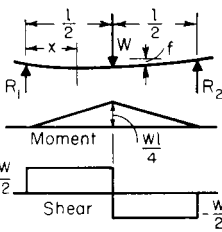
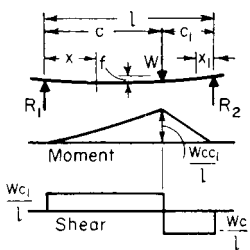
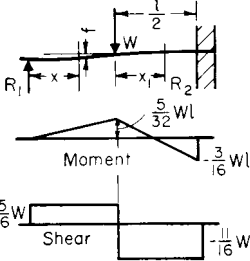
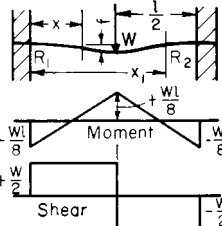
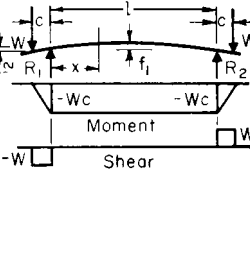
It is assumed that a beam is prismatic, of a length at least 10 times its depth, and that the external forces are all at right angles to the axis of the beam and in a plane of symmetry, and that flexure is slight. Other assumptions are: (1) That the material is homogeneous, and obeys Hooke's law. (2) That stresses are within the elastic limit. (3) That every layer of material is free to expand and contract longitudinally and laterally under stress as if separate from other layers. (4) That the tensile and compressive moduli of elasticity are equal. (5) That the cross section remains a plane surface. (The assumption of plane cross sections is strictly true only when the shear is constant or zero over the cross section, and when the shear is constant throughout the length of the beam.)

It follows then that: (1) The internal forces are in horizontal balance. (2) The **neutral axis contains the center of gravity** of the cross section, where there is no resultant axial stress. (3) The stress intensity varies directly with the distance from the neutral axis.

The moment of the elastic forces about the neutral axis, i.e., the **stress moment** or **moment of resistance**, is $M = SI/c$, where S is an elastic unit stress at outer fiber whose distance from the neutral axis is c ; and I is the rectangular moment of inertia about the neutral axis. I/c is the **section modulus**.

This formula is for the **strength of beams**. For rectangular beams, $M = \frac{1}{6}Sbh^2$, where b = breadth and h = depth; i.e., the elastic **strength of beam sections** varies as follows: (1) for equal width, as the square of the depth; (2) for equal depth, directly as the width; (3) for equal depth and width, directly as the strength of the material; (4) if span varies, then for equal depth, width, and material, inversely as the span.

Table 5.2.2 Beams of Uniform Cross Section, Loaded Transversely

 $R_2 = W$ $M_x = -Wx$ $M_{\max} = -Wl, (x = l)$ $Q_x = -W$ $f = \frac{Wl^3}{3EI} \text{ (max)}$	 $R_1 = \frac{W}{2}, R_2 = \frac{W}{2}$ $M_x = \frac{Wx}{2}$ $M_{\max} = \frac{Wl}{4}, \left(x = \frac{l}{2}\right)$ $Q_x = \pm \frac{W}{2}$ $f = \frac{W}{EI} \frac{l^3}{48} \text{ (max)}$	 $R_1 = \frac{Wc}{l}, R_2 = \frac{W(l-c)}{l}$ $M_x = \frac{Wc_1x}{l}, M_{x'} = \frac{Wc_2x'}{l}$ $M_{\max} = \frac{Wcc_1}{l}, (x_1 = c_1 \text{ or } x = c)$ $Q_x = \frac{Wc_1}{l}, Q_{x_1} = \frac{Wc_2}{l}$ $f = \frac{Wc_1}{3EI} \left[\frac{c(l+c_1)}{3} \right]^{3/2} \text{ (max)}$ <p>Max f occurs at $x = \sqrt{c(l-c_1)}/3$</p>
 $R_1 = \frac{5}{16} W, R_2 = \frac{11}{16} W$ $M_x = \frac{5}{16} Wx$ $M_{x_1} = Wl \left(\frac{5}{32} - \frac{11}{16} \frac{x_1}{l} \right)$ $M_{\max} = -\frac{3}{16} Wl, \left(x_1 = \frac{l}{2}\right)$ $Q_x = +\frac{5}{16} W, Q_{x_1} = -\frac{11}{16} W$ $Q_{\max} = -\frac{11}{16} W,$ $\left(x = \frac{l}{2} \text{ to } x + l\right)$ $f = \frac{W}{EI} \frac{7l^3}{768}$	 $R_1 = \frac{W}{2}, R_2 = \frac{W}{2}$ $M_x = \frac{W}{2} \left(\frac{x}{l} - \frac{1}{4} \right)$ $M_{x_1} = -\frac{Wl}{2} \left(\frac{x}{l} - \frac{3}{4} \right)$ $M_{\max} = \frac{Wl}{8}, \left(x = \frac{l}{2}\right)$ $Q_x = \frac{W}{2}, Q_{x_1} = -\frac{W}{2}$ $f = \frac{W}{EI} \frac{l^3}{192} \text{ (max)}$	 $R_1 = W$ $R_2 = W$ $M_x = -Wc = \text{const}$ $Q_{W \text{ to } R_1} = -W$ $Q_{R_1 \text{ to } R_2} = 0$ $Q_{R_2 \text{ to } W} = +W$ $f_1 = \frac{Wcl^2}{EI8} \text{ (max)}$ $f_2 = \frac{Wc^2}{EI3} \left(c + \frac{3l}{2} \right) \text{ (max)}$

If a beam is cut in halves vertically, the two halves laid side by side each will carry only one-half as much as the original beam.

Tables 5.2.6 to 5.2.8 give the properties of various beam cross sections. For properties of structural-steel shapes, see Sec. 12.2.

Oblique Loading It should be noted that Table 5.2.6 includes certain cases for which the horizontal axis is not a neutral axis, assuming the common case of vertical loading. The rectangular section with the diagonal as a horizontal axis (Table 5.2.6) is such a case. These cases must be handled by the principles of oblique loading.

Every section of a beam has two principal axes passing through the

center of gravity, and these two axes are always at right angles to each other. The principal axes are axes with respect to which the moment of inertia is, respectively, a maximum and a minimum, and for which the product of inertia is zero. For symmetrical sections, axes of symmetry are always principal axes. For unsymmetrical sections, like a **rolled angle section** (Fig. 5.2.32), the inclination of the principal axis with the X axis may be found from the formula $\tan 2\theta = 2I_{xy}/(I_y - I_x)$, in which $\theta =$ angle of inclination of the principal axis to the X axis, $I_{xy} =$ the product of inertia of the section with respect to the X and Y axes, $I_y =$ moment of inertia of the section with respect to the Y axis, $I_x =$ moment of inertia of

Table 5.2.2 Beams of Uniform Cross Section, Loaded Transversely (Continued)

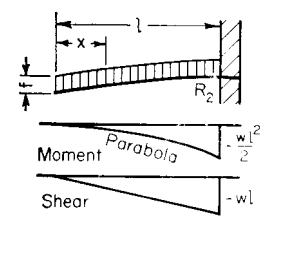
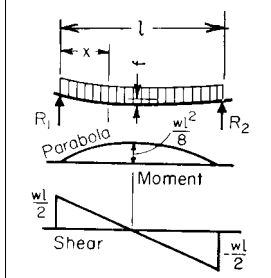
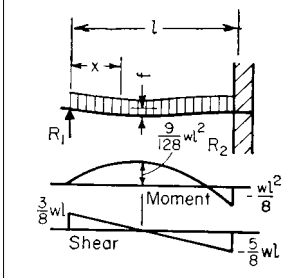
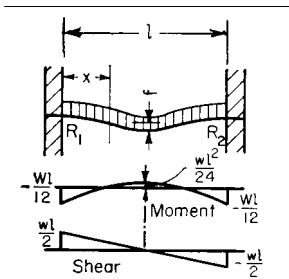
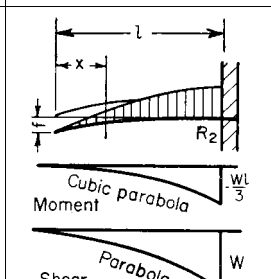
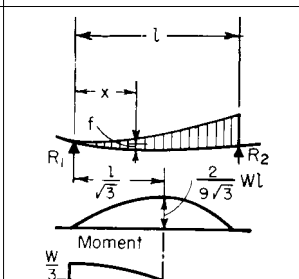
 <p>Moment Parabola $-\frac{wl^2}{2}$</p> <p>Shear $-wl$</p> $R_2 = W = wl$ $M_x = -\frac{wx^2}{2}$ $M_{\max} = -\frac{wl^2}{2}, (x = l)$ $Q_x = -wx$ $Q_{\max} = -wl, (x = l)$ $f = \frac{W}{EI} \frac{l^3}{8} (\max)$	 <p>Moment Parabola $\frac{wl^2}{8}$</p> <p>Shear $\frac{wl}{2}$ $-\frac{wl}{2}$</p> $R_1 = \frac{W}{2} = \frac{wl}{2}$ $R_2 = \frac{W}{2} = \frac{wl}{2}$ $M_x = \frac{wx}{2} (l - x)$ $M_{\max} = \frac{wl^2}{8}, (x = \frac{1}{2}l)$ $Q_x = \frac{wl}{2} - wx$ $Q_{\max} = \frac{wl}{2}, (x = 0)$ $f = \frac{W}{EI} \frac{5l^3}{384} (\max)$	 <p>Moment $\frac{9}{128}wl^2$ $-\frac{wl^2}{8}$</p> <p>Shear $\frac{3}{8}wl$ $-\frac{5}{8}wl$</p> $R_1 = \frac{3}{8}W = \frac{3}{8}wl$ $R_2 = \frac{5}{8}W = \frac{5}{8}wl$ $M_x = \frac{wx}{4} \left(\frac{3}{4}l - x \right)$ $M_{\max} = \frac{9}{128}wl^2, \left(x = \frac{3}{8}l \right)$ $M_{\max} = -\frac{wl^2}{8}, (x = l)$ $Q_x = \frac{3}{8}wl - wx$ $Q_{\max} = -\frac{5}{8}wl$ $f = \frac{W}{EI} \frac{l^3}{185} (\max)$
 <p>Moment $-\frac{wl}{12}$ $\frac{wl}{24}$ $-\frac{wl}{12}$</p> <p>Shear $\frac{wl}{2}$ $-\frac{wl}{2}$</p> $R_1 = \frac{W}{2} = \frac{wl}{2}, R_2 = \frac{W}{2} = \frac{wl}{2}$ $M_x = -\frac{wl^2}{2} \left(\frac{1}{6} - \frac{x}{l} + \frac{x^2}{l^2} \right)$ $M_{\max} = -\frac{1}{12}wl^2, (x = 0, \text{ or } x = l)$ $Q_x = \frac{wl}{2} - wx$ $Q_{\max} = \pm \frac{wl}{2}$ $f = \frac{W}{EI} \frac{l^3}{384} (\max)$	 <p>Moment Cubic parabola $-\frac{Wl}{3}$</p> <p>Shear Parabola W</p> $R_2 = W = \text{total load}$ $M_x = -\frac{W}{3} \frac{x^3}{l^2}$ $M_{\max} = -\frac{Wl}{3}$ $Q_x = -\frac{Wx^2}{l^2}$ $Q_{\max} = -W$ $f = \frac{W}{EI} \frac{l^3}{15} (\max)$	 <p>Moment $\frac{2}{9\sqrt{3}}Wl$ $-\frac{2}{9\sqrt{3}}Wl$</p> <p>Shear $\frac{W}{3}$ $-\frac{2}{3}W$</p> $R_1 = \frac{1}{3}W, R_2 = \frac{2}{3}W$ $M_x = \frac{Wx}{3} \left(1 - \frac{x^2}{l^2} \right)$ $M_{\max} = \frac{2}{9\sqrt{3}}Wl, \left(x = \frac{1}{\sqrt{3}} \right)$ $Q_x = W \left(\frac{1}{3} - \frac{x^2}{l^2} \right)$ $Q_{\max} = -\frac{2}{3}W, (x = l)$ $f = 0.01304 \frac{Wl^3}{EI} (\max)$

Table 5.2.2 Beams of Uniform Cross Section, Loaded Transversely (Continued)

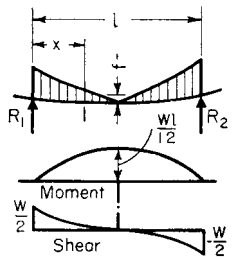
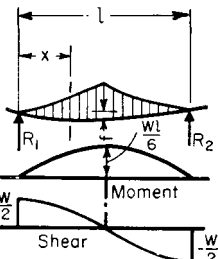
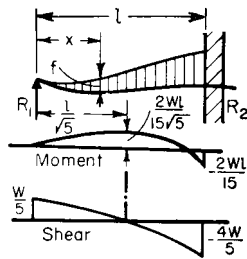
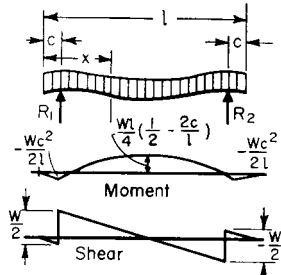
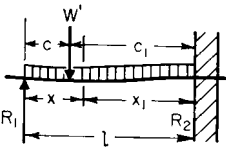
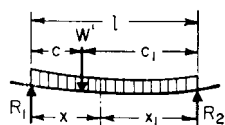
 $R_1 = \frac{W}{2}, R_2 = \frac{W}{2}$ $M_x = Wx \left(\frac{1}{2} - \frac{x}{l} + \frac{2x^2}{3l^2} \right)$ $M_{\max} = \frac{Wl}{12}, \left(x = \frac{1}{2} l \right)$ $Q_x = W \left(\frac{1}{2} - \frac{2x}{l} + \frac{2x^2}{l^2} \right)$ $Q_{\max} = \pm \frac{W}{2}, (x = 0)$ $f = \frac{W}{EI} \frac{3l^3}{320} (\max)$	 $R_1 = \frac{W}{2}, R_2 = \frac{W}{2}$ $M_x = Wx \left(\frac{1}{2} - \frac{2}{3} \frac{x^2}{l^2} \right)$ $M_{\max} = \frac{Wl}{6}, \left(x = \frac{1}{2} l \right)$ $Q_x = W \left(\frac{1}{2} - \frac{2x^2}{l^2} \right)$ $Q_{\max} = \pm \frac{W}{2}, (x = 0)$ $f = \frac{W}{EI} \frac{l^3}{60} (\max)$	 $R_1 = \frac{W}{5}, R_2 = \frac{4W}{5}$ $M_x = Wx \left(\frac{1}{5} - \frac{x^2}{3l^2} \right)$ $M_{\max} = -\frac{2}{15} Wl \text{ at support 2}$ $Q_x = W \left(\frac{1}{5} - \frac{x^2}{l^2} \right)$ $Q_{\max} = -\frac{4W}{5}$ $f = \frac{16Wl^3}{1,500\sqrt{5}EI}$ $= \frac{0.00477Wl^3}{EI} (\max)$
 $R_1 = \frac{W}{2} = \frac{wl}{2}, R_2 = \frac{W}{2} = \frac{wl}{2}$ $M_x = \frac{Wx}{2} \left(1 - \frac{c}{x} - \frac{x}{l} \right), (x > c)$ $M_x = -\frac{Wx^2}{2l}, (x \leq c)$ $M_{\max} = \frac{Wl}{4} \left(\frac{1}{2} - \frac{2c}{l} \right), c \leq \left(\frac{\sqrt{2}-1}{2} \right) l$ $Q_x = \frac{W}{2} - wx (x > c)$ $Q_x = -wx (x \leq c)$	 <p>Concentrated load W' Uniformly dist. load $W = wl$</p> $R_1 = W' \frac{c_1^2(3c + 2c_1)}{2l^3} + \frac{3}{8} W$ $R_2 = W' \frac{(2c^2 + 6cc_1 + 3c_1^2)c}{2l^3} + \frac{5}{8} W$ $M_2 = W' \frac{cc_1(2c + c_1)}{2l^2} + W \left(\frac{l}{8} \right)$ $M_{W'} = W' \frac{cc_1^2(3c + 2c_1)}{2l^3} + W \frac{(3c_1 - c)c}{8l}$ <p>(a) $\frac{W'}{W} < \frac{l^2}{4c_1^2} \frac{5c - 3c_1}{3c + 2c_1}$</p> $M_{c_1 \max} = \frac{R_1^2}{2W} l, \left(x = \frac{R_1 l}{W} \right)$ <p>(b) $\frac{W'}{W} < \frac{l^2(3c_1 - 5c)}{4c(2c^2 + 6cc_1 + 3c_1^2)}$</p> $M_{c_1 \max} = W'c + \frac{(R_1 - W')^2}{2W} l, \left(x = \frac{R_1 - W'}{W} l \right)$ <p>Deflection under W'</p> $f = \frac{W'}{EI} \frac{c^2 c_1^2 (4c + 3c_1)}{12l^3} + \frac{W}{EI} \frac{cc_1^2(3c + c_1)}{48l}$	

Table 5.2.2 Beams of Uniform Cross Section, Loaded Transversely (Continued)



Concentrated load W'
Uniformly dist. load $W = wl; c < c_1$

$$R_1 = W' \frac{c_1}{l} + \frac{W_2}{2}$$

$$R_2 = W' \frac{c}{l} + \frac{W}{2}$$

(a) $\frac{W'}{W} < \frac{c_1 - c}{2c}$

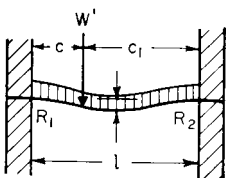
$$M_{\max} = R_2 \frac{x_1}{2} = \frac{R_2^2 l}{2W}, \left(x_1 = \frac{R_2 l}{W} \right)$$

(b) $\frac{W'}{W} > \frac{c_1 - c}{2c}$

$$M_{\max} = \left(W' + \frac{W}{2} \right) \frac{cc_1}{l}, (x_1 = c_1)$$

Deflection of beam under W' :

$$f = \left(W' + \frac{l^2 + cc_1}{8cc_1} W \right) \frac{c^2 c_1^2}{3EI}$$



$c < c_1$

$$R_1 = W' \frac{(3c + c_1)c_1^2}{l^3} + \frac{W}{2}$$

$$R_2 = W' \frac{(c + 3c_1)c^2}{l^3} + \frac{W}{2}$$

$$M_{\max} = M_1 = W' \frac{cc_1^2}{l^2} + \frac{Wl}{12}$$

Deflection under W'

$$f = \frac{1}{EI} \left(W' \frac{c^3 c_1^3}{3l^3} + W \frac{c^2 c_1^2}{24l} \right)$$

Table 5.2.3 Uniformly Distributed Loads on Simply Supported Rectangular Beams 1-in Wide* (Laterally Supported Sufficiently to Prevent Buckling)

[Calculated for unit fiber stress at 1,000 lb/in² (70 kgf/cm²): nominal size]
Total load in pounds (kgf)† including the weight of beam

Span, ft (m)‡	Depth of beam, in (cm)§										
	6	7	8	9	10	11	12	13	14	15	16
5	800	1,090	1,420	1,800	2,220	2,690	3,200	3,750	4,350	5,000	5,690
6	670	910	1,180	1,500	1,850	2,240	2,670	3,130	3,630	4,170	4,740
7	570	780	1,010	1,290	1,590	1,920	2,280	2,680	3,110	3,570	4,060
8	500	680	890	1,120	1,390	1,680	2,000	2,350	2,720	3,130	3,560
9	440	600	790	1,000	1,230	1,490	1,780	2,090	2,420	2,780	3,160
10	400	540	710	900	1,110	1,340	1,600	1,880	2,180	2,500	2,840
11	360	490	650	820	1,010	1,220	1,450	1,710	1,980	2,270	2,590
12	330	450	590	750	930	1,120	1,330	1,560	1,810	2,080	2,370
13	310	420	550	690	850	1,030	1,230	1,440	1,680	1,920	2,190
14	290	390	510	640	790	960	1,140	1,340	1,560	1,790	2,030
15	270	360	470	600	740	900	1,070	1,250	1,450	1,670	1,900
16	250	340	440	560	690	840	1,000	1,170	1,360	1,560	1,780
17	230	320	420	530	650	790	940	1,100	1,280	1,470	1,670
18	220	300	400	500	620	750	890	1,040	1,210	1,390	1,580
19	210	290	380	470	590	710	840	990	1,150	1,320	1,500
20	200	270	360	450	560	670	800	940	1,090	1,250	1,420
22	180	250	320	410	500	610	730	850	990	1,140	1,290
24	160	230	290	370	460	560	670	780	910	1,040	1,180
26	150	210	270	340	420	520	610	720	840	960	1,090
28	140	190	250	320	390	480	570	670	780	890	1,010
30	130	180	240	300	370	450	530	630	730	830	950

* This table is convenient for wooden beams. For any other fiber stress S' , multiply the values in table by $S'/1,000$. See Sec. 12.2 for properties of wooden beams of commercial sizes.
 † To change to kgf, multiply by 0.454.
 ‡ To change to m, multiply by 0.305.
 § To change to cm, multiply by 2.54.

the section with respect to the X axis. When this principal axis has been found, the other principal axis is at right angles to it.

Calling the moments of inertia with respect to the principal axes I'_x and I'_y , the unit stress existing anywhere in the section at a point whose coordinates are x and y (Fig. 5.2.33) is $S = My \cos \alpha / I'_x + Mx \sin \alpha / I'_y$, in which M = bending moment with respect to the section in question, α = the angle which the plane of bending moment or the plane of the

loads makes with the y axis, $M \cos \alpha$ = the component of bending moment causing bending about the principal axis which has been designated as the X axis, $M \sin \alpha$ = the component of bending moment causing bending about the principal axis which has been designated as the Y axis. The sign of the two terms for unit stress may be determined by inspection in the usual way, and the result will be tension or compression as determined by the algebraic sum of the two terms.

Table 5.2.4 Approximate Safe Loads in Pounds (kgf) on Steel Beams,* Simply Supported, Single Span

Allowable fiber stress for steel, 16,000 lb/in² (1,127 kgf/cm²) (basis of table)

Beams simply supported at both ends.

L = distance between supports, ft (m) a = interior area, in² (cm²)
 A = sectional area of beam, in² (cm²) d = interior depth, in (cm)
 D = depth of beam, in (cm) w = total working load, net tons (kgf)

Shape of section	Greatest safe load, lb		Deflection, in	
	Load in middle	Load distributed	Load in middle	Load distributed
Solid rectangle	$\frac{890AD}{L}$	$\frac{1,780AD}{L}$	$\frac{wL^3}{32AD^2}$	$\frac{wL^3}{52AD^2}$
Hollow rectangle	$\frac{890(AD - ad)}{L}$	$\frac{1,780(AD - ad)}{L}$	$\frac{wL^3}{32(AD^2 - ad^2)}$	$\frac{wL^3}{52(AD^2 - ad^2)}$
Solid cylinder	$\frac{667AD}{L}$	$\frac{1,333AD}{L}$	$\frac{wL^3}{24AD^2}$	$\frac{wL^3}{38AD^2}$
Hollow cylinder	$\frac{667(AD - ad)}{L}$	$\frac{1,333(AD - ad)}{L}$	$\frac{wL^3}{24(AD^2 - ad^2)}$	$\frac{wL^3}{38(AD^2 - ad^2)}$
I beam	$\frac{1,795AD}{L}$	$\frac{3,390AD}{L}$	$\frac{wL^3}{58AD^2}$	$\frac{wL^3}{93AD^2}$

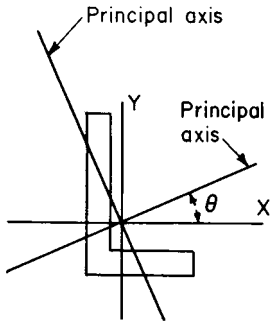


Fig. 5.2.32

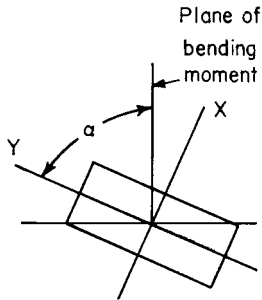


Fig. 5.2.33

In general, it may be stated that when the plane of the bending moment coincides with one of the principal axes, the other principal axis is the neutral axis. This is the ordinary case, in which the ordinary formula for unit stress may be applied. When the plane of the bending moment does not coincide with one of the principal axes, the above formula for oblique loading may be applied.

Internal Moment Beyond the Elastic Limit

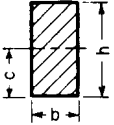
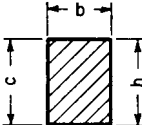
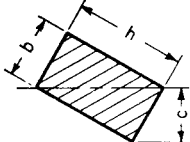
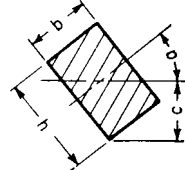
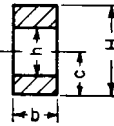
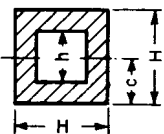
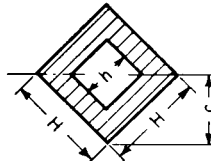
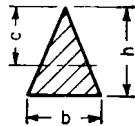
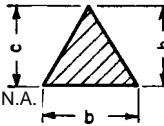
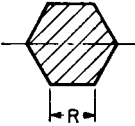
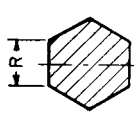
Ordinarily, the expression $M = SI/c$ is used for stresses above the elastic limit, in which case S becomes an experimental coefficient S_R , the **modulus of rupture**, and the formula is empirical. The true relation is obtained by applying to the cross section a stress-strain diagram from a tension and compression test, as in Fig. 5.2.34. Figure 5.2.34 shows the side of a beam of depth d under flexure beyond its elastic limit; line 1-1 shows the distorted cross section; line 3-3, the usual rectilinear

Table 5.2.5 Coefficients for Correcting Values in Table 5.2.4 for Various Methods of Support and of Loading, Single Span

Conditions of loading	Max relative safe load	Max relative deflection under max relative safe load
Beam supported at ends:		
Load uniformly distributed over span	1.0	1.0
Load concentrated at center of span	1/2	0.80
Two equal loads symmetrically concentrated	1/4c	
Load increasing uniformly to one end	0.974	0.976
Load increasing uniformly to center	3/4	0.96
Load decreasing uniformly to center	3/2	1.08
Beam fixed at one end, cantilever:		
Load uniformly distributed over span	1/4	2.40
Load concentrated at end	1/6	3.20
Load increasing uniformly to fixed end	3/8	1.92
Beam continuous over two supports equidistant from ends:		
Load uniformly distributed over span		
1. If distance $a > 0.2071l$	$l^2/(4a^2)$	
2. If distance $a < 0.2071l$	$\frac{l}{l - 4a}$	
3. If distance $a = 0.2071l$	5.83	
Two equal loads concentrated at ends	$l/(4a)$	

NOTE: l = length of beam; c = distance from support to nearest concentrated load; a = distance from support to end of beam.

Table 5.2.6 Properties of Various Cross Sections*
 (I = moment of inertia; I/c = section modulus; $r = \sqrt{I/A}$ = radius of gyration)

 $I = \frac{bh^3}{12}$ $\frac{I}{c} = \frac{bh^2}{6}$ $r = \frac{h}{\sqrt{12}} = 0.289h$	 <p>N.A.</p> $\frac{bh^3}{3}$ $\frac{bh^2}{3}$ $\frac{h}{\sqrt{3}} = 0.577h$	 $\frac{b^3h^3}{6(b^2 + h^2)}$ $\frac{b^2h^2}{6\sqrt{b^2 + h^2}}$ $\frac{bh}{\sqrt{6(b^2 + h^2)}}$	 $\frac{bh}{12} (h^2 \cos^2 a + b^2 \sin^2 a)$ $\frac{bh}{6} \left(\frac{h^2 \cos^2 a + b^2 \sin^2 a}{h \cos a + b \sin a} \right)$ $\sqrt{\frac{h^2 \cos^2 a + b^2 \sin^2 a}{12}}$
 $I = \frac{b}{12} (H^3 - h^3)$ $\frac{I}{c} = \frac{b}{6} \frac{H^3 - h^3}{H}$ $r = \sqrt{\frac{H^3 - h^3}{12(H - h)}}$	 $\frac{H^4 - h^4}{12}$ $\frac{1}{6} \frac{H^4 - h^4}{H}$ $\sqrt{\frac{H^2 + h^2}{12}}$	 $\frac{H^4 - h^4}{12}$ $\frac{\sqrt{2}}{12} \frac{H^4 - h^4}{H}$ $\sqrt{\frac{H^2 + h^2}{12}}$	 $\frac{bh^3}{36}; c = \frac{2}{3}h$ $\frac{bh^2}{24}$ $\frac{h}{\sqrt{18}}$
 <p>N.A.</p> $I = \frac{bh^3}{12}$ $\frac{I}{c} = \frac{bh^2}{12}$ $r = \frac{h}{\sqrt{6}}$	 $\frac{5\sqrt{3}}{16} R^4$ $\frac{5\sqrt{3}}{16} R^3$ $\sqrt{\frac{5}{24}} R$	 $\frac{1 + 2\sqrt{2}}{6} R^4$ $0.6906R^3$ $0.475R$	

NOTE: Square, axis same as first rectangle, side = h ; $I = h^4/12$; $I/c = h^3/6$; $r = 0.289h$.
 Square, diagonal taken as axis: $I = h^4/12$; $I/c = 0.1179h^3$; $r = 0.289h$.

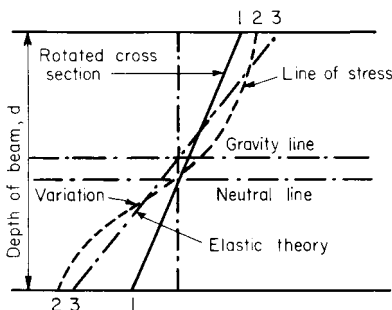


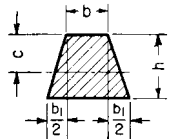
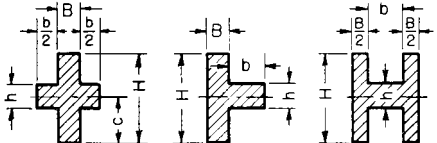
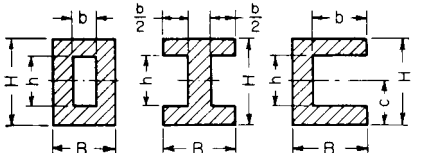
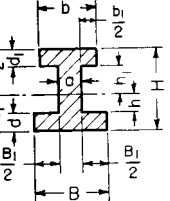
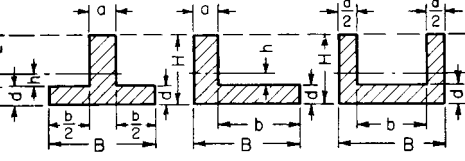
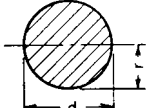
Fig. 5.2.34

relation of stress to strain; and line 2-2, an actual stress-strain diagram, applied to the cross section of the beam, compression above and tension below. The neutral axis is then below the gravity axis. The **outer material** may be expected to develop **greater ultimate strength** than in simple stress, because of the reinforcing action of material nearer the neutral axis that is not yet overstrained. This leads to an **equalization of stress** over the cross section. S_R exceeds the ultimate strength S_M in tension as follows: for cast iron, $S_R = 2S_M$; for sandstone, $S_R = 3S_M$; for concrete, $S_R = 2.2S_M$; for wood (green), $S_R = 2.3S_M$.

In the case of steel I beams, failure begins practically when the elastic limit in the compression flange is reached.

Because of the support of adjoining material, the **elastic limit in flexure** S_p is also greater than in tension, depending upon the relation of breadth to depth of section. For the same breadth, the difference decreases with

Table 5.2.6 Properties of Various Cross Sections* (Continued)

<p>Equilateral Polygon <i>A</i> = area <i>R</i> = rad circumscribed circle <i>r</i> = rad inscribed circle <i>n</i> = no. sides <i>a</i> = length of side Axis as in preceding section of octagon</p>	$I = \frac{A}{24} (6R^2 - a^2)$ $= \frac{A}{48} (12r^2 + a^2)$ $= \frac{AR^2}{4} \text{ (approx)}$	$\frac{I}{c} = \frac{I}{r}$ $= \frac{I}{R \cos \frac{180^\circ}{n}}$ $= \frac{AR}{4} \text{ (approx)}$	$\sqrt{\frac{I}{A}} = \sqrt{\frac{6R^2 - a^2}{24}} \approx \frac{R}{2}$ $= \sqrt{\frac{12r^2 + a^2}{48}}$
	$I = \frac{6b^2 + 6bb_1 + b_1^2}{36(2b + b_1)} h^3$ $c = \frac{1}{3} \frac{3b + 2b_1}{2b + b_1} h$	$\frac{I}{c} = \frac{6b^2 + 6bb_1 + b_1^2}{12(3b + 2b_1)} h^2$	$r = \frac{h\sqrt{12b^2 + 12bb_1 + 2b_1^2}}{6(2b + b_1)}$
	$I = \frac{BH^3 + bh^3}{12}$ $\frac{I}{c} = \frac{BH^3 + bh^3}{6H}$	$r = \sqrt{\frac{BH^3 + bh^3}{12(BH + bh)}}$	
	$I = \frac{BH^3 - bh^3}{12}$ $\frac{I}{c} = \frac{BH^3 - bh^3}{6H}$	$r = \sqrt{\frac{BH^3 - bh^3}{12(BH - bh)}}$	
	$I = \frac{1}{2} (Bc_1^3 - B_1h^3 + bc_2^3 - b_1h_1^3)$ $c_1 = \frac{1}{2} \frac{aH^2 + B_1d^2 + b_1d_1(2H - d_1)}{aH + B_1d + b_1d_1}$	$r = \sqrt{\frac{I}{Bd + b_1d_1 + a(h + h_1)}}$	
	$I = \frac{1}{2} (Bc_1^3 - bh^3 + ac_2^3)$ $c_1 = \frac{1}{2} \frac{aH^2 + bd^2}{aH + bd}$ $c_2 = H - c_1$ $r = \sqrt{\frac{I}{Bd + a(H - d)}}$		
	$I = \frac{\pi d^4}{64} = \frac{\pi r^4}{4} = \frac{A}{4} r^2$ $= 0.05d^4 \text{ (approx)}$	$\frac{I}{c} = \frac{\pi d^3}{32} = \frac{\pi r^3}{4} = \frac{A}{4} r$ $= 0.1d^3 \text{ (approx)}$	$\sqrt{\frac{I}{A}} = \frac{r}{2} = \frac{d}{4}$

increase of height. No difference will occur in the case of an I beam, or with hard materials.

Wide plates will not expand and contract freely, and the value of *E* will be increased on account of side constraint. As a consequence of lateral contraction of the fibers of the tension side of a beam and lateral swelling of fibers at the compression side, the cross section becomes distorted to a trapezoidal shape, and the neutral axis is at the center of gravity of the trapezoid. Strictly, this shape is one with a curved perimeter, the radius being r_c/μ , where r_c is the radius of curvature of the neutral line of the beam, and μ is Poisson's ratio.

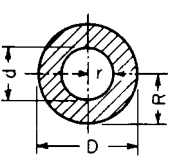
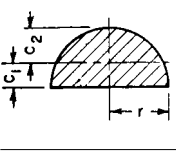
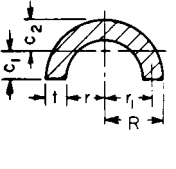
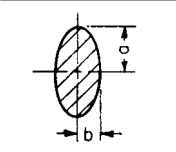
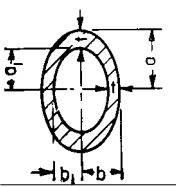
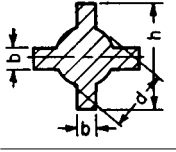
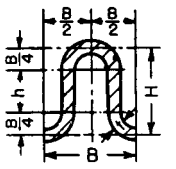
Deflection of Beams

When a beam is subjected to bending, the fibers on one side elongate, while the fibers on the other side shorten (Fig. 5.2.35). These changes in length cause the beam to deflect. All points on the beam except those directly over the support fall below their original position, as shown in Figs. 5.2.31 and 5.2.35.

The **elastic curve** is the curve taken by the neutral axis. The radius of curvature at any point is

$$r_c = EI/M$$

Table 5.2.6 Properties of Various Cross Sections* (Continued)

 <p>$d_m = \frac{1}{2}(D + d)$ $s = \frac{1}{2}(D - d)$</p>	$I = \frac{\pi}{64}(D^4 - d^4)$ $= \frac{\pi}{4}(R^4 - r^4)$ $= \frac{1}{4}A(R^2 + r^2)$ $= 0.05(D^4 - d^4)$ <p>(approx)</p>	$\frac{I}{c} = \frac{\pi}{32} \frac{D^4 - d^4}{D}$ $= \frac{\pi}{4} \frac{R^4 - r^4}{R}$ $= 0.8d_m^2s$ <p>(approx)</p> <p>when $\frac{s}{d_m}$ is very small</p>	$\sqrt{\frac{I}{A}} = \frac{\sqrt{R^2 + r^2}}{2} = \frac{\sqrt{D^2 + d^2}}{4}$
	$I = r^4 \left(\frac{\pi}{8} - \frac{8}{9\pi} \right)$ $= 0.1098r^4$	$\frac{I}{c_2} = 0.1908r^3$ $\frac{I}{c_1} = 0.2587r^2$ $c_1 = 0.4244r$	$\sqrt{\frac{I}{A}} = \frac{\sqrt{9\pi^2 - 64}}{6\pi} r = 0.264r$
	$I = 0.1098(R^4 - r^4)$ $- \frac{0.283R^2r^2(R - r)}{R + r}$ $= 0.3tr_1^3$ <p>(approx)</p> <p>when $\frac{t}{r_1}$ is very small</p>	$c_1 = \frac{4}{3\pi} \frac{R^2 + Rr + r^2}{R + r}$ $c_2 = R - c_1$	$\sqrt{\frac{I}{A}} = \sqrt{\frac{2I}{\pi(R^2 - r^2)}}$ $= 0.31r_1$ <p>(approx)</p>
	$I = \frac{\pi a^3 b}{4} = 0.7854a^3 b$	$\frac{I}{c} = \frac{\pi a^2 b}{4} = 0.7854a^2 b$	$r = \frac{a}{2}$
	$I = \frac{\pi}{4}(a^3 b - a_1^3 b_1)$ $= \frac{\pi}{4} a^2(a + 3b)t$ <p>(approx)</p>	$\frac{I}{c} = \frac{\pi}{4} a(a + 3b)t$ <p>(approx)</p>	$r = \sqrt{\frac{I}{\pi ab - a_1 b_1}}$ $= \frac{a}{2} \sqrt{\frac{a + 3b}{a + b}}$ <p>(approx)</p>
	$I = \frac{1}{12} \left[\frac{3\pi}{16} d^4 + b(h^3 - d^3) + b^3(h - d) \right]$ $\frac{I}{c} = \frac{1}{6h} \left[\frac{3\pi}{16} d^4 + b(h^3 + d^3) + b^3(h - d) \right]$		$r = \sqrt{\frac{I}{\pi \frac{d^2}{4} + 2b(h - d)}}$ <p>(approx)</p>
	$I = \frac{t}{4} \left(\frac{\pi B^3}{16} + B^2 h + \frac{\pi B h^2}{2} + \frac{2}{3} h^3 \right)$ $h = H - \frac{1}{2} B$ $\frac{I}{c} = \frac{2I}{H + t}$		$r = \sqrt{\frac{I}{2 \left(\frac{\pi B}{4} + h \right) t}}$

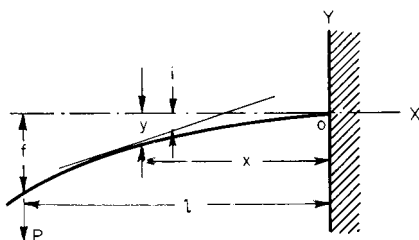


Fig. 5.2.35

A beam bent to a **circular curve** of constant radius has a constant bending moment.

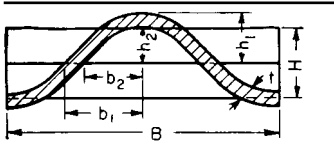
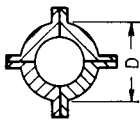
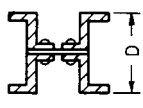
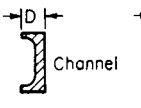
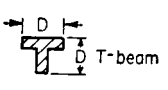
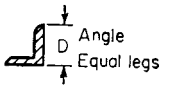
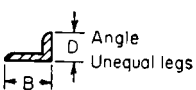
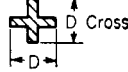
Replacing r_c in the equation by its approximate geometrical value, $1/r_c = d^2y/dx^2$, the fundamental equation from which the elastic curve of a bent beam can be developed and the deflection of any beam obtained is,

$$M = EI \frac{d^2y}{dx^2} \quad (\text{approx})$$

Substituting the value of M , in terms of x , and integrating once, gives the slope of the tangent to the elastic curve of the beam at point x ;

$\tan i = dy/dx = \int_0^x M dx/(EI)$. Since i is usually small, $\tan i = i$,

Table 5.2.6 Properties of Various Cross Sections* (Continued)

 <p>Corrugated sheet iron, parabolically curved</p>	$I = \frac{64}{105} (b_1 h_1^3 - b_2 h_2^3), \text{ where}$ $h_1 = \frac{1}{2}(H + t) \quad \left \quad b_1 = \frac{1}{4}(B + 2.6t)\right.$ $h_2 = \frac{1}{2}(H - t) \quad \left \quad b_2 = \frac{1}{4}(B - 2.6t)\right.$ $\frac{I}{c} = \frac{2I}{H + t}$	$r = \sqrt{\frac{3I}{t(2B + 5.2H)}}$
Approximate values of least radius of gyration r		
 <p>$r = 0.36336D$</p>	 <p>$0.295D$</p>	 <p>$D/4.58$</p>
 <p>$r = D/4.74$</p>	 <p>$D/5$</p>	 <p>$BD/[2.6(B + D)]$</p>
 <p>$D/4.74$</p>		

* Some of the cross sections depicted in this table will be encountered most often in machinery as castings, forgings, or individual sections assembled and joined mechanically (or welded). A number of the sections shown are obsolete and will be encountered mainly in older equipment and/or building structures.

expressed in radians. A second integration gives the vertical deflection of any point of the elastic curve from its original position.

EXAMPLE. In the cantilever beam shown in Fig. 5.2.35, the bending moment at any section $= -P(l - x) = EI d^2y/(dx)^2$. Integrate and determine constant by the condition that when $x = 0, dy/dx = 0$. Then $EI dy/dx = -Px + \frac{1}{2}Px^2$. Integrate again; and determine constant by the condition that when $x = 0, y = 0$. Then $EIy = -\frac{1}{2}Plx^2 + Px^3/6$. This is the equation of the elastic curve. When $x = l, y = f = -Pl^3/(3EI)$. In general, the two constants of integration must be determined simultaneously.

Deflection in general, f , may be expressed by the equation $f = Pl^3/(mEI)$, where m is a coefficient. See Tables 5.2.2 and 5.2.4 for values of f for beams of various sections and loadings. For coefficients of deflection of wooden beams and structural steel shapes, see Sec. 12.2.

Since I varies as the cube of the depth, the **stiffness**, or inverse deflection, of various **beams** varies, other factors remaining constant, inversely as the load, inversely as the cube of the span, and directly as the cube of the depth. This deflection is due to bending moment only. In general, however, the bending of beams involves transverse shearing stresses which cause **shearing strains** and thus **add to the total deflection**. The contribution of shearing strain to overall deflection becomes significant only when the beam span is very short. These strains may affect substantially the strength as well as the deflection of beams. When deflection due to transverse shear is to be accounted for, the differential equation of the elastic curve takes the form

$$EI \frac{d^2y}{dx^2} = EI \left(\frac{d^2y_b}{dx^2} + \frac{d^2y_s}{dx^2} \right) = M - \frac{kEI}{AG} \times \frac{d^2M}{dx^2}$$

where k is a factor dependent upon the beam cross section. Sergiev Sergev, in "The Effect of Shearing Forces on the Deflection and Strength of Beams" (*Univ. Wash. Eng. Exp. Stn. Bull.* 114) gives $k = 1.2$ for rectangular sections, $10/9$ for circular sections, and 2.4 for I beams. He also points out that in the case of a deep, rectangular-section cantilever, carrying a concentrated load at the free end, the deflection due to shear may be up to 3.1 percent of that due to bending moment; if this beam supports a uniformly distributed load, it may be up to 4.1 percent. A deep, simple beam deflection may increase up to 15.6 percent when carrying a uniformly distributed load and up to 12.5 percent when the load is concentrated at midspan.

Design of beams may be based on **strength** (stress) or on **stiffness** if deflection must be limited. Deflection rather than stress becomes the

crit^{er}ion for design, e.g., of machine tools, for which the relative positions of tool and workpiece must be maintained while the cutting loads are applied during operation. Similarly, large steam-turbine shafts supported on two end bearings must maintain alignment and tight critical clearances between the rotating blade assemblies and the stationary stator blades during operation. When more than one beam shares a load, each beam will assume a portion of the load that is proportional to its stiffness. **Superposition** may be used in connection with both stresses and deflections.

EXAMPLE. (Fig. 5.2.36). Two wooden stringers—one (A) 8×16 in in cross section and 20 ft in span, the other (B) $8 \text{ in} \times 8 \text{ in} \times 16 \text{ ft}$ —carrying the center load $P_0 = 22,000$ lb are required, the load carried by each stringer. The deflections f of the two stringers must be equal. Load on A $= P_1$, and on B $= P_2$. $f = P_1 l^3 / (48EI_1) = P_2 l^3 / (48EI_2)$. Then $P_1 / P_2 = I_2^3 / (I_1^3) = 4$. $P_0 = P_1 + P_2 = 4P_2 + P_2$, whence $P_2 = 22,000/5 = 4,400$ lb (1,998 kgf) and $P_1 = 4 \times 4,400 = 17,600$ lb (7,990 kgf).

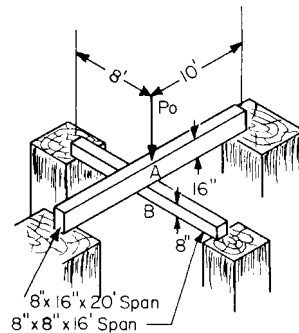


Fig. 5.2.36

Relation between Deflection and Stress

Combine the formula $M = SI/c = Pl/n$, where n is a constant, $P =$ load, and $l =$ span, with formula $f = Pl^3/(mEI)$, where m is a constant. Then

$$f = C'' SI^2 / (Ec)$$

where C'' is a new constant $= n/m$. Other factors remaining the same, the **deflection varies directly as the stress and inversely as E** . If the span is

Table 5.2.7

Beam	Load	n	m	C''
Cantilever	Concentrated at end	1	3	$\frac{1}{3}$
Cantilever	Uniform	2	8	$\frac{1}{4}$
Simple	Concentrated at center	4	48	$\frac{1}{12}$
Simple	Uniform	8	$\frac{384}{5}$	$\frac{5}{48}$
Fixed ends	Concentrated at center	8	192	$\frac{1}{24}$
Fixed ends	Uniform	12	384	$\frac{1}{52}$
One end fixed, one end supported	Concentrated at center	$\frac{16}{3}$	$\frac{768}{7}$	$\frac{7}{144}$
One end fixed, one end supported	Uniform	$\frac{128}{9}$	185	$\frac{1}{13}$
Simple	Uniformly varying, maximum at center	6	60	$\frac{1}{10}$

constant, a shallow beam will submit to greater deformations than a deeper beam without exceeding a safe stress. If depth is constant, a beam of double span will attain a given deflection with only one-quarter the stress. Values of n , m , and C'' are given in Table 5.2.7 (for other values, see Table 5.2.2).

Graphical Relations

Referring to Fig. 5.2.37, the shear V acting at any section is equal to the total load on the right of the section, or

$$V = \int w \, dx$$

Since $w \, dx$ is the product of w , a loading intensity (which is expressed as a vertical height in the load diagram), and dx , an elementary length along the horizontal, evidently $w \, dx$ is the area of a small vertical strip of the **load diagram**. Then $\int w \, dx$ is the summation of all such vertical strips between two indefinite points. Thus, to obtain the shear in any

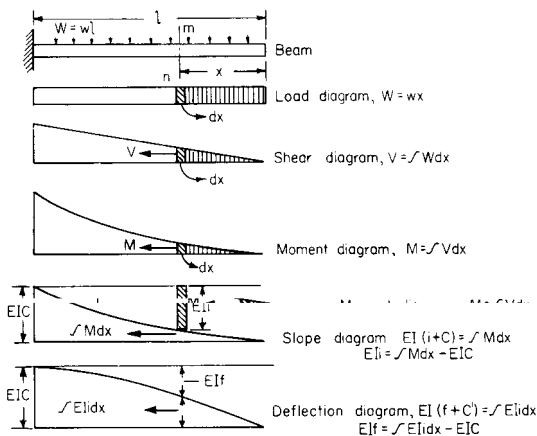


Fig. 5.2.37

section mn , find the area of the load diagram up to that section, and draw a second diagram called the **shear diagram**, any ordinate of which is proportional to the shear, or to the area in the load diagram to the right of mn . Since $V = dM/dx$,

$$\int V \, dx = M$$

By similar reasoning, a **moment diagram** may be drawn, such that the ordinate at any point is proportional to the area of the shear diagram to the right of that point. Since $M = EI \, d^2f/dx^2$,

$$\int M \, dx = EI (df/dx + C) = EI(i + C)$$

if I is constant. Here C is a constant of integration. Thus i , the slope or grade of the elastic curve at any point, is proportional to the area of the

moment diagram $\int M \, dx$ up to that point; and a **slope diagram** may be derived from the moment diagram in the same manner as the moment diagram was derived from the shear diagram.

If I is not constant, draw a new curve whose ordinates are M/I and use these M/I ordinates just as the M ordinates were used in the case where I was constant; that is, $\int (M/I) \, dx = E(i + C)$. The ordinate at any point of the slope curve is thus proportional to the area of the M/I curve to the right of that point. Again, since $iE = E \, df/dx$,

$$\int iE \, dx = \int E \, df = E(f + C)$$

and thus the ordinate f to the elastic curve at any point is proportional to the area of the slope diagram $\int i \, dx$ up to that point. The equilibrium polygon may be used in drawing the **deflection curve** directly from the M/I diagram.

Thus, the five curves of load, shear, moment, slope, and deflection are so related that each curve is derived from the previous one by a process of graphical integration, and with proper regard to scales the deflection is thereby obtained.

The vertical distance from any point A (Fig. 5.2.38) on the elastic curve of a beam to the tangent at any other point B equals the moment of the area of the $M/(EI)$ diagram from A to B about A . This distance, the **tangential deviation** t_{AB} , may be used with the slope-area relation and the geometry of the elastic curve to obtain deflections. These theorems, together with the equilibrium equations, can be used to compute reactions in the case of statically **indeterminate beams**.

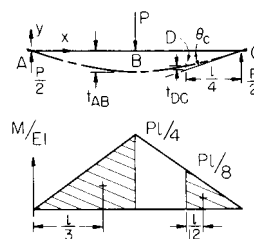


Fig. 5.2.38

EXAMPLE. The deflections of points B and D (Fig. 5.2.38) are

$$\begin{aligned}
 y_B &= -t_{AB} = \text{moment area} \frac{M}{EI} \Big|_A^B \\
 &= -\frac{1}{EI} \times \frac{Pl}{4} \times \frac{l}{4} \times \frac{l}{3} = -\frac{Pl^3}{48EI} \\
 \theta_C &= \nabla \theta \Big|_B^C = \text{area} \frac{M}{EI} \Big|_B^C = \frac{1}{EI} \times \frac{Pl}{4} \times \frac{l}{4} = \frac{Pl^2}{16EI} \\
 y_D &= -\left(\theta_C \times \frac{l}{4} - t_{DC} \right) \\
 &= -\frac{Pl^2}{16EI} \times \frac{l}{4} + \frac{l}{EI} \times \frac{Pl}{8} \times \frac{l}{8} \times \frac{l}{12} = -\frac{11Pl^3}{768EI}
 \end{aligned}$$

Resilience of Beams

The external work of a load gradually applied to a beam, and which increases from zero to P , is $\frac{1}{2}Pf$ and equals the **resilience** U . But, from the formulas $P = nSI/(cl)$ and $f = nSI^2/(mcE)$, where n and m are constants that depend upon loading and supports, S = fiber stress, c = distance from neutral axis to outer fiber, and l = length of span. Substitute for P and f , and

$$U = \frac{n^2}{m} \left(\frac{k}{c}\right)^2 \frac{S^2V}{2E}$$

where k is the radius of gyration and V the volume of the beam. For values of U , see Table 5.2.1.

The resilience of beams of similar cross section at a given stress is proportional to their volumes. The **internal resilience**, or the elastic deformation energy in the material of a beam in a length x is dU , and

$$U = \frac{1}{2} \int M^2 dx/(EI) = \frac{1}{2} \int M di$$

where M is the moment at any point x , and di is the angle between the tangents to the elastic curve at the ends of dx . The values of resilience and deflection in special cases are easily developed from this equation.

Rolling Loads

Rolling or moving loads are those loads which may change their position on a beam. Figure 5.2.39 represents a beam with two equal concentrated moving loads, such as two wheels on a crane girder, or the wheels of a

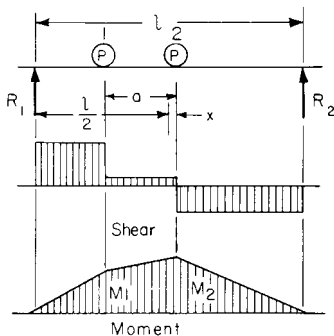


Fig. 5.2.39

truck on a bridge. Since the maximum moment occurs where the shear is zero, it is evident from the shear diagram that the maximum moment will occur under a wheel. $x < a/2$:

$$R_1 = P \left(1 - \frac{2x}{l} + \frac{a}{l} \right)$$

$$M_2 = \frac{Pl}{2} \left(1 - \frac{a}{l} + \frac{2x}{l} \frac{a}{l} - \frac{4x^2}{l^2} \right)$$

$$R_2 = P \left(1 + \frac{2x}{l} - \frac{a}{l} \right)$$

$$M_1 = \frac{Pl}{2} \left(1 - \frac{a}{l} - \frac{2a^2}{l^2} + \frac{2x}{l} \frac{3a}{l} - \frac{4x^2}{l^2} \right)$$

M_2 max when $x = \frac{1}{4}a$

M_1 max when $x = \frac{3}{4}a$

$$M_{\max} = \frac{Pl}{2} \left(1 - \frac{a}{2l} \right)^2 = \frac{P}{2l} \left(l - \frac{a}{2} \right)^2$$

EXAMPLE. Two wheel loads of 3,000 lb each, spaced on 5-ft centers, move on a span of $l = 15$ ft, $x = 1.25$ ft, and $R_2 = 2,500$ lb. $\therefore M_{\max} = M_2 = 2,500 \times 6.25$ (1,135 \times 1.90) = 15,600 lb \cdot ft (2,159 kgf \cdot m).

Figure 5.2.40 shows the condition when two equal loads are equally distant on opposite sides of the center. The moment is equal under the two loads

If the **two moving loads are of unequal weight**, the condition for **maximum moment** is that the maximum moment will occur under the heavy wheel when the center of the beam bisects the distance between the resultant of the loads and the heavy wheel. Figure 5.2.41 shows this position and the shear and moment diagrams.

When several **wheel loads** constituting a system occur, the several suspected wheels must be examined in turn to determine which will cause the greatest moment. The **position for the greatest moment** that can occur under a given wheel is, as stated, when the center of the span bisects the distance between the wheel in question and the resultant of all the loads then on the span. The **position for maximum shear** at the support will be when one wheel is passing off the span.

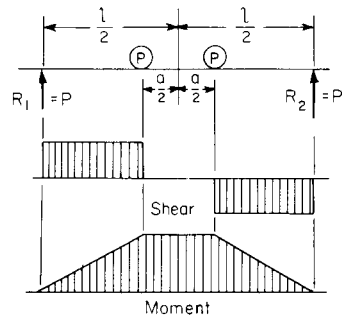


Fig. 5.2.40

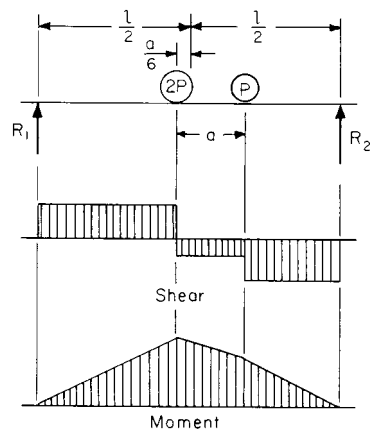


Fig. 5.2.41

Constrained Beams

Constrained beams are those so held or "built in" at one or both ends that the tangent to the elastic curve remains fixed in direction. These beams are held at the ends in such a manner as to allow free horizontal motion, as illustrated by Fig. 5.2.42. A constrained beam is stiffer than a simple beam of the same material, because of the modification of the moment by an end resisting moment. Figure 5.2.43 shows the two most common cases of constrained beams. See also Table 5.2.2.

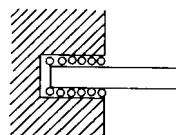


Fig. 5.2.42

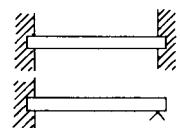


Fig. 5.2.43

Continuous Beams

A continuous beam is one resting upon several supports which may or may not be in the same horizontal plane. The general discussion for

beams holds for continuous beams. $S_v A = V$, $SI/c = M$, and $d^2f/dx^2 = M/(EI)$. The shear at any section is equal to the algebraic sum of the components parallel to the section of all external forces on either side of the section. The bending moment at any section is equal to the moment of all external forces on either side of the section. The relations stated above between shear and moment diagrams hold true for continuous beams. The bending moment at any section is equal to the bending moment at any other section, plus the shear at that section times its arm, plus the product of all the intervening external forces times their respective arms. To illustrate (Fig. 5.2.44):

$$V_x = R_1 + R_2 + R_3 - P_1 - P_2 - P_3$$

$$M_x = R_1(l_1 + l_2 + x) + R_2(l_2 + x) + R_3x - P_1(l_2 + c + x) - P_2(b + x) - P_3a$$

$$M_x = M_3 + V_3x - P_3a$$

Table 5.2.8 gives the value of the moment at the various supports of a uniformly loaded continuous beam over equal spans, and it also gives the values of the shears on each side of the supports. Note that the shear is of opposite sign on either side of the supports and that the sum of the two shears is equal to the reaction.

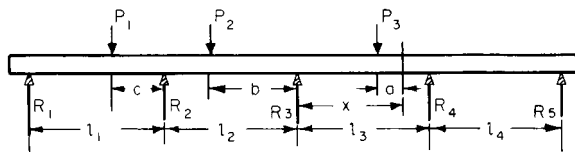


Fig. 5.2.44

Figure 5.2.45 shows the relation between the moment and shear diagrams for a uniformly loaded continuous beam of four equal spans (see Table 5.2.8). Table 5.2.8 also gives the maximum bending moment which will occur between supports, and in addition the position of this moment and the points of inflection (see Fig. 5.2.46).

Figure 5.2.46 shows the values of the functions for a uniformly loaded continuous beam resting on three equal spans with four supports. Continuous beams are stronger and much stiffer than simple beams. However, a small, unequal subsidence of piers will cause serious

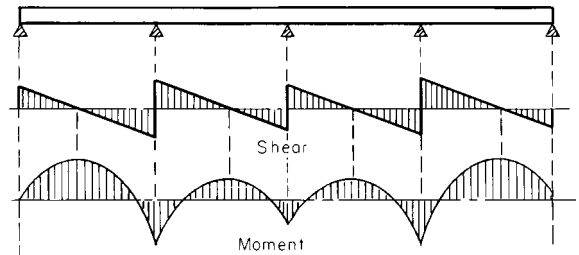


Fig. 5.2.45

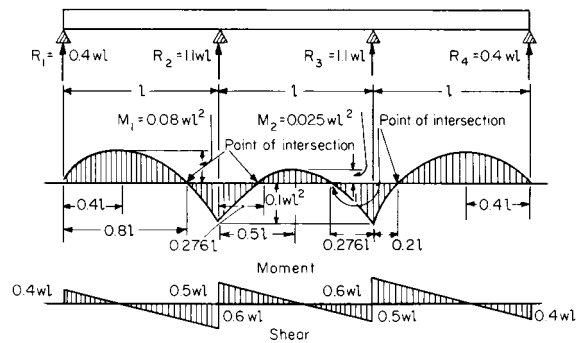


Fig. 5.2.46

Table 5.2.8 Uniformly Loaded Continuous Beams over Equal Spans (Uniform load per unit length = w ; length of equal span = l)

Number of supports	Notation of support of span	Shear on each side of support. $L = \text{left}, R = \text{right}$. Reaction at any support is $L + R$		Moment over each support	Max moment in each span	Distance to point of max moment, measured to right from support	Distance to point of inflection, measured to right from support
		L	R				
2	1 or 2	0	$\frac{1}{2}$	0	0.125	0.500	None
3	1	0	$\frac{3}{8}$	0	0.0703	0.375	0.750
	2	$\frac{5}{8}$	$\frac{5}{8}$	$\frac{1}{8}$	0.0703	0.625	0.250
4	1	0	$\frac{4}{10}$	0	0.080	0.400	0.800
	2	$\frac{9}{10}$	$\frac{5}{10}$	$\frac{1}{10}$	0.025	0.500	0.276, 0.724
5	1	0	$\frac{11}{28}$	0	0.0772	0.393	0.786
	2	$\frac{17}{28}$	$\frac{15}{28}$	$\frac{3}{28}$	0.0364	0.536	0.266, 0.806
	3	$\frac{13}{28}$	$\frac{13}{28}$	$\frac{2}{28}$	0.0364	0.464	0.194, 0.734
6	1	0	$\frac{15}{38}$	0	0.0779	0.395	0.789
	2	$\frac{23}{38}$	$\frac{20}{38}$	$\frac{4}{38}$	0.0332	0.526	0.268, 0.783
	3	$\frac{18}{38}$	$\frac{19}{38}$	$\frac{3}{38}$	0.0461	0.500	0.196, 0.804
7	1	0	$\frac{41}{104}$	0	0.0777	0.394	0.788
	2	$\frac{63}{104}$	$\frac{55}{104}$	$\frac{11}{104}$	0.0340	0.533	0.268, 0.790
	3	$\frac{49}{104}$	$\frac{51}{104}$	$\frac{9}{104}$	0.0433	0.490	0.196, 0.785
	4	$\frac{53}{104}$	$\frac{53}{104}$	$\frac{9}{104}$	0.0433	0.510	0.215, 0.804
8	1	0	$\frac{56}{142}$	0	0.0778	0.394	0.789
	2	$\frac{86}{142}$	$\frac{75}{142}$	$\frac{15}{142}$	0.0338	0.528	0.268, 0.788
	3	$\frac{67}{142}$	$\frac{70}{142}$	$\frac{11}{142}$	0.0440	0.493	0.196, 0.790
	4	$\frac{72}{142}$	$\frac{71}{142}$	$\frac{12}{142}$	0.0405	0.500	0.215, 0.785

Values apply to:

wl wl wl^2 wl^2 l l

NOTE: The numerical values given are coefficients of the expressions at the foot of each column.

Table 5.2.9 Beams of Uniform Strength (in Bending)

Beam	Cross section	Elevation and plan	Formulas
1. Fixed at one end, load P concentrated at other end			
	Rectangle: width (b) constant, depth (g) variable	Elevation: 1, top, straight line; bottom, parabola. 2, complete pa- rabola Plan: rectangle	$y^2 = \frac{6P}{bS_s} x$ $h = \sqrt{\frac{6Pl}{bS_s}}$ <hr/> Deflection at A: $f = \frac{8P}{bE} \left(\frac{l}{h}\right)^3$
	Rectangle: width (y) variable, depth (h) constant	Elevation: rec- tangle Plan: triangle	$y = \frac{6P}{h^2S_s} x$ $b = \frac{6Pl}{h^2S_s}$ <hr/> Deflection at A: $f = \frac{6P}{bE} \left(\frac{l}{h}\right)^3$
	Rectangle: width (z) variable, depth (y) variable $\frac{z}{y} = k(\text{const.})$	Elevation: cubic parabola Plan: cubic pa- rabola	$y^3 = \frac{6P}{kS_s} x$ $z = ky$ $h = \sqrt[3]{\frac{6Pl}{kS_s}}$ $b = kh$
	Circle: diam (y) variable	Elevation: cubic parabola Plan: cubic pa- rabola	$y^3 = \frac{32P}{\pi S_s} x$ $d = \sqrt[3]{\frac{32Pl}{\pi S_s}}$
2. Fixed at one end, load of total magnitude P uniformly distributed			
	Rectangle width (b) constant, depth (y) variable	Elevation: triangle Plan: rectangle	$y = x \sqrt{\frac{3P}{blS}}$ $h = \sqrt{\frac{3Pl}{bS_s}}$ <hr/> $f = 6 \frac{P}{bE} \left(\frac{l}{h}\right)^3$
	Rectangle: width (y) variable, depth (h) constant	Elevation: rec- tangle Plan: two para- bolic curves with vertices at free end	$y = \frac{3Px^2}{lS_s h^2}$ $b = \frac{3Pl}{S_s h^2}$ <hr/> Deflection at A: $f = \frac{3P}{bE} \left(\frac{l}{h}\right)^3$

Table 5.2.9 Beams of Uniform Strength (in Bending) (Continued)

Beam	Cross section	Elevation and plan	Formulas
2. Fixed at one end, load of total magnitude P uniformly distributed			
	Rectangle: width (z) variable, depth (y) variable, $z = ky$	Elevation: semi-cubic parabola Plan: semicubic parabola	$y^3 = \frac{3Px^2}{kS_s l}$ $z = ky$ $h = \sqrt[3]{\frac{3Pl}{kS_s}}$ $b = kh$
	Circle: diam (y) variable	Elevation: semi-cubic parabola Plan: semicubic parabola	$y^3 = \frac{16P}{\pi S_s} x^2$ $d = \sqrt[3]{\frac{16Pl}{\pi S_s}}$
3. Supported at both ends, load P concentrated at point C			
	Rectangle: width (b) constant, depth (y) variable	Elevation: two parabolas, vertices at points of support Plan: rectangle	$y = \sqrt{\frac{3P}{S_s b}} x$ $h = \sqrt{\frac{3Pl}{2bS_s}}$ $f = \frac{P}{2Eb} \left(\frac{l}{h}\right)^3$
	Rectangle: width (y) variable, depth (h) constant	Elevation: rectangle Plan: two triangles, vertices at points of support	$y = \frac{3P}{S_s h^2} x$ $b = \frac{3Pl}{2S_s h^2}$ $f = \frac{3P l^3}{8Ebh^3}$
	Rectangle: width (b) constant, depth (y or y_1) variable	Elevation: two parabolas, vertices at points of support Plan: rectangle	$y^2 = \frac{6P(l-p)}{bS_s} x$ $y_1^2 = \frac{6P_p}{bS_s} x_1$ $h = \sqrt{\frac{6P(l-p)p}{bS_s}}$
Load P moving across span			
	Rectangle: width (b) constant, depth (y) variable	Elevation: ellipse Major axis = l Minor axis = $2h$ Plan: rectangle	$\frac{x^2}{\left(\frac{l}{2}\right)^2} + \frac{y^2}{\frac{3Pl}{2bS_s}} = 1$ $h = \sqrt{\frac{3Pl}{2bS_s}}$

Table 5.2.9 Beams of Uniform Strength (in Bending) (Continued)

Beam	Cross section	Elevation and plan	Formulas
4. Supported at both ends, load of total magnitude P uniformly distributed			
	Rectangle: width (b) constant, depth (y) variable	Elevation: ellipse Plan: rectangle	$\frac{x^2}{\left(\frac{l}{2}\right)^2} + \frac{y^2}{\frac{3Pl}{4bS_s}} = 1$ $h = \sqrt{\frac{3Pl}{4bS_s}}$ Deflection at O : $f = \frac{1}{64} \frac{Pl^3}{EI}$ $= \frac{3}{16} \frac{P}{bE} \left(\frac{l}{h}\right)^3$
	Rectangle: width (y) variable, depth (h) constant	Elevation: rectangle Plan: two parabolas with vertices at center of span	$y = \frac{3P}{S_s h^2} \left(x - \frac{x^2}{l}\right)$ $b = \frac{3Pl}{4S_s h^2}$

changes in sign and magnitude of the bending stresses, reactions, and shears.

Maxwell's Theorem When a number of loads rest upon a beam, the deflection at any point is equal to the sum of the deflections at this point due to each of the loads taken separately. Maxwell's theorem states that if unit loads rest upon a beam at two points A and B , the deflection at A due to the unit load at B equals the deflection at B due to the unit load at A .

Castigliano's theorem states that the deflection of the point of application of an external force acting on a beam is equal to the partial derivative of the work of deformation with respect to this force. Thus, if P is the force, f the deflection, and U the work of deformation, which equals the resilience,

$$dU/dP = f$$

According to the **principle of least work**, the deformation of any structure takes place in such a manner that the work of deformation is a minimum.

Beams of Uniform Strength

Beams of uniform strength vary in section so that the unit stress S remains constant, the I/c varies as M . For **rectangular beams**, of breadth b and depth d , $I/c = bd^2/6$; and $M = Sbd^2/6$. Thus, for a cantilever beam of rectangular cross section, under a load P , $Px = Sbd^2/6$. If b is constant, d^2 varies with x , and the profile of the beam will be a parabola, as Fig. 5.2.47. If d is constant, b will vary as x and the beam will be triangular in plan, as shown in Fig. 5.2.48.

Shear at the end of a beam necessitates a modification of the forms determined above. The area required to resist shear will be P/S , in a cantilever and R/S , in a simple beam. The dotted extensions in Figs. 5.2.47 and 5.2.48 show the changes necessary to enable these cantilevers to resist shear. The extra material and cost of fabrication, however, make many of the forms impractical.

Table 5.2.9 shows some of the simple **sections of uniform strength**. In none of these, however, is shear taken into account.

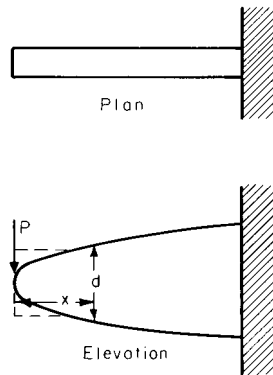


Fig. 5.2.47

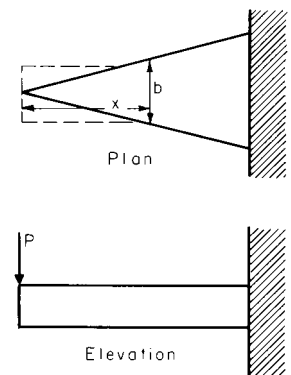


Fig. 5.2.48

TORSION

Under torsion, a bar (Fig. 5.2.49) is twisted by a couple of magnitude $P\rho$. Elements of the surface becomes helices of angle d , and a radius rotates through an angle θ in a length l , both d and θ being expressed in radians. S_v = shearing unit stress at distance r from center; I_p = *polar moment of inertia*; G = shearing modulus of elasticity. It is assumed that the cross sections remain plane surfaces. The strain on the cross section is wholly tangential, and is zero at the center of the section. Note that $ld = r\theta$.

In the case of a **circular cross section**, the stress S_v increases directly as the distance of the strained element from the center.

The polar moment of inertia I_p for any section may be obtained from $I_p = I_1 + I_2$, where I_1 and I_2 are the rectangular moments of inertia of the section about any two lines at right angles to each other, through the center of gravity.

The external twisting moment M_t is balanced by the internal resisting moment.

For strength, $M_t = S_v I_p / r$.

For stiffness, $M_t = a G I_p / l$.

The torsional resilience $U = \frac{1}{2} P p a = S_v^2 I_p l / (2 r^2 G) = a^2 G I_p / (2 l)$.

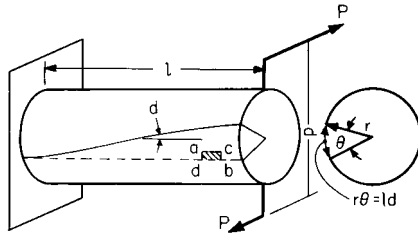


Fig. 5.2.49

The state of stress on an element taken from the surface of the shaft, as in Fig. 5.2.50, is pure shear. Pure tension exists at right angles to one 45° helix and pure compression at right angles to the opposite helix.

Reduced formulas for shafts of various sections are given in Table 5.2.11. When the ratio of shaft length to the largest lateral dimension in the cross section is less than approximately 2, the end effects may drastically affect the torsional stresses calculated.

Failure under torsion in brittle materials is a tensile failure at right angles to a helical element on the surface. Plastic materials twist off squarely. Fibrous materials separate in long strips.

Torsion of Noncircular Sections When a section is not circular, the unit stress no longer varies directly as the distance from the center. Cross sections become warped, and the greatest unit stress usually occurs at a point on the perimeter of the cross section nearest the axis of twist; thus, there is no stress at the corners of square and rectangular sections. The analyses become complex for noncircular sections, and the methods for solution of design problems using them most often admit only of approximations.

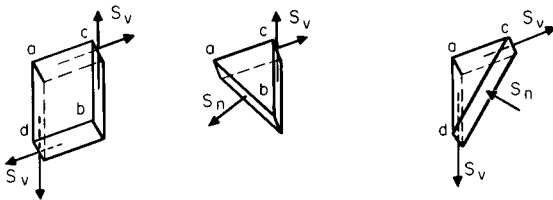


Fig. 5.2.50

Torsion problems have been solved for many different noncircular cross sections by utilizing the **membrane analogy**, due to Prandtl, which makes use of the fact that the mathematical treatment of a twisted bar is governed by the same equations as for a membrane stretched over a hole

which has the same shape as the bar and then inflated. The resulting three-dimensional surface provides the following: (1) The torque transmitted is proportional to twice the volume under the inflated membrane, and (2) the shear stress at any point is proportional to the slope of the curve measured perpendicular to that slope. In recent years, several other mathematical techniques have become widely used, especially with the aid of faster computational methods available from electronic computers.

By using **finite-difference methods**, the differential operators of the governing equations are replaced with difference operators which are related to the desired unknown values at a gridwork of points in the outline of the cross section being investigated.

The **finite-element method**, commonly referred to as **FEM**, deals with a spatial approximation of a complex shape which is then analyzed to determine deformations, stresses, etc. By using FEM, the exact structure is replaced with a set of simple structural elements interconnected at a finite number of nodes. The governing equations for the approximate structure can be solved exactly. Note that inasmuch as there is an exact solution for an approximate structure, the end result must be viewed, and the results thereof used, as approximate solutions to the real structure.

Using a finite-difference approach to Poisson's partial differential equation, which defines the stress functions for solid and hollow shafts with generalized contours, along with Prandtl's membrane analogy, Isakower has developed a series of practical design charts (ARRADCOM-MISD Manual UN 80-5, January 1981, Department of the Army). Dimensionless charts and tables for transmitted torque and maximum shearing stress have been generated. Information for circular shafts with rectangular and circular keyways, external splines and milled flats, as well as rectangular and X-shaped torsion bars, is presented.

Assuming the stress distribution from the point of maximum stress to the corner to be parabolic, Bach derived the approximate expression, $S_v M = 9 M_t / (2 b^2 h)$ for a rectangular section, b by h , where $h > b$. For closer results, the shearing stresses for a **rectangular section** (Fig. 5.2.51) may be expressed $S_A = M_t / (\alpha_A b^2 h)$ and $S_B = M_t / (\alpha_B b^2 h)$. The angle of twist for these shafts is $\theta = M_t l / (\beta G b^3 h)$. The factors α_A , α_B , and β are functions of the ratio h/b and are given in Table 5.2.10.

In the case of **composite sections**, such as a tee or angle, the torque that can be resisted is $M_t = G \theta \sum \beta h b^3$; the summation applies to each of the rectangles into which the section can be divided. The maximum stress occurs on the component rectangle having the largest b value. It is computed from

$$S_A = M_t \beta_A b_A / (\alpha_A \sum \beta h b^3)$$

Torque, deflection, and work relations for some additional sections are given in Table 5.2.11.

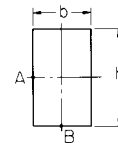
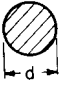
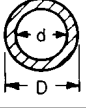
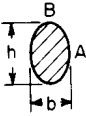
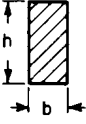
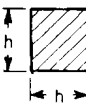




Fig. 5.2.51

Table 5.2.10 Factors for Torsion of Rectangular Shafts (Fig. 5.2.51)

b/b	1.00	1.50	1.75	2.00	2.50	3.00	4.00	5.00	6.00	8.00	10.0	∞
α_A	0.208	0.231	0.239	0.246	0.258	0.267	0.282	0.291	0.299	0.307	0.312	0.333
α_B	0.208	0.269	0.291	0.309	0.336	0.355	0.378	0.392	0.402	0.414	0.421	
β	0.141	0.196	0.214	0.229	0.249	0.263	0.281	0.291	0.299	0.307	0.312	0.333

Table 5.2.11 Torsion of Shafts of Various Cross Sections
(For strength and stiffness of shafts, see Sec. 8.2)

Cross section	Torsional resisting moment M_t	Angular twist, θ_1 (length = 1 in, radius = 1 in)		Work of torsion (V = volume)
		In terms of torsional moment	In terms of max shear	
	$\frac{\pi}{16} d^3 S_v$	$\frac{M_t}{G I_p} = \frac{32}{\pi d^4} \frac{M_t}{G}$	$2 \frac{S_{v_{max}}}{G} \frac{1}{d}$	$\frac{1}{4} \frac{S_{v_{max}}^2}{G} V$ (Note 1)
	$\frac{\pi}{16} \frac{D^4 - d^4}{D} S_v$	$\frac{32}{\pi(D^4 - d^4)} \frac{M_t}{G}$	$2 \frac{S_{v_{max}}}{G} \frac{1}{D}$	$\frac{1}{4} \frac{S_{v_{max}}^2}{G} \frac{D^2 + d^2}{D^2} V$ (Note 2)
	$\frac{\pi}{16} b^2 h S_v$ ($h > b$)	$\frac{16}{\pi} \frac{b^2 + h^2}{b^3 h^3} \frac{M_t}{G}$	$\frac{S_{v_{max}}}{G} \frac{b^2 + h^2}{b h^2}$	$\frac{1}{8} \frac{S_{v_{max}}^2}{G} \frac{b^2 + h^2}{h^2} V$ (Note 3)
	$\frac{3}{8} b^2 h S_v$ ($h > b$)	$3.6 \frac{b^2 + h^2}{b^3 h^3} \frac{M_t}{G}$	$0.8 \frac{S_{v_{max}}}{G} \frac{b^2 + h^2}{b h^2}$	$\frac{4}{45} \frac{S_{v_{max}}^2}{G} \frac{b^2 + h^2}{h^2} V$ (Note 4)
	$\frac{3}{8} h^3 S_v$	$7.2 \frac{1}{h^4} \frac{M_t}{G}$	$1.6 \frac{S_{v_{max}}}{G} \frac{1}{h}$	$\frac{8}{45} \frac{S_{v_{max}}^2}{G} V$ (Note 5)
	$\frac{b^2}{20} S_v$	$46.2 \frac{1}{b^4} \frac{M_t}{G}$	$2.31 \frac{S_{v_{max}}}{G} \frac{1}{b}$	
	$\frac{b^3}{1.09} S_v$	$0.967 \frac{1}{b^4} \frac{M_t}{G}$	$0.9 \frac{S_{v_{max}}}{G} \frac{1}{b}$	

*When $h/b =$ 1 2 4 8
Coefficient 3.6 becomes = 3.56 3.50 3.35 3.21
Coefficient 0.8 becomes = 0.79 0.78 0.74 0.71

NOTES: (1) $S_{v_{max}}$ at circumference. (2) $S_{v_{max}}$ at outer circumference. (3) $S_{v_{max}}$ at A; $S_{v_B} = 16M_t/\pi b h^2$. (4) $S_{v_{max}}$ at middle of side h ; in middle of b , $S_v = 9M_t/2bh^2$. (5) $S_{v_{max}}$ at middle of side.

COLUMNS

Members subjected to direct compression can be grouped into three classes. **Compression blocks** are so short (slenderness ratios below 30) that bending of member is unlikely. At the other limit, columns so slender that bending is primary, are the **long columns** defined by Euler's theory. The intermediate columns, quite common in practice, are called **short columns**.

Long columns and the more slender short columns usually fail by **buckling** when the **critical load** is reached. This is a matter of **instability**; that is, the column may continue to yield and deflect even though the load is not increased above critical. The **slenderness ratio** is the unsupported length divided by the least radius of gyration, parallel to which it can bend.

Long columns are handled by Euler's column formula,

$$P_{cr} = n \pi^2 EI / l^2 = n \pi^2 EA / (l/r)^2$$

The coefficient n accounts for **end conditions**. When the column is pivoted at both ends, $n = 1$; when one end is fixed and other rounded, $n = 2$;

when both are fixed, $n = 4$; and when one end is fixed with the other free, $n = 1/4$. The slenderness ratio that separates long columns from short ones depends upon the modulus of elasticity and the yield strength of the column material. When Euler's formula results in $(P_{cr}/A) > S_y$, strength rather than buckling causes failure, and the column ceases to be long. In round numbers, this **critical slenderness ratio** falls between 120 and 150. Table 5.2.12 gives additional facts concerning long columns.

Short Columns The stress in a short column may be considered partly due to compression and partly due to bending. A theoretical equation has not been derived. Empirical, though rational, expressions are, in general, based on the assumption that the permissible stress must be reduced below that which could be permitted were it due to compression only. The manner in which this reduction is made determines the type of equation as well as the slenderness ratio beyond which the **equation does not apply**. Figure 5.2.52 illustrates the situation. Some typical formulas are given in Table 5.2.13.

EXAMPLE. A machine member unsupported for a length of 15 in has a square cross section 0.5 in on a side. It is to be subjected to compression. What maximum safe load can be applied centrally, according to the AISC formula? At the com-

Table 5.2.12 Strength of Round-ended Columns according to Euler's Formula*

Material	Cast iron	Wrought iron†	Low-carbon steel	Medium-carbon steel
Ultimate compressive strength, lb/in ²	107,000	53,400	62,600	89,000
Allowable compressive stress, lb/in ² (maximum)	7,100	15,400	17,000	20,000
Modulus of elasticity	14,200,000	28,400,000	30,600,000	31,300,000
Factor of safety	8	5	5	5
Smallest <i>I</i> allowable at worst section, in ⁴	$\frac{Pl^2}{17,500,000}$	$\frac{Pl^2}{56,000,000}$	$\frac{Pl^2}{60,300,000}$	$\frac{Pl^2}{61,700,000}$
Limit of ratio, <i>l/r</i>	50.0	60.6	59.4	55.6
Rectangle ($r = b\sqrt{1/2}$), <i>l/b</i> >	14.4	17.5	17.2	16.0
Circle ($r = 1/2d$), <i>l/d</i> >	12.5	15.2	14.9	13.9
Circular ring of small thickness ($r = d\sqrt{1/8}$), <i>l/d</i> >	17.6	21.4	21.1	19.7

* *P* = allowable load, lb; *l* = length of column, in; *b* = smallest dimension of a rectangular section, in; *d* = diameter of a circular section, in; *r* = least radius of gyration of section.

† This material is no longer manufactured but may be encountered in existing structures and machinery.

Table 5.2.13 Typical Short-Column Formulas

Formula	Material	Code	Slenderness ratio
$S_w = 17,000 - 0.485 \left(\frac{l}{r}\right)^2$	Carbon steels	AISC	$l/r < 20$
$S_w = 16,000 - 70 (l/r)$	Carbon steels	Chicago	$l/r < 120$
$S_w = 15,000 - 50 \left(\frac{l}{r}\right)$	Carbon steels	AREA	$l/r < 150$
$S_w = 19,000 - 100 (l/r)$	Carbon steels	Am. Br. Co.	$60 < \frac{l}{r} < 120$
$S_{cr}^* = 135,000 - \frac{15.9}{c} \left(\frac{l}{r}\right)^2$	Alloy-steel tubing	ANC	$\frac{1}{\sqrt{cr}} < 65$
$S_w = 9,000 - 40 \left(\frac{l}{r}\right)$	Cast iron	NYC	$\frac{l}{r} < 70$
$S_{cr}^* = 34,500 - \frac{245}{\sqrt{c}} \left(\frac{l}{r}\right)$	2017ST Aluminum	ANC	$\frac{1}{\sqrt{cr}} < 94$
$S_{cr}^* = 5,000 - \frac{0.5}{c} \left(\frac{l}{r}\right)^2$	Spruce	ANC	$\frac{l}{\sqrt{cr}} < 72$
$S_{cr}^* = S_y \left[1 - \frac{S_y}{4n\pi^2E} \left(\frac{l}{r}\right)^2 \right]$	Steels	Johnson	$\frac{l}{r} < \sqrt{\frac{2n\pi^2E}{S_y}}$
$S_{cr}^{*\dagger} = \frac{S_y}{1 + \frac{ec}{r^2} \sec \left(\frac{l}{r} \sqrt{\frac{P}{4AE}}\right)}$	Steels	Secant	$\frac{l}{r} < \text{critical}$

* *S_{cr}*^{*} = theoretical maximum, *c* = end fixity coefficient.
c = 2, both ends pivoted; *c* = 2.86, one pivoted, other fixed;
c = 4, both ends fixed; *c* = 1, one end fixed, one end free.

† *e* is initial eccentricity at which load is applied to center of column cross section.

puted load, what size section (also square) would be needed, if it were to be designed according to the AREA formula?

$$l/r = 15/0.5\sqrt{12} = 104 \quad \therefore \text{short column}$$

$$P/A = 17,000 - 0.485 (104)^2 = 11,730$$

or $P = 0.25 \times 11,730 = 2,940 \text{ lb (1,335 kgf)}$

and $\frac{2,940}{a^2} \leq 15,000 - 50 \left(\frac{15a}{\sqrt{12}}\right) = 15,000 - \frac{2,600}{a}$

thus $a^2 - 0.173a - 0.196 = 0$ or $a = 0.536 \text{ in (1.36 cm)}$

Combined Flexure and Longitudinal Force Figure 5.2.53 shows a bar under flexure due to transverse and longitudinal loads. The maximum fiber stress *S* is made up of *S*₀, due to the direct action of load *P*, and *S*_b, due to the entire bending moment *M*. *M* is the algebraic sum of

two bending moments, *M*₁ due to longitudinal load (+ for compression and - for tension), and *M*₂ due to transverse load. $M = M_2 \pm M_1$. Here $M_1 = Pf$ and $f = CS_b^2/(Ec)$.

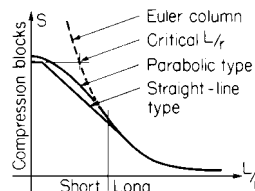


Fig. 5.2.52

FOR THE CASE OF LONGITUDINAL COMPRESSION. $S_b I/c = M_2 + CPS_b I^2/(Eo)$, or $S_b = M_2 c/(I - CPI^2/E)$. The maximum stress is $S = S_b + S_0$ compression. The constant C for the case of Fig. 5.2.53 is derived from the equations $P'l/4 = S_b I/c$ and $f = P'l^3/(48EI)$. Solving for f ; $f = \frac{1}{12} S_b I^2/(Ec)$, or $C = \frac{1}{12}$. For a beam supported at the ends and uniformly loaded, $C = \frac{5}{48}$. Other cases can be similarly calculated.

FOR THE CASE OF LONGITUDINAL TENSION. $M = M_2 - Pf$, and $S_b = M_2 c/(I + CPI^2/E)$. The maximum stress is $S = S_b + S_0$, tension.

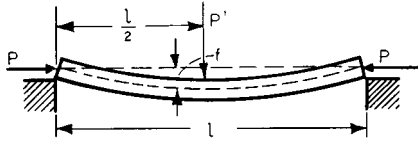


Fig. 5.2.53

ECCENTRIC LOADS

When short blocks are loaded eccentrically in compression or in tension, i.e., not through the center of gravity (cg), a combination of axial and bending stress results. The maximum unit stress S_M is the algebraic sum of these two unit stresses.

In Fig. 5.2.54 a load P acts in a line of symmetry at the distance e from cg; $r =$ radius of gyration. The unit stresses are (1) S_c , due to P , as if it acted through cg, and (2) S_b , due to the bending moment of P acting with a leverage of e about cg. Thus unit stress S at any point y is

$$S = S_c \pm S_b$$

$$= P/A \pm Pe y/I$$

$$= S_c (1 \pm e y/r^2)$$

y is positive for points on the same side of cg as P , and negative on the opposite side. For a rectangular cross section of width b , the maximum stress $S_M = S_c (1 + 6e/b)$. When P is outside the middle third of width b and is a compressive load, tensile stresses occur.

For a circular cross section of diameter d , $S_M = S_c (1 + 8e/d)$. The stress due to the weight of the solid will modify these relations.

NOTE. In these formulas e is measured from the gravity axis, and gives tension when e is greater than one-sixth the width (measured in the same direction as e), for rectangular sections; and when greater than one-eighth the diameter for solid circular sections.

If, as in certain classes of masonry construction, the material cannot withstand tensile stress and thus no tension can occur, the center of moments (Fig. 5.2.55) is taken at the center of stress. For a rectangular section, P acts at distance k from the nearest edge. Length under compression = $3k$, and $S_M = \frac{2}{3}P/(hk)$. For a circular section, $S_M = [0.372 + 0.056(k/r)]P/k\sqrt{rk}$, where $r =$ radius and $k =$ distance of P from circumference. For a circular ring, $S =$ average compressive stress on cross section produced by P ; $e =$ eccentricity of P ; $z =$ length of diameter under compression (Fig. 5.2.56). Values of z/r and of the ratio of S_{max} to average S are given in Tables 5.2.14 and 5.2.15.

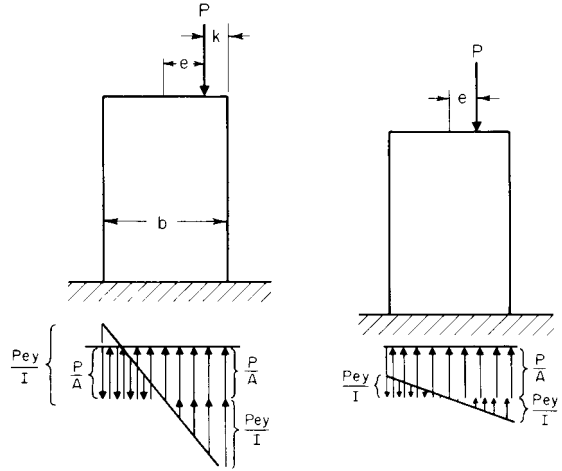


Fig. 5.2.54

CHIMNEY PROBLEM. Weight of chimney = 563,000 lb; $e = 1.56$ ft; OD of chimney = 10 ft 8 in; ID = 6 ft 6 1/2 in. Overturning moment = $Pe = 878,000$ ft · lb, $r_1/r = 0.6$, $e/r = 0.29$. This gives $z/r > 2$. Therefore, the entire area of the base is under compression. Area under compression = 55.8 ft²; $I = 546$; $S = 563,000/55.8 \pm (878,000 \times 5.33)/546 = 18,700$ (max) and 1,500 (min) lb compression per ft². From Table 5.2.15, by interpolation, $S_{max}/S_{av} = 1.85$. $\therefore S_{max} = (563,000/55.8) \times 1.85 = 18,685$ lb/ft² (91,313 kgf/m²).

The kern is the area around the center of gravity of a cross section within which any load applied will produce stress of only one sign throughout the entire cross section. Outside the kern, a load produces stresses of different sign. Figure 5.2.57 shows kerns (shaded) for various sections.

For a circular ring, the radius of the kern $r = D[1 + (d/D)^2]/8$.

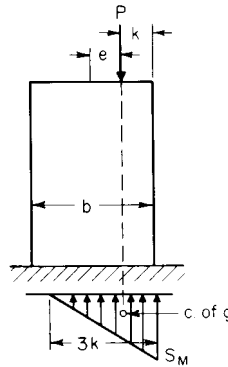


Fig. 5.2.55

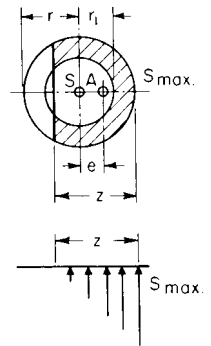


Fig. 5.2.56

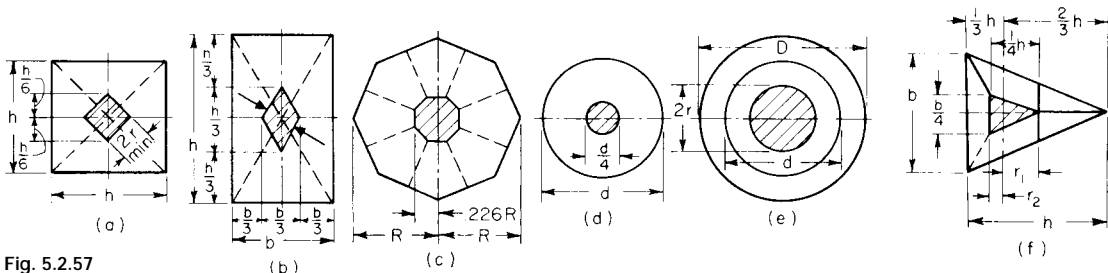


Fig. 5.2.57

Table 5.2.14 Values of the Ratio z/r (Fig. 5.2.56)

$\frac{e}{r}$	$\frac{r_1}{r}$							$\frac{e}{r}$
	0.0	0.5	0.6	0.7	0.8	0.9	1.0	
0.25	2.00							0.25
0.30	1.82							0.30
0.35	1.66	1.89	1.98					0.35
0.40	1.51	1.75	1.84	1.93				0.40
0.45	1.37	1.61	1.71	1.81	1.90			0.45
0.50	1.23	1.46	1.56	1.66	1.78	1.89	2.00	0.50
0.55	1.10	1.29	1.39	1.50	1.62	1.74	1.87	0.55
0.60	0.97	1.12	1.21	1.32	1.45	1.58	1.71	0.60
0.65	0.84	0.94	1.02	1.13	1.25	1.40	1.54	0.65
0.70	0.72	0.75	0.82	0.93	1.05	1.20	1.35	0.70
0.75	0.59	0.60	0.64	0.72	0.85	0.99	1.15	0.75
0.80	0.47	0.47	0.48	0.52	0.61	0.77	0.94	0.80
0.85	0.35	0.35	0.35	0.36	0.42	0.55	0.72	0.85
0.90	0.24	0.24	0.24	0.24	0.24	0.32	0.49	0.90
0.95	0.12	0.12	0.12	0.12	0.12	0.12	0.25	0.95

Table 5.2.15 Values of the Ratio S_{max}/S_{avg}
(In determining S average, use load P divided by total area of cross section)

$\frac{e}{r}$	$\frac{r_1}{r}$							$\frac{e}{r}$
	0.0	0.5	0.6	0.7	0.8	0.9	1.0	
0.00	1.00	1.00	1.00	1.00	1.00	1.00	1.00	0.00
0.05	1.20	1.16	1.15	1.13	1.12	1.11	1.10	0.05
0.10	1.40	1.32	1.29	1.27	1.24	1.22	1.20	0.10
0.15	1.60	1.48	1.44	1.40	1.37	1.33	1.30	0.15
0.20	1.80	1.64	1.59	1.54	1.49	1.44	1.40	0.20
0.25	2.00	1.80	1.73	1.67	1.61	1.55	1.50	0.25
0.30	2.23	1.96	1.88	1.81	1.73	1.66	1.60	0.30
0.35	2.48	2.12	2.04	1.94	1.85	1.77	1.70	0.35
0.40	2.76	2.29	2.20	2.07	1.98	1.88	1.80	0.40
0.45	3.11	2.51	2.39	2.23	2.10	1.99	1.90	0.45
0.50	3.55	2.80	2.61	2.42	2.26	2.10	2.00	0.50
0.55	4.15	3.14	2.89	2.67	2.42	2.26	2.17	0.55
0.60	4.96	3.58	3.24	2.92	2.64	2.42	2.26	0.60
0.65	6.00	4.34	3.80	3.30	2.92	2.64	2.42	0.65
0.70	7.48	5.40	4.65	3.86	3.33	2.95	2.64	0.70
0.75	9.93	7.26	5.97	4.81	3.93	3.33	2.89	0.75
0.80	13.87	10.05	8.80	6.53	4.93	3.96	3.27	0.80
0.85	21.08	15.55	13.32	10.43	7.16	4.50	3.77	0.85
0.90	38.25	30.80	25.80	19.85	14.60	7.13	4.71	0.90
0.95	96.10	72.20	62.20	50.20	34.60	19.80	6.72	0.95
1.00	∞	∞	∞	∞	∞	∞	∞	1.00

For a hollow square (H and h = lengths of outer and inner sides), the kern is a square similar to Fig. 5.2.57a, where

$$r_{min} = \frac{H}{6} \frac{1}{\sqrt{2}} \left[1 + \left(\frac{h}{H} \right)^2 \right] = 0.1179H \left[1 + \left(\frac{h}{H} \right)^2 \right]$$

For a hollow octagon R_o and R_i = radii of circles circumscribing the outer and inner sides; thickness of wall = $0.9239(R_o - R_i)$, the kern is an octagon similar to Fig. 5.2.57c, where $0.2256R$ becomes $0.2256R_o[1 + (R_i/R_o)^2]$.

CURVED BEAMS

The application of the flexure formula for a straight beam to the case of a curved beam results in error. When all "fibers" of a member have the same center of curvature, the **concentric** or common type of curved beam exists (see Fig. 5.2.58). Such a beam is defined by the Winkler-Bach theory. The stress at a point y units from the centroidal axis is

$$S = \frac{M}{AR} \left[1 + \frac{y}{Z(R + y)} \right]$$

M is the bending moment, positive when it increases curvature; Y is positive when measured toward the convex side; A is the cross-sectional area; R is the radius of the centroidal axis; Z is a cross-section property defined by

$$Z = -\frac{1}{A} \int \frac{y}{R+y} dA$$

Analytical expressions for Z of certain sections are given in Table 5.2.16. Also Z can be found by graphical integration methods (see any advanced

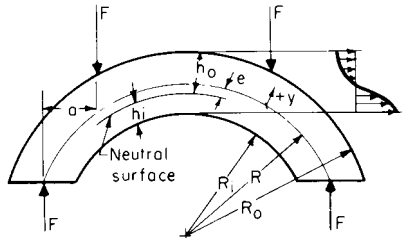


Fig. 5.2.58

strength book). The **neutral surface** shifts toward the center of curvature, or inside fiber, an amount equal to $e = ZR/(Z + 1)$. The Winkler-Bach theory, though practically satisfactory, disregards radial stresses as well as lateral deformations and assumes pure bending. The **maximum stress** occurring on the inside fiber is $S = Mh_i/(AeR_i)$, while that on the outside fiber is $S = Mh_o/(AeR_o)$.

EXAMPLE. A split steel ring of rectangular cross section is subjected to a diametral force of 1,000 lb as shown in Fig. 5.2.59a. Compute the stress at the point 0.5 in from the outside fiber on plane mm . Also compute the maximum stress.

$$Z = -1 + \frac{R}{h} \ln \frac{R+C}{R-C}$$

$$= -1 + \frac{10}{4} \ln \frac{10+2}{10-2} = 0.0133$$

$$S_{1.5} = \frac{M}{AR} \left[1 + \frac{y}{Z(R+y)} \right] + \frac{F}{A}$$

$$= \frac{-1,000 \times 10}{8 \times 10} \left[1 + \frac{1.5}{0.0133(10+1.5)} \right] + \frac{1,000}{8}$$

$$= -1,250 + 125 = -1,125 \text{ lb/in}^2 \text{ (compr.) (79 kgf/cm}^2\text{)}$$

$$S_M = \frac{-1,000}{8} \left[1 + \frac{-2}{0.0133(10-2)} \right] + \frac{1,000}{8}$$

$$= 2,230 + 125 = 2,355 \text{ lb/in}^2 \text{ (166 kgf/cm}^2\text{)}$$

or
$$e = \frac{ZR}{Z+1} = \frac{0.0133 \times 10}{0.0133 + 1} = 0.131$$

and
$$S_M = \frac{Mh_i}{AeR_i} + \frac{F}{A} = \frac{1,000 \times 10 \times 1.87}{8 \times 0.131 \times 8} + \frac{1,000}{8}$$

$$= 2,355 \text{ lb/in}^2 \text{ (166 kgf/cm}^2\text{)}$$

The **deflection** in curved beams can be computed by means of the moment-area theory. If the origin of axes is taken at the point whose deflection is wanted, it can be shown that the component displacements in the x and y directions are

$$\Delta_x = \int_0^s \frac{My ds}{EI} \quad \text{and} \quad \Delta_y = \int_0^s \frac{Mx ds}{EI}$$

The resultant deflection is then equal to $\Delta_0 = \sqrt{\Delta_x^2 + \Delta_y^2}$ in the direction defined by $\tan \theta = \Delta_y/\Delta_x$. Deflections can also be found conveniently by use of **Castigliano's theorem**. It states that in an elastic system the displacement in the direction of a force (or couple) and due to that force (or couple) is the partial derivative of the strain energy with respect to the force (or couple). Stated mathematically, $\Delta_z = \partial U/\partial F_z$. If a force does not exist at the point and/or in the direction desired, a dummy force

may be applied. This force must then be eliminated by equating it to zero at the end.

EXAMPLE. A quadrant of radius R is fixed at one end as shown in Fig. 5.2.59b. The force F is applied in the radial direction at the free end B . Find the deflection of B .

By moment area:

$$y = R \sin \theta \quad x = R(1 - \cos \theta)$$

$$ds = R d\theta \quad M = FR \sin \theta$$

$${}_B \Delta_x = \frac{FR^3}{EI} \int_0^{\pi/2} \sin^2 \theta d\theta = \frac{\pi FR^3}{4EI}$$

$${}_B \Delta_y = \frac{FR^3}{EI} \int_0^{\pi/2} \sin \theta (1 - \cos \theta) d\theta = -\frac{FR^3}{2EI}$$

and

$$\Delta_B = \frac{FR^3}{2EI} \sqrt{1 + \frac{\pi^2}{4}}$$

at
$$\theta_x = \tan^{-1} \left(-\frac{FR^3}{2EI} \times \frac{4EI}{\pi FR^3} \right) = \tan^{-1} \frac{2}{\pi} = 32.5^\circ$$

By Castigliano:

$${}_B \Delta_x = \frac{\partial U}{\partial F} = \frac{\partial}{\partial F_x} \int_0^{\pi/2} \frac{F^2 R^3}{2EI} \sin^2 \theta d\theta = \frac{\pi FR^3}{4EI}$$

$${}_B \Delta_y = \frac{\partial U}{\partial F_y} = \frac{\partial}{\partial F_y} \int_0^{\pi/2} \frac{[FR \sin \theta - F_y R (1 - \cos \theta)]^2 R d\theta}{2EI}$$

$$= -\frac{FR^3}{2EI}$$

The F_y , assumed downward, is equated to zero, after the integration and differentiation are performed to find ${}_B \Delta_y$. The remainder of the computation is exactly as in the moment-area method.

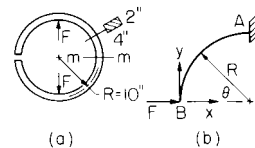


Fig. 5.2.59

Eccentrically Curved Beams These beams (Fig. 5.2.60) are bounded by arcs having different centers of curvature. In addition, it is possible for either radius to be the larger one. The one in which the section depth shortens as the central section is approached may be called the **arch beam**. When the central section is the largest, the beam is of the **crescent type**. **Crescent I** denotes the beam of larger outside radius and **crescent II** of larger inside radius. The stress at the **central section** of such beams may be found from $S = KMC/I$. In the case of rectangular cross section, the equation becomes $S = 6KM/(bh^2)$ where M is the bending moment, b is the width of the beam section, and h its height. The **stress factors K for the inner boundary**, established from photoelastic data, are given in Table 5.2.17. The outside radius is denoted by R_o and the inside by R_i . The geometry of crescent beams is such that the stress can be larger in **off-center sections**. The stress at the central section determined above must then be multiplied by the **position factor k** , given in Table 5.2.18. As in the concentric beam, the **neutral surface** shifts slightly toward the inner boundary (see Vidosic, Curved Beams with Eccentric Boundaries, *Trans. ASME*, 79, pp., 1317–1321).

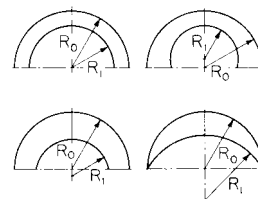


Fig. 5.2.60

Table 5.2.16 Analytical Expressions for Z

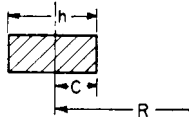
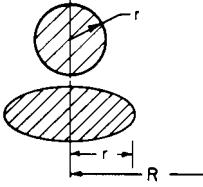
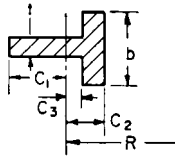
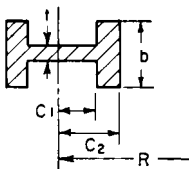
Section	Expression
	$Z = -1 + \frac{R}{h} \ln \frac{R+C}{R-C}$
	$Z = -1 + 2 \left(\frac{R}{r} \right) \left[\frac{R}{r} - \sqrt{\left(\frac{R}{r} \right)^2 - 1} \right]$
	$Z = -1 + \frac{R}{A} \left[t \ln(R + C_1) + (b - t) \ln(R - C_3) - b \ln(R - C_3) \right]$ $A = tC_1 - (b - t)C_3 + bC_2$
	$Z = -1 + \frac{R}{A} \left[b \ln \frac{R + C_2}{R - C_2} + (t - b) \ln \frac{R + C_1}{R - C_1} \right]$ $A = 2[(t - b)C_1 + bC_2]$

Table 5.2.17 Stress Factors for Inner Boundary at Central Section (See Fig. 5.2.60)

- For the arch-type beams
 - $K = 0.834 + 1.504 \frac{h}{R_o + R_i}$ if $\frac{R_o + R_i}{h} < 5$.
 - $K = 0.899 + 1.181 \frac{h}{R_o + R_i}$ if $5 < \frac{R_o + R_i}{h} < 10$.
 - In the case of larger section ratios use the equivalent beam solution.
- For the crescent I-type beams
 - $K = 0.570 + 1.536 \frac{h}{R_o + R_i}$ if $\frac{R_o + R_i}{h} < 2$.
 - $K = 0.959 + 0.769 \frac{h}{R_o + R_i}$ if $2 < \frac{R_o + R_i}{h} < 20$.
 - $K = 1.092 \left(\frac{h}{R_o + R_i} \right)^{0.0298}$ if $\frac{R_o + R_i}{h} > 20$.
- For the crescent II-type beams
 - $K = 0.897 + 1.098 \frac{h}{R_o + R_i}$ if $\frac{R_o + R_i}{h} < 8$.
 - $K = 1.119 \left(\frac{h}{R_o + R_i} \right)^{0.0378}$ if $8 < \frac{R_o + R_i}{h} < 20$.
 - $K = 1.081 \left(\frac{h}{R_o + R_i} \right)^{0.0270}$ if $\frac{R_o + R_i}{h} > 20$.

Table 5.2.18 Crescent-Beam Position Stress Factors (See Fig. 5.2.60)

Angle θ , deg	k	
	Inner	Outer
10	$1 + 0.055H/h$	$1 + 0.03H/h$
20	$1 + 0.164H/h$	$1 + 0.10H/h$
30	$1 + 0.365H/h$	$1 + 0.25H/h$
40	$1 + 0.567H/h$	$1 + 0.467H/h$
50	$1.521 - \frac{(0.5171 - 1.382H/h)^{1/2}}{1.382}$	$1 + 0.733H/h$
60	$1.756 - \frac{(0.2416 - 0.6506H/h)^{1/2}}{0.6506}$	$1 + 1.123H/h$
70	$2.070 - \frac{(0.4817 - 1.298H/h)^{1/2}}{0.6492}$	$1 + 1.70H/h$
80	$2.531 - \frac{(0.2939 - 0.7084H/h)^{1/2}}{0.3542}$	$1 + 2.383H/h$
90		$1 + 3.933H/h$

NOTE: All formulas are valid for $0 < H/h \leq 0.325$. Formulas for the inner boundary, except for 40 deg, may be used to $H/h \leq 0.36$. H = distance between centers.

IMPACT

A force or stress is considered **suddenly applied** when the duration of load application is less than one-half the **fundamental natural period** of vibration of the member upon which the force acts. Under impact, a

compression wave propagates through the member at a velocity $c = \sqrt{E/\rho}$, where ρ is the mass density. As this compression wave travels back and forth by reflection from one end of the bar to the other, a maximum stress is produced which is many times larger than what it would be statically. An exact determination of this stress is most difficult. However, if conservation of kinetic and strain energies is applied, the **impact stress** is found to be

$$S' = S \sqrt{\frac{W}{W_b} \left(\frac{3W}{3W + W_b} \right)}$$

The weight of the striking mass is here denoted by W , that of the struck bar by W_b , while S is the static stress, W/A (A is the cross-sectional area of the bar). Above is the case of **sudden impact**. When the ratio W/W_b is small, the stress computed by the above equation may be erroneous. A better solution of this problem may result from

$$S' = S + S \sqrt{\frac{W}{W_b} + \frac{2}{3}}$$

If a weight W falls a distance h before striking a bar of mass W_b , energy conservation will yield the relation

$$S' = S \left(1 + \sqrt{1 + \frac{2h}{e} \times \frac{3W}{3W + W_b}} \right)$$

The elongation $e = \epsilon l = SI/E$. When the striking mass W is assumed rigid, the elasticity factor is taken equal to 1. Thus the equation becomes

$$S' = S (1 + \sqrt{1 + 2h/e})$$

If, in addition, h is taken equal to zero (**sudden impact**), the radical equals 1, and so the stress becomes $S' = 2S$. Since Hooke's law is applicable, the relations

$$e' = e (1 + \sqrt{1 + 2h/e}) \quad \text{and} \quad e' = 2e$$

are also true for the same conditions.

The expression may be converted, by using $v^2 = 2gh$, to

$$S' = S [1 + \sqrt{1 + v^2/(eg)}]$$

This might be called the **energy impact** form. If the **natural frequency** f_n of the bar is used, the stress equation is

$$S' = S (1 + \sqrt{1 + 0.204hf_n^2})$$

In general, the **maximum impact stress** in a **beam** and a **shaft** can be approximated from the simplified falling-weight equation. It is necessary, though, to substitute the maximum **deflection** y for e , in the case of beams, and for the **angle of twist** θ in the case of shafts. Of course $S = Mc/I$ and $M, c/J$, respectively. Thus

$$S' = S \left[1 + \sqrt{1 + \frac{2h}{y \text{ (or } \theta)}} \right]$$

For a more exact solution, elastic yield in each member must be considered. The theory then yields

$$S' = S \left[1 + \sqrt{1 + \frac{2h}{y} \left(\frac{35W}{35W + 17W_b} \right)} \right]$$

for a **simply supported beam** struck in the middle by a weight W .

THEORY OF ELASTICITY

Loaded members in which the stress distribution cannot be estimated fail of solution by elementary strength-of-material methods. To such cases, the more advanced mathematical principles of the **theory of elasticity** must be applied. When this is not possible, experimental stress analysis has to be used. Because of the complexity of solution, only some of the more practical problems have been solved by the theory of elasticity. The more general concepts and methods are presented.

Two kinds of forces may act on a body. **Surface forces** are distributed over the surface as the result of, for instance, the pressure of one body

on another. Forces due to gravity, inertia, magnetism, etc., which act over the entire volume of a body, are called **body forces**. Both surface and body forces can be best handled if resolved into three orthogonal components. Surface forces are thus designated \bar{X} , \bar{Y} , and \bar{Z} , while body forces are labeled X , Y , and Z .

In general, there exists a normal stress σ and a shearing stress τ at each point of a loaded member. It is convenient to deal with components of each of these stresses on each of six orthogonal planes that bound the point element. Thus there are at each point **six stress components**, $\sigma_x, \sigma_y, \sigma_z, \tau_{yx} = \tau_{xy}, \tau_{zx} = \tau_{xz}$, and $\tau_{zy} = \tau_{yz}$. Similarly, if the normal unit strain is designated by the letter ϵ and shearing unit strain by γ , the **six components of strain** are defined by

$$\begin{aligned} \epsilon_x &= \partial u/\partial x & \epsilon_y &= \partial v/\partial y & \epsilon_z &= \partial w/\partial z \\ \gamma_{xy} &= \partial u/\partial y + \partial v/\partial x & \gamma_{yz} &= \partial v/\partial z + \partial w/\partial y \\ \text{and} & & \gamma_{xz} &= \partial u/\partial z + \partial w/\partial x \end{aligned}$$

The elastic **displacements** of particles on the body in the x , y , and z directions are identified as the u , v , and w **components**, respectively.

Since metals have the usually assumed elastic as well as isotropic properties, Hooke's law holds. Therefore, the interrelationships between stress and strain can easily be obtained.

$$\epsilon_x = \frac{1}{E} [\sigma_x - \mu(\sigma_y + \sigma_z)]$$

$$\epsilon_y = \frac{1}{E} [\sigma_y - \mu(\sigma_x + \sigma_z)]$$

$$\epsilon_z = \frac{1}{E} [\sigma_z - \mu(\sigma_x + \sigma_y)]$$

$$\text{and} \quad \begin{aligned} \gamma_{xy} &= \tau_{xy}/G & \gamma_{xz} &= \tau_{xz}/G \\ \gamma_{yz} &= \tau_{yz}/G \end{aligned}$$

The general case of strain can be obtained by superposing the elongation strains upon the shearing strains.

Problems depending upon theories of elasticity are considerably simplified if the stresses are all parallel to one plane or if all deformations occur in planes perpendicular to the length of the member. The first case is one of **plane stress**, as when a thin plate of uniform thickness is subjected to central, boundary forces parallel to the plane of the plate. The second is a case of **plane strain**, such as a gate subjected to hydrostatic pressure, the intensity of which does not vary along the gate's length. All particles therefore displace at right angles to the length, and so cross sections remain plane. In plane-stress problems, three of the six stress components vanish, thus leaving only σ_x, σ_y , and τ_{xy} . Similarly, in plane strain, only ϵ_x, ϵ_y , and γ_{xy} will not equal zero; thus the same three stresses σ_x, σ_y , and τ_{xy} remain to be considered. Plane problems can thus be represented by the element shown in Fig. 5.2.61. Equilibrium considerations applied to this particle result in the **differential equations of equilibrium** which reduce to

$$\frac{\partial \sigma_x}{\partial x} + \frac{\partial \tau_{xy}}{\partial y} + X = 0$$

$$\text{and} \quad \frac{\partial \sigma_y}{\partial y} + \frac{\partial \tau_{xy}}{\partial x} + Y = 0$$

Since the two differential equations of equilibrium are insufficient to find the three stresses, a third equation must be used. This is the **compatibility equation** relating the three strain components. It is

$$\frac{\partial^2 \epsilon_x}{\partial y^2} + \frac{\partial^2 \epsilon_y}{\partial x^2} = \frac{\partial^2 \gamma_{xy}}{\partial x \partial y}$$

If strains are expressed in terms of the stresses, the compatibility equation becomes

$$\left(\frac{\partial^2}{\partial x^2} + \frac{\partial^2}{\partial y^2} \right) (\sigma_x + \sigma_y) = 0$$

Now, in any **two-dimensional** problem, the compatibility equation along with the differential equilibrium equations must be simultaneously

solved for the three unknown stresses. This is accomplished using **stress functions**, which permit the integration and satisfy boundary conditions in each particular situation.

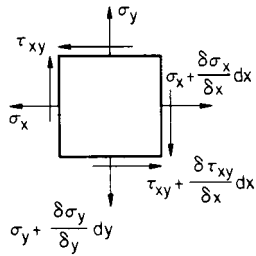


Fig. 5.2.61

In **three-dimensional** problems, the third dimension must be considered. This results in three differential equations of equilibrium, as well as three compatibility equations. The six stress components can thus be found. The complexity involved in the solution of these equations is such, however, that only a few special cases have been solved.

In certain problems, such as rotating circular disks, **polar coordinates** become more convenient. In such cases, the stress components in a two-dimensional field are the **radial stress** σ_r , the **tangential stress** σ_θ , and the **shearing stress** $\tau_{r\theta}$. In terms of these stresses the **polar differential equations** become

$$\frac{\partial \sigma_r}{\partial r} + \frac{1}{r} \frac{\partial \tau_{r\theta}}{\partial \theta} + \frac{\sigma_r - \sigma_\theta}{r} + R = 0$$

and
$$\frac{1}{r} \frac{\partial \sigma_\theta}{\partial \theta} + \frac{\partial \tau_{r\theta}}{\partial r} + \frac{2\tau_{r\theta}}{r} = 0$$

The body force per unit volume is represented by R . The **compatibility equation** in polar coordinates is

$$\left(\frac{\partial^2}{\partial r^2} + \frac{1}{r} \frac{\partial}{\partial r} + \frac{1}{r^2} \frac{\partial^2}{\partial \theta^2} \right) \left(\frac{\partial^2 \phi}{\partial r^2} + \frac{1}{r} \frac{\partial \phi}{\partial r} + \frac{1}{r^2} \frac{\partial^2 \phi}{\partial \theta^2} \right) = 0$$

ϕ is again a stress function of r and θ that will provide a solution of the differential equations and satisfy boundary conditions. As an example, the exact solution of a **simply supported beam** carrying a uniformly distributed load w yields

$$\sigma_x = \frac{w}{2I} (l^2 - x^2) y + \frac{w}{2I} \left(\frac{2y^3}{3} - \frac{2c^2 y}{5} \right)$$

The origin of coordinates is at the center of the beam, $2c$ is the beam depth, and $2l$ is the span length. Thus the maximum stress at $x = 0$ and $y = c$ is $\sigma_x = \frac{wl^2c}{2I} + \frac{2}{15} \frac{wc^3}{I}$. The first term represents the stress as obtained by the elementary flexure theory; the second is a correction. The second term becomes negligible when c is small compared to l .

The important case of a **flat plate** of unit width with a **circular hole** of diameter $2a$ at its center, subjected to a uniform tensile load, has been solved using polar coordinates. If S is the uniform stress at some distance from the hole, r is measured from the center of the hole, and θ is the angle of r with respect to the longitudinal axis of the member, the stresses are

$$\begin{aligned} \sigma_r &= \frac{S}{2} \left(1 - \frac{a^2}{r^2} \right) + \frac{S}{2} \left(1 + \frac{3a^4}{r^4} - \frac{4a^2}{r^2} \right) \cos 2\theta \\ \sigma_\theta &= \frac{S}{2} \left(1 + \frac{a^2}{r^2} \right) - \frac{S}{2} \left(1 + \frac{3a^4}{r^4} \right) \cos 2\theta \\ \tau_{r\theta} &= -\frac{S}{2} \left(1 - \frac{3a^4}{r^4} + \frac{2a^2}{r^2} \right) \sin 2\theta \end{aligned}$$

CYLINDERS AND SPHERES

A **thin-wall cylinder** has a wall thickness such that the assumption of constant stress across the wall results in negligible error. Cylinders having internal-diameter-to-thickness (D/t) ratios greater than 10 are usually considered thin-walled. Boilers, drums, tanks, and pipes are often treated as such. Equilibrium equations reveal the circumferential, or hoop, stress to be $S = pr/t$ under an internal pressure p (see Fig. 5.2.62). If the cylinder is closed at the ends, a longitudinal stress of $pr/(2t)$ is developed. The tensile stress developed in a thin hollow sphere subjected to internal pressure is also $pr/(2t)$.

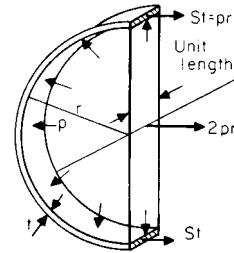


Fig. 5.2.62

When thin-walled cylinders, such as vacuum tanks and submarines, are subjected to **external pressure**, **collapse** becomes the mode of failure. The shell is assumed perfectly round and of uniform thickness, the material obeys Hooke's law, the radial stress is negligible, and the normal stress distribution is linear. Other, lesser assumptions are also made. Using the theory of elasticity, R. G. Sturm (*Univ. Ill. Eng. Exp. Sm. Bull.*, no 12, Nov. 11, 1941) derived the **collapsing pressure** as

$$W_c = KE \left(\frac{t}{D} \right)^3 \text{ lb/in}^2$$

The factor K , a numerical coefficient, depends upon the L/R and D/t ratios (D is outside-shell diameter), the kind of end support, and whether pressure is applied radially only, or at the ends as well. Figures 5.2.63 to 5.2.66, reproduced from the bulletin, supply the K values. N on these charts indicates the number of lobes into which the shell collapses. These values are for materials having Poisson's ratio $\mu = 0.3$. It may also be pointed out that in the case of long cylinders (infinitely long, theoretically) the value of K approaches $2/(1 - \mu^2)$.

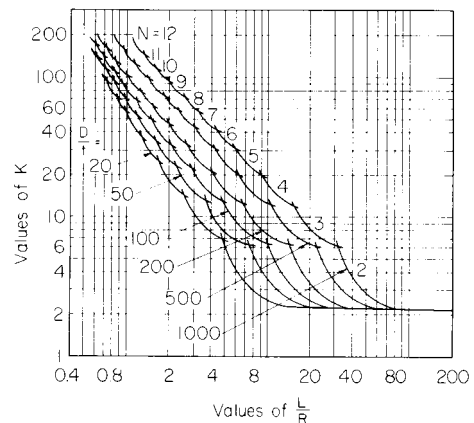


Fig. 5.2.63 Radial external pressure with simply supported edges.

When the **cylinder is stiffened with rings**, the shell may be assumed to be divided into a series of shorter shells, equal in length to the ring spacing. The previous equation can then be applied to a ring-to-ring length of cylinder. However, the flexural rigidity of the combined

stiffener and shell EI_c necessary to withstand the pressure is $EI_c = W_s D^3 L_s / 24$. W_s is the pressure, L_s the length between rings, and I_c the combined moment of inertia of the ring and that portion of the shell assumed acting with the ring.

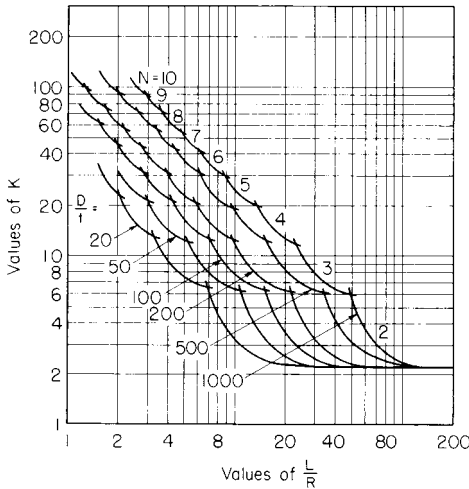


Fig. 5.2.64 Radial external pressure with fixed edges.

In some instances, cylinders collapse only after a stress in excess of the elastic limit has been reached; that is, **plastic range** stresses are present. In such cases the same equation applies, but the modulus of elasticity must be modified.

When the average stress S_a is less than the proportional limit S_p , and the maximum stress (direct, plus bending) is S , the modified modulus

$$E' = E \left[1 - \frac{1}{4} \left(\frac{S - S_f}{S_u - S_a} \right)^2 \right]$$

S_u is the modulus of rupture. When the average stress is larger than the proportional limit, the modified modulus is taken as the tangent at the average stress.

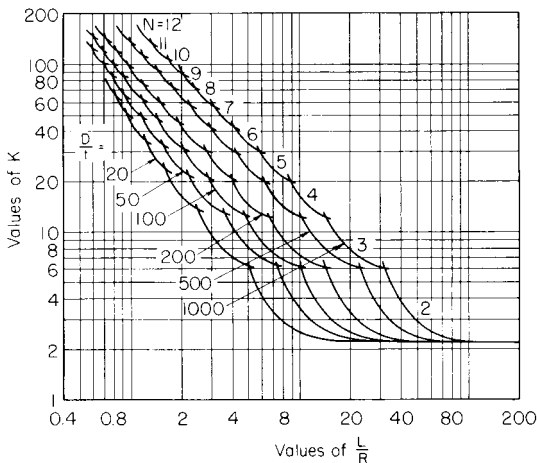


Fig. 5.2.65 Radial and end external pressure with simply supported edges.

In **thick-walled cylinders** (Fig. 5.2.67a) the circumferential, hoop, or tangential stress S_t is not uniform. In addition a radial stress S_r is present. When equilibrium is applied to the annulus taken out of Fig. 5.2.67a and

shown in Fig. 5.2.67b and the equation is integrated, the general tangential and radial stress relations, called the **Lamé** equations, are derived.

$$S_t = \frac{r_1^2 p_1 - r_2^2 p_2 + (p_1 - p_2) r_1^2 r_2^2 / r^2}{r_2^2 - r_1^2}$$

and

$$S_r = \frac{r_1^2 p_1 - r_2^2 p_2 - (p_1 - p_2) r_1^2 r_2^2 / r^2}{r_2^2 - r_1^2}$$

When the external pressure $p_2 = 0$, the equations reduce to

$$S_t = \frac{r_1^2 p_1}{r_2^2 - r_1^2} \left(1 + \frac{r_2^2}{r^2} \right)$$

and

$$S_r = \frac{r_1^2 p_1}{r_2^2 - r_1^2} \left(1 - \frac{r_2^2}{r^2} \right)$$

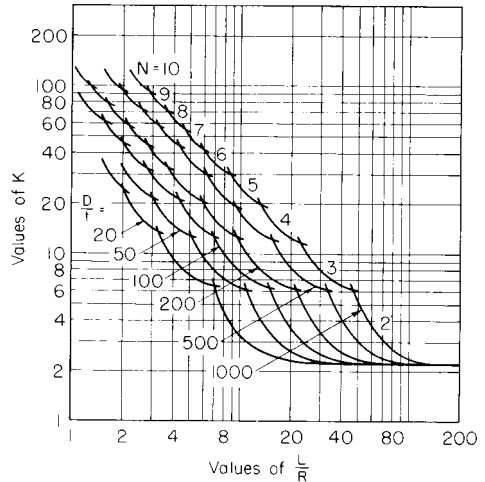


Fig. 5.2.66 Radial and end external pressure with fixed edges.

At the inner boundary the tangential elongation ϵ_t is equal to

$$\epsilon_t = (S_t - \mu S_r) / E$$

The increase in the bore radius Δr_1 resulting therefrom is

$$\Delta r_1 = \frac{r_1 p_1}{E_h} \left(\frac{1 + r_1^2 / r_2^2}{1 - r_1^2 / r_2^2} + \mu \right)$$

Similarly a solid shaft of r radius under external pressure p_2 will have its radius decreased by the amount

$$\Delta r = - \frac{r p_2}{E_s} (1 - \mu)$$

In the case of a **press or shrink fit**, $p_1 = p_2 = p$. The sum of Δr_1 and Δr_2 absolute is the radial interference; twice this sum is the **diametral interference** Δ or

$$\Delta = 2 r_1 p \left[\frac{1}{E_h} \left(\frac{1 + r_1^2 / r_2^2}{1 - r_1^2 / r_2^2} + \mu \right) + \frac{1 - \mu}{E_s} \right]$$

If the hub and shaft materials are the same, $E_h = E_s = E$, and

$$\Delta = \frac{4 r_1 r_2^2 p}{E (r_2^2 - r_1^2)}$$

If the equation is solved for p and this value is substituted in Lamé's equation, the maximum tangential stress on the inner surface of the hub is found to be

$$S_t = \frac{E \Delta}{4 r_1 r_2^2} (r_2^2 + r_1^2)$$

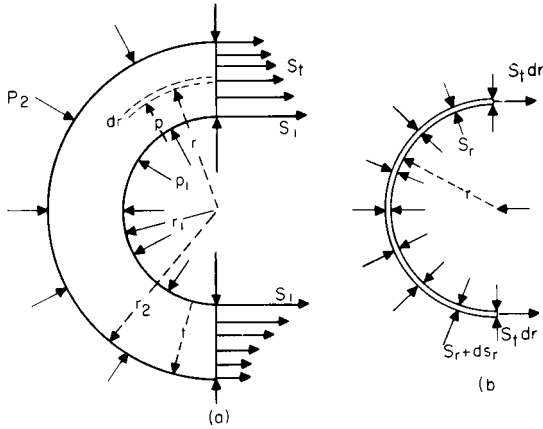


Fig. 5.2.67

EXAMPLE. The barrel of a field gun has an outside diameter of 9 in and a bore of 4.7 in. An internal pressure of 16,000 lb/in² is developed during firing. What maximum stress occurs in the barrel? An investigation of Lamé's equations for internal pressure reveals the maximum stress to be the tangential one on the inner surface. Thus,

$$S_t = p_1 \frac{r_2^2 + r_1^2}{r_2^2 - r_1^2} = \frac{16,000 (2.35^2 + 4.5^2)}{4.5^2 - 2.35^2} = 28,000 \text{ lb/in}^2 (1,972 \text{ kgf/cm}^2)$$

Oval Hollow Cylinders In Fig. 5.2.68, let a and b be the semiminor and semimajor axes. The bending moments at A and C will then be

$$M_0 = pa^2/2 - pI_x/(2S) - pI_y/(2S) \\ M_1 = M_0 - p(a^2 - b^2)/2$$

where I_x and I_y are the moments of inertia of the arc AC about the x and y axes, respectively. The bending moment at any point will be

$$M = M_0 - pa^2/2 + px^2/2 + py^2/2$$

Thick Hollow Spheres With an internal pressure p , where $p < T/0.65$.

$$r_2 = r_1 [(T + 0.4p)/(T - 0.65p)]^{1/3}$$

The maximum tensile stress is on the inner surface, in the direction of the circumference. With an external pressure p , where $p < T/1.05$,

$$r_2 = r_1 [T/(T - 1.05p)]^{1/3}$$

In both cases T is the true stress.

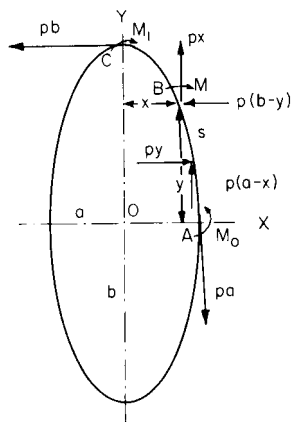


Fig. 5.2.68

PRESSURE BETWEEN BODIES WITH CURVED SURFACES

(See Hertz, "Gesammelte Werke," vol. 1, pp. 159 et seq., Barth.)

Two Spheres The radius A of the compressed area is obtained from the formula $A^3 = 0.68P(c_1 + c_2)/(1/r_1 + 1/r_2)$, in which P is the compressing force, c_1 and c_2 ($= 1/E_1$ and $1/E_2$) are reciprocals of the respective moduli of elasticity, and r_1 and r_2 are the radii. (Reciprocal of Poisson's ratio is assumed to be $n = 10/3$) The greatest contact pressure in the middle of the compressed surface will be $S_{max} = 1.5(P/\pi A^2)$, and

$$S_{max}^3 = 0.235P(1/r_1 + 1/r_2)^2/(c_1 + c_2)^2$$

The total deformation of the two spheres will be Y , which is obtained from

$$Y^3 = 0.46P^2(c_1 + c_2)^2/(r_1 + 1/r_2)$$

For $c_1 = c_2 = 1/E$, i.e., two spheres with the same modulus of elasticity, it follows that $A^3 = 1.36 P/E(1/r_1 + 1/r_2)$, $S_{max}^3 = 0.059PE^2/(1/r_1 + 1/r_2)^2$, and $Y^3 = 1.84P^2(1/r_1 + 1/r_2)/E^2$. If the radii of these spheres are also equal, $A^3 = 0.68Pr/E = 0.34Pd/E$; $S_{max}^3 = 0.235PE^2/r^2 = 0.94PE^2/d^2$; and $Y^3 = 3.68P^2/(E^2r) = 7.36P^2/(E^2d)$.

Sphere and Flat Plate In this case $r_1 = r$ and $r_2 = \infty$, and the above formulas become $A^3 = 0.68Pr(c_1 + c_2) = 1.36Pr/E$, and

$$S_{max}^3 = 0.235P/[r^2(c_1 + c_2)^2] = 0.059PE^2/r^2 \\ Y^3 = 0.46P^2(c_1 + c_2)^2/r = 1.84P^2/(E^2r)$$

Two Cylinders The width b of the rectangular pressure surface is obtained from $(b/4)^2 = 0.29P/c_1 + c_2/l[(1/r_1) + (1/r_2)]$, where r_1 and r_2 are the radii, and l the length

$$S_{max}^2 = [4P/(\pi bl)]^2 = 0.35P(1/r_1 + 1/r_2)/l(c_1 + c_2)$$

For cylinders with the same moduli of elasticity, $c_1 = c_2 = 1/E$, and $(b/4)^2 = 0.58PE/l[(1/r_1) + (1/r_2)]$; and $S_{max}^2 = 0.175PE(1/r_1 + 1/r_2)/l$. When $r_1 = r_2 = r$, $(b/4)^2 = 0.29Pr/(El)$, and $S_{max}^2 = 0.35PE/(lr)$.

Cylinder and Flat Plate Here $r_1 = r$, $r_2 = \infty$, and the above formulas reduce to $(b/4)^2 = 0.29Pr(c_1 + c_2)/l = 0.58Pr/(El)$, and

$$S_{max}^2 = 0.35P/[lr(c_1 + c_2)] = 0.175PE/(lr)$$

For application to ball and roller bearings and to gear teeth, see Sec. 8.

FLAT PLATES

The analysis of flat plates subjected to lateral loads is very involved because plates bend in all vertical planes. Strict mathematical derivations have therefore been accomplished only in some special cases. Most of the available formulas contain some amount of rational empiricism. Plates may be classified as (1) **thick plates**, in which transverse shear is important; (2) **average-thickness plates**, in which flexure stress predominates; (3) **thin plates**, which depend in part upon direct tension; and (4) **membranes**, which are subject to direct tension only. However, exact lines of demarcation do not exist.

The flat-plate formulas given apply primarily to symmetrically loaded **average-thickness plates** of constant thickness. They are valid only if the maximum deflection is small relative to the plate thickness; usually, $y \leq 0.4t$. In the mathematical analyses, allowance for stress redistribution, because of slight local yielding, is usually not made. Since this yielding, especially in ductile materials, is beneficial, the formulas generally err on the side of safety. Certain cases of symmetrically loaded **circular and rectangular plates** are presented in Figs. 5.2.69 and 5.2.70. The maximum stresses are calculated from

$$S_M = k \frac{wR^2}{t^2} \quad S_M = k \frac{P}{t^2} \quad \text{or} \quad S_M = k \frac{C}{t^2}$$

The first equation is for a uniformly distributed load w , lb/in²; the second supports a concentrated load P , lb; and the third a couple C , per unit length, uniformly distributed along the edge. Combinations of these loadings may be treated by superposition. The factors k and k_1 are given

Table 5.2.19 Coefficients k and k_1 for Circular Plates ($\mu = 0.3$)

Case	k	k_1	R/r											
			1.25		1.5		2		3		4		5	
Case	k	k_1	k	k_1	k	k_1	k	k_1	k	k_1	k	k_1	k	k_1
1	1.24	0.696												
2	0.75	0.171												
3	6.0	4.2												
4	0.592	0.184	0.976	0.414	1.440	0.664	1.880	0.824	2.08	0.830	2.19	0.813		
5	0.105	0.0025	0.259	0.0129	0.481	0.057	0.654	0.130	0.708	0.163	0.730	0.176		
6	1.10	0.341	1.26	0.519	1.48	0.672	1.88	0.734	2.17	0.724	2.34	0.704		
7	0.195	0.0036	0.320	0.024	0.455	0.081	0.670	0.171	1.00	0.218	1.30	0.238		
8	0.660	0.202	1.19	0.491	2.04	0.902	3.34	1.220	4.30	1.300	5.10	1.310		
9	0.135	0.0023	0.410	0.0183	1.04	0.0938	2.15	0.293	2.99	0.448	3.69	0.564		
10	0.122	0.00343	0.336	0.0313	0.740	0.1250	1.21	0.291	1.45	0.417	1.59	0.492		
11	0.072	0.00068	0.1825	0.005	0.361	0.023	0.546	0.064	0.627	0.092	0.668	0.112		
12	6.865	0.2323	7.448	0.6613	8.136	1.493	8.71	2.555	8.930	3.105	9.036	3.418		
13	6.0	0.196	6.0	0.485	6.0	0.847	6.0	0.940	6.0	0.801	6.0	0.658		
14	0.115	0.00129	0.220	0.0064	0.405	0.0237	0.703	0.062	0.933	0.092	1.13	0.114		
15	0.090	0.00077	0.273	0.0062	0.710	0.0329	1.54	0.110	2.23	0.179	2.80	0.234		

in Tables 5.2.19 and 5.2.20; R is the radius of circular plates or one side of rectangular plates, and t is the plate thickness.

[In Figs. 5.2.69 and 5.2.70, $r = R$ for circular plates and $r =$ smaller side rectangular plates.]

The maximum deflection for the same cases is given by

$$y_M = k_1 \frac{wR^4}{Et^3} \quad y_M = k_1 \frac{PR^2}{Et^3} \quad \text{and} \quad y_M = k_1 \frac{CR^2}{Et^3}$$

The factors k_1 are also given in the tables. For additional information, including shells, refer to ASME Handbook, "Metals Engineering: Design," McGraw-Hill.

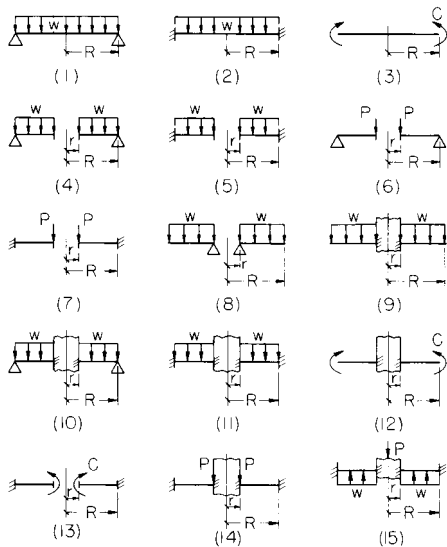


Fig. 5.2.69 Circular plates. Cases (4), (5), (6), (7), (8), and (13) have central hole of radius r ; cases (9), (10), (11), (12), (14), and (15) have a central piston of radius r to which the plate is fixed.

THEORIES OF FAILURE

Material properties are usually determined from tests in which specimens are subjected to **simple stresses** under static or fluctuating loads. The attempt to apply these data to **bi- or triaxial stress fields** has resulted

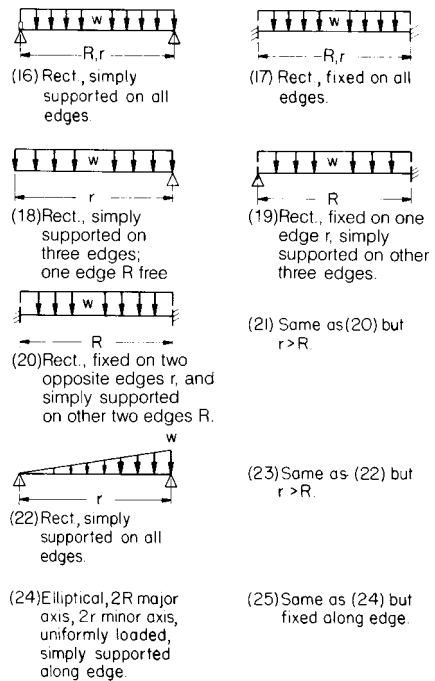


Fig. 5.2.70 Rectangular and elliptical plates. [R is the longer dimension except in cases (21) and (23).]

in the proposal of various theories of failure. Figure 5.2.71 shows the principal stresses on a triaxially stressed element. It is assumed, for simplicity, that $S_1 > S_2 > S_3$. Compressive stresses are negative.

1. **Maximum-stress theory** (Rankine) assumes failure occurs when the largest principal stress reaches the yield stress in a tension (or compression) specimen. That is, $S_1 = \pm S_y$.

2. **Maximum-shear theory** (Coulomb) assumes yielding (failure) occurs when the maximum shearing stress equals that in a simple tension (or compression) specimen at yield. Mathematically, $S_1 - S_3 = \pm S_y$.

3. **Maximum-strain-energy theory** (Beltrami) assumes failure occurs when the energy absorbed per unit volume equals the strain energy per

Table 5.2.20 Coefficients k and k_1 for Rectangular and Elliptical Plates ($\mu = 0.3$)

Case	R/r									
	1.0		1.5		2.0		3.0		4.0	
	k	k_1	k	k_1	k	k_1	k	k_1	k	k_1
16	0.287	0.0443	0.487	0.0843	0.610	0.1106	0.713	0.1336	0.741	0.1400
17	0.308	0.0138	0.454	0.0240	0.497	0.0277	0.500	0.028	0.500	0.028
18	0.672	0.140	0.768	0.160	0.792	0.165	0.798	0.166	0.800	0.166
19	0.500	0.030	0.670	0.070	0.730	0.101	0.750	0.132	0.750	0.139
20	0.418	0.0209	0.626	0.0582	0.715	0.0987	0.750	0.1276	0.750	
21*	0.418	0.0216	0.490	0.0270	0.497	0.0284	0.500	0.0284	0.500	0.0284
22	0.160	0.0221	0.260	0.0421	0.320	0.0553	0.370	0.0668	0.380	0.0700
23*	0.160	0.0220	0.260	0.0436	0.340	0.0592	0.430	0.0772	0.490	0.0908
24	1.24	0.70	1.92	1.26	2.26	1.58	2.60	1.88	2.78	2.02
25	0.75	0.171	1.34	0.304	1.63	0.379	1.84	0.419	1.90	0.431

* Length ratio is r/R in cases 21 and 23.

unit volume in a tension (or compression) specimen at yield. Mathematically, $S_1^2 + S_2^2 + S_3^2 - 2\mu(S_1S_2 + S_2S_3 + S_3S_1) = S_y^2$.

4. **Maximum-distortion-energy theory** (Huber, von Mises, Hencky) assumes yielding occurs when the distortion energy equals that in simple tension at yield. The distortion energy, that portion of the total energy which causes distortion rather than volume change, is

$$U_d = \frac{1 + \mu}{3E} (S_1^2 + S_2^2 + S_3^2 - S_1S_2 - S_2S_3 - S_3S_1)$$

Thus failure is defined by

$$S_1^2 + S_2^2 + S_3^2 - (S_1S_2 + S_2S_3 + S_3S_1) = S_y^2$$

5. **Maximum-strain theory** (Saint-Venant) claims failure occurs when the maximum strain equals the strain in simple tension at yield or $S_1 - \mu(S_2 + S_3) = S_y$.

6. **Internal-friction theory** (Mohr). When the ultimate strengths in tension and compression are the same, this theory reduces to that of maximum shear. For principal stresses of opposite sign, failure is defined by $S_1 - (S_{uc}/S_u) S_2 = -S_{uc}$; if the signs are the same $S_1 = S_u$ or $-S_{uc}$, where S_{uc} is the ultimate strength in compression. If the principal stresses are both either tension or compression, then the larger one, say S_1 , must equal S_u when S_1 is tension or S_{uc} when S_1 is compression.

A graphical representation of the first four theories applied to a biaxial stress field is presented in Fig. 5.2.72. Stresses outside the bounding lines in the case of each theory mean failure (yield or fracture). A comparison with experimental data proves the distortion-energy theory (4) best for ductile materials of equal tension-compression properties. When these properties are unequal, the internal friction theory (6) appears best. In practice, judging by some accepted codes, the maximum-

above holds for **fluctuating stresses**, provided that principal stresses at the maximum load are used and the **endurance strength** in simple bending is substituted for the yield strength.

EXAMPLE. A steel shaft, 4 in in diameter, is subjected to a bending moment of 120,000 in · lb, as well as a torque. If the yield strength in tension is 40,000 lb/in², what maximum torque can be applied under the (1) maximum-shear theory and (2) the distortion-energy theory?

$$S_x = \frac{M_c}{I} = \frac{120,000 \times 2}{12.55} = 19,100 \text{ lb/in}^2 \quad S_{xy} = \frac{TC}{J} = \frac{T \times 2}{25.1} = 0.0798T$$

and
$$S_{M,m} = \frac{S_x}{2} \pm \sqrt{\left(\frac{S_x}{2}\right)^2 + S_{xy}^2}$$

$$S_M - S_m = S_y \quad \text{or} \quad 2\sqrt{\left(\frac{19,100}{2}\right)^2 + (0.0798T)^2} = (40,000)^2$$

or
$$T = 221,000 \text{ in} \cdot \text{lb} \quad (254,150 \text{ cm} \cdot \text{kgf})$$

$$S_M^2 + S_m^2 - S_M S_m = S_y^2$$

substituting and simplifying,

$$(9,550)^2 + 3\sqrt{\left(\frac{19,100}{2}\right)^2 + (0.0798T)^2} = (40,000)^2$$

or
$$T = 255,000 \text{ in} \cdot \text{lb} \quad (293,250 \text{ cm} \cdot \text{kgf})$$

PLASTICITY

The reaction of materials to stress and strain in the plastic range is not fully defined. However, some concepts and theories have been proposed.

Ideally, a **purely elastic material** is one complying explicitly with Hooke's law. In a **viscous material**, the shearing stress is proportional to the shearing strain. The **purely plastic material** yields indefinitely, but only after reaching a certain stress. Combinations of these are the **elasto-viscous** and the **elastoplastic materials**.

Engineering materials are not ideal, but usually contain some of the elastoplastic characteristics. The **total strain** ϵ_t is the sum of the **elastic strain** ϵ_o plus the **plastic strain** ϵ_p , as shown in Fig. 5.2.73, where the stress-strain curve is approximated by two straight lines. The **natural strain**, which is at the same time the total strain, is $\epsilon = \int_{l_o}^l dl/l = \ln(l/l_o)$. In this equation, l is the instantaneous length, while l_o is the original length. In terms of the normal strain, the natural strain becomes $\bar{\epsilon} = \ln(1 + \epsilon_o)$. Since it is assumed that the volume remains constant, $l/l_o = A_o/A$, and so the natural stress becomes $\bar{S} = P/A = (P/A_o)(1 + \epsilon_o)$. A_o is the original cross-sectional area. If the natural stress is plotted against strain on log-log paper, the graph is very nearly a straight line. The plastic-range relation is thus approximated by $\bar{S} = K\bar{\epsilon}^n$, where the proportionality factor K and the **strain-hardening coefficient** n are deter-

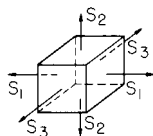


Fig. 5.2.71

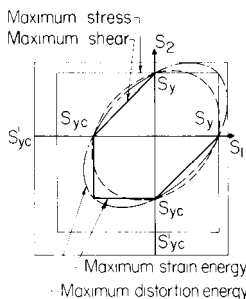


Fig. 5.2.72

shear theory (2) is generally used for ductile materials, and the maximum-stress theory (1) for brittle materials.

Fatigue failures cannot be related, theoretically, to elastic strength and thus to the theories described. However, experimental results justify this, at least to a limited extent. Therefore, the theory evaluation given

mined from best fits to experimental data. Values of K and n determined by Low and Garofalo (*Proc. Soc. Exp. Stress Anal.*, vol. IV, no. 2, 1947) are given in Table 5.2.21.

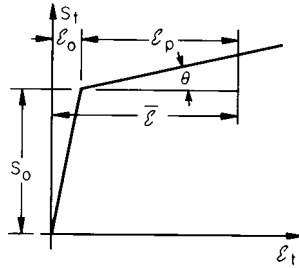


Fig. 5.2.73

The geometry of Fig. 5.2.73 can be used to arrive at a second approximate relation

$$\bar{S} = S_o + (\epsilon_p - \epsilon_o) \tan \theta = S_o \left(1 - \frac{H}{E} \right) + \epsilon_p H$$

where $H = \tan \theta$ is a kind of **plastic modulus**.

The **deformation theory of plastic flow** for the general case of combined stress is developed using the above concepts. Certain additional assumptions involved include: principal plastic-strain directions are the same as principal stress directions; the elastic strain is negligible compared to plastic strain; and the ratios of the three principal shearing strains— $(\bar{\epsilon}_1 - \bar{\epsilon}_2)$, $(\bar{\epsilon}_2 - \bar{\epsilon}_3)$, $(\bar{\epsilon}_3 - \bar{\epsilon}_1)$ —to the principal shearing stresses— $(\bar{S}_1 - \bar{S}_2)/2$, $(\bar{S}_2 - \bar{S}_3)/2$, $(\bar{S}_3 - \bar{S}_1)/2$ —are equal. The relations between the principal strains and stresses in terms of the simple tension quantities become

$$\begin{aligned} \bar{\epsilon}_1 &= \bar{\epsilon} \bar{S} [\bar{S}_1 - (\bar{S}_2 + \bar{S}_3)/2] \\ \bar{\epsilon}_2 &= \bar{\epsilon} \bar{S} [\bar{S}_2 - (\bar{S}_3 + \bar{S}_1)/2] \\ \bar{\epsilon}_3 &= \bar{\epsilon} \bar{S} [\bar{S}_3 - (\bar{S}_1 + \bar{S}_2)/2] \end{aligned}$$

If these equations are added, the plastic-flow theory is expressed:

$$\frac{\bar{S}}{\bar{\epsilon}} = \sqrt{\frac{[(\bar{S}_1 - \bar{S}_2)^2 + (\bar{S}_2 - \bar{S}_3)^2 + (\bar{S}_3 - \bar{S}_1)^2]/2}{2(\bar{\epsilon}_1^2 + \bar{\epsilon}_2^2 + \bar{\epsilon}_3^2)/3}}$$

In the above equation

$$\sqrt{[(\bar{S}_1 - \bar{S}_2)^2 + (\bar{S}_2 - \bar{S}_3)^2 + (\bar{S}_3 - \bar{S}_1)^2]/2} = \bar{S}_e$$

and

$$\sqrt{2(\bar{\epsilon}_1^2 + \bar{\epsilon}_2^2 + \bar{\epsilon}_3^2)/3} = \epsilon_e$$

are the effective, or significant, stress and strain, respectively.

EXAMPLE. An annealed, stainless-steel type 430 tank has a 41-in inside diameter and has a wall 0.375 in thick. The ultimate strength of the stainless steel is 85,000 lb/in². Compute the maximum strain as well as the pressure at fracture.

The tank constitutes a biaxial stress field where $S_1 = pd/(2t)$, $S_2 = pd/(4t)$, and $S_3 = 0$. Taking the power stress-strain relation

$$\bar{S}_e = K \bar{\epsilon}_e^n \quad \text{or} \quad \bar{\epsilon} \bar{S} = \bar{S}_e^{(1-n)/n} / K^{1/n}$$

thus

$$\bar{\epsilon}_1 = \frac{\bar{S}_e^{(1-n)/n}}{K^{1/n}} \left(\frac{3}{4} \bar{S}_1 \right) \bar{\epsilon} = 0,$$

$$\text{and} \quad \bar{\epsilon}_3 = \frac{\bar{S}_e^{(1-n)/n}}{K^{1/n}} \left(-\frac{3}{4} \bar{S}_1 \right) = -\bar{\epsilon}_1$$

The maximum-shear theory, which is applicable to a ductile material under combined stress, is acceptable here. Thus rupture will occur at

$$\bar{S}_1 - \bar{S}_3 = \bar{S}_u, \text{ and}$$

$$\bar{S}_e = \sqrt{\frac{1}{2} \left[\left(\frac{\bar{S}_1}{2} \right)^2 + \left(\frac{\bar{S}_1}{2} \right)^2 + \bar{S}_1^2 \right]} = \sqrt{\frac{3}{4} \bar{S}_1^2} = \left(\frac{3}{4} \right)^{1/2} \bar{S}_u$$

$$\bar{\epsilon}_1 = \frac{[(3/4)^{1/2} \bar{S}_u]^{(1-n)/n}}{K^{1/n}} \left(\frac{3}{4} \bar{S}_u \right) = \left(\frac{3}{4} \right)^{1+0.229/0.458} \left(\frac{85,000}{143,000} \right)^{1/0.229}$$

$$= 0.0475 \text{ in/in (0.0475 cm/cm)}$$

$$\text{Since} \quad \bar{S}_u = S_1 = \frac{pd}{2t}, \text{ then } p = \frac{2t\bar{S}_u}{d}$$

$$\text{or} \quad p = \frac{2 \times 0.375 \times 85,000}{41} = 1,550 \text{ lb/in}^2 \text{ (109 kgf/cm}^2\text{)}$$

ROTATING DISKS

Rotating circular disks may be of various profiles, of constant or variable thickness, with or without centrally and noncentrally located holes, and with radial, tangential, and shearing stresses.

Solution starts with the differential equations of equilibrium and compatibility and the subsequent application of appropriate boundary conditions for the derivation of working-stress equations.

If the disk thickness is small compared with the diameter, the variation of stress with thickness can be assumed to be negligible, and symmetry eliminates the shearing stress. In the rotating case, the disk weight is neglected, but its inertia force becomes the body-force term in the equilibrium equations.

Thus solved, the stress components in a solid disk become

$$\sigma_r = \frac{3 + \mu}{8} \rho \omega^2 (R^2 - r^2)$$

$$\sigma_\theta = \frac{3 + \mu}{8} \rho \omega^2 R^2 - \frac{1 + 3\mu}{8} \rho \omega^2 r^2$$

where μ = Poisson's ratio; ρ = mass density, lb · s²/in⁴; ω = angular speed, rad/s; R = outside disk radius; and r = radius to point in question.

The largest stresses occur at the center of the solid disk and are

$$\sigma_r = \sigma_\theta = \frac{3 + \mu}{8} \rho \omega^2 R^2$$

A disk with a central hole of radius r_h (no external forces) is subjected to the following stresses:

$$\sigma_r = \frac{3 + \mu}{8} \rho \omega^2 \left(R^2 + r_h^2 - \frac{R^2 r_h^2}{r^2} - r^2 \right)$$

$$\sigma_\theta = \frac{3 + \mu}{8} \rho \omega^2 \left(R^2 + r_h^2 + \frac{R^2 r_h^2}{r^2} - \frac{1 + 3\mu}{3 + \mu} r^2 \right)$$

The maximum radial stress σ_{rM} occurs at $r = \sqrt{Rr_h}$, and

$$\sigma_{rM} = \frac{3 + \mu}{8} \rho \omega^2 (R - r_h)^2$$

Table 5.2.21 Constants K and n for Sheet Materials

Material	Treatment	K , lb/in ²	n
0.05% C rimmed steel	Annealed	77,100	0.261
0.05% C killed steel	Annealed and tempered	73,100	0.234
Decarburized 0.05% C steel	Annealed in wet H ₂	75,500	0.284
0.05/0.07% phos. low C	Annealed	93,330	0.156
SAE 4130	Annealed	169,400	0.118
SAE 4130	Normalized and tempered	154,500	0.156
Type 430 stainless	Annealed	143,000	0.229
Alcoa 24-S	Annealed	55,900	0.211
Reynolds R-301	Annealed	48,450	0.211

The largest tangential stress $\sigma_{\theta|M}$ exists at the inner boundary, and

$$\sigma_{\theta|M} = \frac{3 + \mu}{4} \rho \omega^2 \left(R^2 + \frac{1 - \mu}{3 + \mu} r_h^2 \right)$$

As the hole radius r_h approaches zero, the tangential stress assumes a value twice that at the center of a rotating solid disk, given above.

Stresses in Turbine Disks Explicit solutions for cases other than those cited are not available; so approximate solutions, such as those proposed by Stodola, Thomson, Hetényi, and Robinson, are necessary. Manson uses the calculus of finite differences. See commentary under previous discussion of torsion for alternate methods of approximate solution. The problem illustrated below is a prime example of the elegance of the combination of approximate methods and electronic computers, which allow a rapid solution to be obtained. The speed with which the repetitive calculations are done allows equally rapid solutions with changes in design variables.

The customary, simplifying assumptions of axial symmetry—no variation of stress in the thickness direction and a completely elastic stress situation—are made. The differential equations of equilibrium and comparibility are rewritten in finite-difference form.

Solution of the finite-difference equations, appreciation of their linear nature, and successive application of them yield the stresses at any station in terms of those at a boundary station such as r_0 . The equations thus derived are

$$\begin{aligned} \sigma_{r,n} &= A_{r,n} \sigma_{r,0} + B_{r,n} \\ \sigma_{t,n} &= A_{t,n} \sigma_{t,0} + B_{t,n} \end{aligned} \quad (5.2.1)$$

The finite-difference expressions yield Eqs. (5.2.2), which permit the coefficients at station n to be computed from those at station $n - 1$.

$$\begin{aligned} A_{r,n} &= K_n A_{r,n-1} + L_n A_{t,n-1} \\ A_{t,n} &= K'_n A_{r,n-1} + L'_n A_{t,n-1} \\ B_{r,n} &= K_n B_{r,n-1} + L_n B_{t,n-1} + M_n \\ B_{t,n} &= K'_n B_{r,n-1} + L'_n B_{t,n-1} + M'_n \end{aligned} \quad (5.2.2)$$

The coefficients at the first station can be established by inspection. For a solid disk, for instance, where both stresses are equal to the tangential stress at the center, the coefficients in Eqs. (5.2.1) are $A_{r,1} = A_{t,1} = 1$ and $B_{r,1} = B_{t,1} = 0$. In the case of the disk with a central hole, where $\sigma_{r,h} = 0$, $A_{r,h} = B_{r,h} = B_{t,h} = 0$ and $A_{t,h} = 1$. Knowing these, all others can be found from Eqs. (5.2.2).

At the outer boundary, $\sigma_{r,R} = A_{r,R} \sigma_{r,0} + B_{r,R}$ and $\sigma_{t,0} = (\sigma_{r,R} - B_{r,R})/A_{r,R}$. The radial and tangential stresses at each station are successively obtained, knowing $\sigma_{r,0}$ and all the coefficients, using Eqs. (5.2.1).

The remaining coefficients in Eqs. (5.2.2), extracted from the finite-difference equations, are defined below, where E is Young's modulus at the temperature of the point in question, h is the profile thickness, α is the thermal coefficient of expansion, ΔT is the temperature increment above that at which the thermal stress is zero, μ is Poisson's ratio, ω is angular velocity of disk, and ρ is the mass density of disk material.

$$\begin{aligned} C_n &= r_n/h_n \\ C'_n &= \mu_n/E_n + (1 + \mu_n)(r_n - r_{n-1})/(2E_n r_n) \\ D_n &= 1/2(r_n - r_{n-1})h_n \\ D'_n &= 1/E_n + (1 + \mu_n)(r_n - r_{n-1})/(2E_n r_n) \\ F_n &= r_{n-1}h_{n-1} \\ F'_n &= (\mu_{n-1}/E_{n-1}) - (1 + \mu_{n-1})(r_n - r_{n-1})/(2E_{n-1}r_{n-1}) \\ G_n &= 1/2(r_n - r_{n-1})h_{n-1} \\ G'_n &= (1/E_{n-1}) - (1 + \mu_{n-1})(r_n - r_{n-1})/(2E_{n-1}r_{n-1}) \\ H_n &= 1/2\omega^2(r_n - r_{n-1})(\rho_n h_n r_n^2 + \rho_{n-1} h_{n-1} r_{n-1}^2) \\ H'_n &= \alpha_n \Delta T_n - \alpha_{n-1} \Delta T_{n-1} \\ K_n &= (F'_n D_n - F_n D'_n)/(C'_n D_n - C_n D'_n) \\ K'_n &= (C_n F'_n - C'_n F_n)/(C'_n D_n - C_n D'_n) \\ L_n &= -(G'_n D_n + G_n D'_n)/(C'_n D_n - C_n D'_n) \\ L'_n &= -(C'_n G_n + C_n G'_n)/(C'_n D_n - C_n D'_n) \\ M_n &= (H'_n D_n + H_n D'_n)/(C'_n D_n - C_n D'_n) \\ M'_n &= (C'_n H_n + C_n H'_n)/(C'_n D_n - C_n D'_n) \end{aligned}$$

Situations need not be equally spaced between the two boundaries. It is best to space them more closely where the profile, temperature, or

other property is changing rapidly. In cases of sudden or abrupt section changes, it is best to fair in across the change; the material density should, however, be adjusted to give a total mass equal to the actual. Six to ten stations are often sufficient.

The modulus of elasticity has a significant effect, and its exact value at the temperature of each station should be used. The coefficients of thermal expansion are usually averaged for the temperature between the station and at which no thermal stress occurs.

The first two Eqs. (5.2.2) and the last two must be worked simultaneously.

At the outer boundary, loads external to the disk may be imposed, e.g., the radial stress $\sigma_{r,R}$ from the centrifuged pull of a bucket. At the center, the disk may be shrunk on a shaft with the fit pressures causing a radial external push at this boundary.

Numerical solutions are most expeditiously accomplished by use of a table with column-to-column procedures. This technique lends itself readily to programmable computers or calculators.

Disks with Noncentral Holes This case has not been solved explicitly, but approximations are useful (e.g., Armstrong, Stresses in Rotating Tapered Disks with Noncentral Holes, Ph.D. dissertation, Iowa State University, 1960). The area between the holes is considered removed and replaced by uniform spokes, each one with a cross-sectional area equal to the original minimum spoke area and with a length equal to the diameter of the noncentral holes. The higher stress in such a spoke results in an additional extension, which is then applied to the outer annulus according to thin-ring theory and based on the average radius of the ring. The additional stress is considered constant and is added to the tangential stress which would be present in a disk of the same dimensions but filled (that is, no noncentral holes).

The stress in the substitute spoke is computed by adjusting the stress at the hole-center radius in the solid or filled disk in proportion to the areas, or $S_{sp} = \sigma_{r,h}(A_g/A_{sp})$, where $\sigma_{r,h}$ is the radial stress in the filled disk at the radius of the hole circle, A_g is the gross circumferential area at the same radius of the filled disk, and A_{sp} is the area of the substitute spoke. The increase in total strain is $\delta = \sigma_{r,h}/[E(A_g/A_{sp} - 1)l_{sp}]$, where l_{sp} is the length of the substitute spoke.

The spoke-effect correction to be applied to the tangential stress is therefore $\sigma_{\theta} = \delta E/r'$, where r' is the average outer-rim or annulus radius. This is added to the tangential stress found at the corresponding radius in the filled disk. The final step is to adjust the tangential and radial stresses as determined for stress concentrations caused by the holes in the actual disk. The factors for this adjustment are those in an infinite plate of uniform thickness having the same size hole. The method is claimed to yield stresses within 5 percent of those measured photoelastically at points of highest stress.

EXPERIMENTAL STRESS ANALYSIS

Analytical methods of stress analysis can reach limits of applicability. Many experimental techniques have been suggested and tried; several have been developed to a state of great usefulness, e.g., photoelasticity, strain-gage measurement, brittle coating, birefringent coating, and holography.

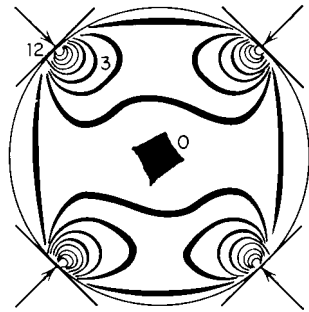
Photoelasticity

Most transparent materials exhibit temporary double refraction, or **birefringence**, when stressed. Light is resolved into components along the two principal plane directions. The effect is temporary as long as the elastic stress is not exceeded and is in direct proportion to the applied load. The stress magnitude can be established by the amount of component wave retardation, as given in the white and black band field (fringe pattern) obtained when a monochromatic light source is used. The polariscope, consisting of the light source, the polarizer, the model in a loading frame, an analyzer (same as polarizer), and a screen or camera, is used to produce and evaluate the fringe effect. Quarter-wave plates may be placed on either side of the model, making the light components through the model independent of the absolute orientation of polarizer and analyzer. The polarizer is a plane polariscope and yields the direc-

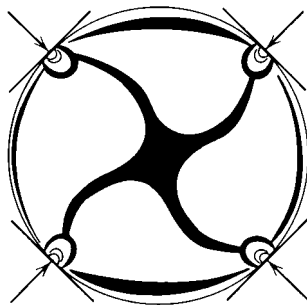
tions of principal stresses (the isoclinics); the analyzer is a circular polariscope yielding the fringes (isochromatics) as well.

Figure 5.2.74 shows the fringe pattern and the 20° isoclinics of a disk loaded radially at four places.

The isochromatics in the fringe pattern depict the **difference** between principal stresses. At free boundaries where the normal stress is zero, the difference automatically becomes the tangential stress. Starting at such a boundary and proceeding into the interior, the stresses can be separated by numerical calculation.



(a) Fringe pattern



(b) 20° isoclinics

Fig. 5.2.74

The Stress-Optic Law In a transparent, isotropic plate subjected to a biaxial stress field within the elastic limit, the relative retardation R_r between the two components produced by temporary double refraction is $R_r = Ct(p - q) = n\lambda$, where C is the stress-optic coefficient, t is the plate thickness, p and q are the principal stresses, n is the fringe order (the number of fringes which have passed the point during application of load), and λ is the wavelength of monochromatic light used. Thus,

$$(p - q)/2 = \tau_M = n\lambda/(2Ct) = nft$$

If the **material-fringe value** f is determined with the same light source (generally a mercury-vapor lamp emitting light having a wavelength of $5,461 \text{ \AA}$) as used in the model study, the maximum shearing stress, or one-half the difference between the principal stresses, is directly determined. The calibration is a matter of obtaining the material-fringe value in lb/in^2 per fringe per inch (kgf/cm^2 per fringe per cm).

Isoclinics, or the direction of the principal planes, can be obtained with a plane polariscope. A new isoclinic parameter is observed each time the polarizer and analyzer are rotated simultaneously into a new position. A white-light source reveals a more distinct isoclinic, as the black curve is more distinguishable against a colored background.

Isostatics, or stress trajectories, are curves the tangents to which represent the progressive change in principal-plane directions. They are constructed graphically using the isoclinics. Since there are two princi-

pal planes at each point, two families of orthogonal curves are drawn. Care must be exercised in the drawing of trajectories for practical accuracy.

Stress Separation If knowledge of each principal stress is required, the photoelastic data must be treated to separate the stresses from the difference given by the data. If the sum of the two stresses is also obtained somehow, a simultaneous solution of the sum and difference values will yield each principal stress. One can also start at a boundary where the normal stress value is zero. There, the photoelastic reading gives the principal stress parallel to the boundary. Starting with the single value, methods have been developed which can be used to proceed with the separation. Typical of the former are lateral-extensometer, iteration, and membrane-analogy techniques; typical of the latter are the slope-equilibrium, shear-difference, graphical-integration, alternating-summation methods, and oblique incidence. Often, however, the surface stresses are the maximum valued ones. (See Frocht, "Photoelasticity," McGraw-Hill.)

EXAMPLE. The fringe pattern of a Homalite disk 1.31 in in diam, 0.282 in thick, and carrying four radial loads of 155 lb each is shown in Fig. 5.2.74.

A closed solution is not known. However, by counting the fringe order at any point, the stress can be determined photoelastically. For instance, the dark spot at the center marks a fringe of zero order, as do the disk edges except in the immediate vicinity of the concentrated loads. The point at the center, which remained dark throughout the loading, is an isotropic point (zero stress difference and normal stresses are equal in all directions). Counting out from the center toward the load, the first "circular" fringe is of order 3. Therefore, anywhere along it $(p - q)/2 = \tau_M = nft = 3 \times 65/0.282 = 692 \text{ lb/in}^2$ (49 kgf/cm^2). Carefully inspected, fringe 12 can be counted at the point of load application. Therefore, $r|M = 12 \times 65/0.282 = 2,770 \text{ lb/in}^2$ (195 kgf/cm^2).

THREE-DIMENSIONAL PHOTOELASTICITY

Stress "freezing" and slicing, wherein a plastic model is brought up to its critical temperature, loaded as desired, and while loaded, slowly brought back to room temperature, are techniques which freeze the fringe pattern into the model. The model can be cut into slices without disturbing the "frozen" strains. Two-dimensional models are usually machined from plate stock, and three-dimensional models are cast. The frozen stress model is sliced so that the desired information can be obtained by normal incidence using the previous formulations.

When normal incidence is not possible, **oblique incidence** becomes necessary. Oblique-incidence patterns are usable in two-dimensional as well as three-dimensional stress separation. The measurement of fractional fringes is often required when using oblique incidence. With a crossed, circular, monochromatic polariscope, oriented to the principal stresses at a point, the analyzer is rotated through some angle ϕ until extinction occurs. The fringe value n is $n = n_n \pm \phi/180$, where n_n is the order of the last visible fringe. Whether the fractional term is added or subtracted depends upon the direction in which the analyzer is rotated (established by inspection).

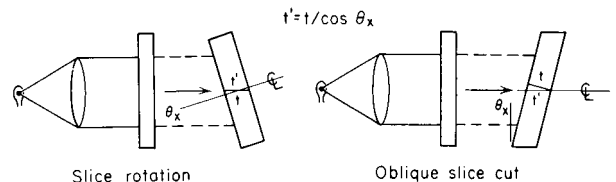


Fig. 5.2.75

Oblique-incidence calculations are based on the stress-optic law: $n_n = R_1 = t(p - q)/f = tp/f - tq/f = n_p - n_q$. Also, when polarized light is directed through the slice at an angle θ_x to a principal plane, either by rotating the slice away from normal to the light ray or by cutting it at the angle θ_x (see Fig. 5.2.75), the fringe order becomes

$$\begin{aligned} n_{\theta_x} &= \frac{t'}{f} (p' - q') = \frac{t}{f \cos \theta_x} (p - q \cos^2 \theta_x) \\ &= (n_p - n_q \cos^2 \theta_x) / \cos \theta_x \end{aligned}$$

Solving algebraically,

$$n_p = (n_{\theta_x} \cos \theta_x - n_n \cos^2 \theta_x) / \sin^2 \theta_x$$

and

$$n_q = (n_{\theta_x} \cos \theta_x + n_n) / \sin^2 \theta_x$$

If orders n_p and n_q are thus measured at a point, n_p and n_q can be computed. The principal stresses are then determined from $p = fn_p/t$ and $q = fn_q/t$.

The material-fringe value f in these equations is at the "freezing" temperature (critical temperature). The angle of incidence, as well as the fringe orders, must be accurately measured if errors are to be minimized.

Bonded Metallic Gages

Strain measurements down to one-millionth inch per inch (one-millionth cm/cm) are possible with electrical-resistance wire gages. Such gages can be used to measure surface strains (stress by Hooke's law) on any shape or size of object. Figure 5.2.76 illustrates schematically the gage construction with a grid of fine alloy wire or thin foil, bonded to paper and covered for protection with a felt pad. In use, the gage is cemented rigidly to the surface of the member to be analyzed. The strain relation is $\epsilon = (\Delta R/R)(1/G_f)$ in/in (cm/cm). Thus, if the resistance R and gage factor G_f (given by the gage manufacturer) are known and the change in resistance ΔR is measured, the strain which caused the resistance change can be determined and Hooke's law can be applied to determine the stress.

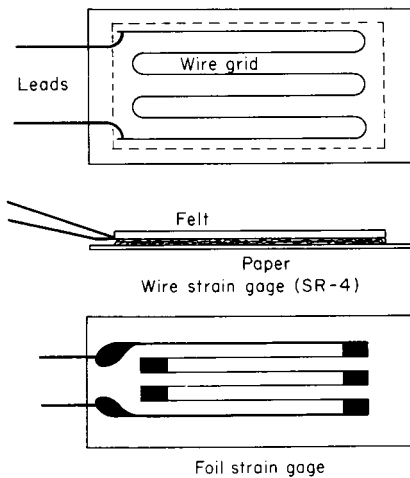


Fig. 5.2.76

Gages must be properly selected in accordance with manufacturer's recommendations. The surface to which the gage is applied must be clean, the proper cement must be used, and the gage assembly must be coated for protection against environmental conditions (e.g., moisture).

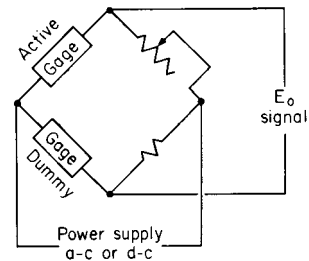
A gaging unit, usually a Wheatstone bridge or a ballast circuit (see Fig. 5.2.77 and Sec. 15), is needed to detect the signal resulting from the change in resistance of the strain gage. The strain and, therefore, the signal are often too small for direct handling, so that amplification is needed, with a metering discriminator for magnitude evaluation.

The signal is read or recorded by a galvanometer, oscilloscope, or other device. Equipment specifically constructed for strain measurement is available to indicate or record the signal directly in strain units.

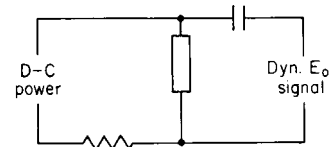
Static strains are best gaged on a **Wheatstone bridge**, with strain gages wired to it as indicated in Fig. 5.2.77a. With the bridge set so that the only unbalance is the change of resistance in the active-strain gage, the potential difference between the output terminals becomes a measurement of strain. Since the gage is sensitive to temperature as well as strain, it will measure the combined effect. However, if a "dummy" gage, cemented to an unstressed piece of the same metal subjected to the same climatic conditions, is wired into the bridge leg adjacent to the one

containing the "active" gage, the electric-resistance temperature effect is canceled out. Thus the active gage reports only that which is taking place in the stressed plate. The power supply can be either ac or dc.

It is sometimes useful to make both gages active—e.g., mounted on opposite sides of a beam, with one gage subjected to tension and the other to compression. Temperature effects are still compensated, but the bridge output is doubled. In other instances, it may be desirable to make all four bridge arms active gages. The experimenter must determine the most practical arrangement for the problem at hand and must bear in mind that the bridge unbalances in proportion to the difference in the strains of gages located in adjacent legs and to the sum of strain in gages located in opposite legs.



(a) Wheatstone bridge circuit



(b) Ballast circuit

Fig. 5.2.77

Dynamic strains can be detected using circuits such as the **ballast** type shown in Fig. 5.2.77b. The capacitor coupling passes only rapidly varying or dynamic strains. The capacitor's infinite impedance to a steady voltage filters out any static effects or strains. The circuit is dc powered.

Transverse Sensitivity Grid-type gages possess some strain sensitivity in the direction perpendicular to the gage axis. In a uniaxial stress field, this transverse sensitivity is of no concern because the gage factor was obtained in such a field. However, in a biaxial stress field, neglect of transverse sensitivity will give slightly erroneous strains. When accounted for, the true strains in the axial direction of gage, ϵ_1 , and at right angles to it, ϵ_2 , are $\epsilon_1 = (1 - \mu k)(\epsilon_{a1} - k\epsilon_{a2})/(1 - k^2)$ and $\epsilon_2 = (1 - \mu k)(\epsilon_{a2} - k\epsilon_{a1})/(1 - k^2)$, where the apparent strains are $\epsilon_{a1} = \Delta R_1/(RG_f)$ and $\epsilon_{a2} = \Delta R_2/(RG_f)$, measured by cementing a gage in each direction 1 and 2. The factor μ is Poisson's ratio of the material to which gages are cemented, and k (usually provided by the gage manufacturer) is the coefficient of transverse sensitivity of the gage. The gage is cemented to the test piece, a uniaxial stress is applied in its axial direction, and the resistance change and strain are measured. The gage factor $G_1 = \Delta R_1/(R\epsilon_1)$ is computed. A uniaxial stress is next applied transversely to the gage. Again the resistance change and strain are measured and G_2 computed. Then $k = (G_2 + \mu G_1)/(G_1 + \mu G_2)$.

Strain Rosettes In a general biaxial stress field, the principal plane directions, as well as the stresses, are unknown. Thus, three gages mounted in three differing directions are needed if the three unknowns are to be determined. Three standard gage combinations, called strain rosettes, are commercially available and are best for the purpose. These are the **rectangular strain rosette** (Fig. 5.2.78a), which covers a minimum of area and is therefore best where the strain gradient is high; the **equiangular strain rosette** (Fig. 5.2.78b), where the gages do not overlap and which can be used where the strain gradient is low; the **T-delta strain rosette** (Fig. 5.2.78c), which occupies no more area than the equiangular rosette and which provides an extra check, or "insurance"

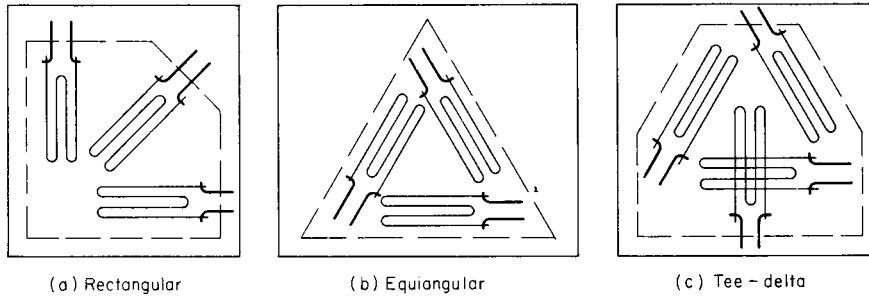


Fig. 5.2.78

gage. The wiring and instrumentation of gages in rosettes do not differ from those of individual gages.

The true strains along the gage-length directions are found according to the following equations, in which $R_n = \Delta R_n/[RF_1(1 - k^2)]$ and $b = 1/k$.

RECTANGULAR ROSETTE (SEE FIG. 5.2.78a)

$$\begin{aligned}\epsilon_1 &= R_1 - R_3/b \\ \epsilon_2 &= R_2(1 + 1/b) - (1/b)(R_1 + R_3) \\ \epsilon_3 &= R_3 - R_1/b\end{aligned}$$

EQUIANGULAR ROSETTE (SEE FIG. 5.2.78b)

$$\begin{aligned}\epsilon_1 &= R_1 - (1/b)(R_2 + R_3) \\ \epsilon_2 &= R_2 - (1/b)(R_1 + R_3) \\ \epsilon_3 &= R_3 - (1/b)(R_1 + R_3)\end{aligned}$$

T-DELTA ROSETTE (SEE FIG. 5.2.78c)

$$\begin{aligned}\epsilon_1 &= R_1(1 + 1/b) - (1/b)(R_3 + R_4) \\ \epsilon_2 &= R_2(1 + 1/b) - (1/b)(R_3 + R_4) \\ \epsilon_3 &= R_3 - (1/b)R_4 \\ \epsilon_4 &= R_4 - (1/b)R_3\end{aligned}$$

Foil Gages Foil gages are produced from thin foil by photoetching techniques and are applied, instrumented, read, and evaluated just like the wire-grid type. Foil gages, being much thinner, may be applied easily to curved surfaces, have lower transverse sensitivity, exhibit negligible hysteresis under cycling loads, creep little under sustained loads, and can be stacked on top of each other.

Brittle-Coating Analysis

Brittle coatings which adhere to the surface well can reveal the strain in the underlying material. Probably the first such coating used was mill scale, a thin iron oxide which forms on hot-rolled steel stock. Many coatings such as whitewash, portland cement, and shellac have been tried.

The most popular of presently available strain-indicating brittle coatings are the wood-rosin lacquers supplied by the Magnaflux Corporation under the trade name **Stresscoat**. Several Stresscoat compositions are available; the suitability of a particular lacquer depends upon the prevailing temperature and humidity. The lacquer is usually sprayed to a thickness of 0.004 to 0.008 in (0.01 to 0.02 cm) upon the surface, which must be clean and free of grease and loose particles. Calibration bars are sprayed at the same time. Both must be dried at an even temperature for up to 24 h. To facilitate observation of cracks, an undercoating of bright aluminum is often applied.

When the cured test piece is subjected to loads, the lacquer will first begin to crack at its threshold sensitivity in the area of the largest principal stress, with the parallel cracks perpendicular to the principal stress. This information is often sufficient, as it reveals the critical area and the direction of normal stress.

The threshold sensitivity of Stresscoat lacquers is 600 to 800 microinches per inch (600 to 800 microcentimeters per centimeter) in a uniaxial stress field. Exact control of lacquer selection, thickness, curing, and testing temperatures may reduce the threshold to 400 mi-

croinches per inch (400 microcentimeters per centimeter). If desired, the approximate strain (probably within 10 percent) may be established using the calibration strip sprayed with the test part. The strip is placed in a loading device and bent as a cantilever beam by means of a cam at the free end, causing the coating to crack on the tension surface. Crack spacing varies with the strain, being close at the fixed end and diminishing toward the free end down to threshold sensitivity values. The strip is placed in a holder containing strain graduations. A visual comparison of cracks on the testpart surface with those on the strip reveals the strain magnitude which caused the cracks.

Birefringent Coatings

A birefringent coating is one which becomes double refractive when strained. The principle is quite old, but plastics, which adhere to all kinds of materials, which have stable optical-strain constants, and which are sufficiently sensitive to be practical, are of recent development. The trade name applied to this technique is **Photostress**. Photostress plastics can be obtained either as thin sheets (0.040, 0.080, and 0.20 in) or in liquid form. The sheet material can be bonded to a surface with a special adhesive. The liquid can be brushed or sprayed on, or the part can be dipped in the liquid. The layer should be at least 0.004 in (0.010 cm) thick. It is often necessary to apply several successive coatings, with heat curing of each layer in turn. Two sheet types and two liquids are available; these differ in stretching ability and in magnitude of the strain-optical constant. Each of the sheet materials is available metalized on one face, to reflect polarized light even when cemented to a dull surface.

The principles involved are the same as those for conventional photoelasticity. One frequent advantage is the fact that the plastic (sheet or liquid) can be applied directly to the part, which can then be subjected to actual operating loads. A special reflecting polariscope must be used. It contains only one polarizer and quarter-wave disk because the light passes back through the same pair after reflection by the stressed surface-plastic interface. The only limitation rests in the geometry of the structural component to be examined; not only must it be possible to apply the plastic to the surface, but the surface must be accessible to light.

The strain-optic law, since the light passes the plastic thickness twice, becomes

$$p - q = \frac{n}{2t} \frac{E}{K(1 + \mu)}$$

where n is fringe order, E is modulus, μ is Poisson's ratio of workpiece material, and K (supplied by the manufacturer) is the strain-optic coefficient of the plastic. As in conventional photoelasticity, isoclinics are present as well.

Holography

A more recently developed technique applicable to stress, or rather, strain analysis as well as to many other purposes is that of holography. It is made possible by the laser, an instrument which produces a highly concentrated, thin beam of light of single wavelength. The helium-neon (He-Ne) laser, emitting at the red end of the visible spectrum at a wave-

length of 633 nanometers, has found much favor. The output of a helium-cadmium (He-Cd) laser is at half the wavelength of the He-Ne laser; accordingly, the He-Ne laser is twice as sensitive to displacements.

The laser beam is split into two components, one of which is directed upon the object (or specimen) and then onto the photographic plate. It is identified as the object beam. The other component, referred to as the reference beam, propagates directly to the plate. Interference between the beams resulting from retardations caused by displacements or strains forms fringes which in turn provide a measure of the disturbance. Spacing of such fringes depends upon Bragg's law:

$$d = \frac{\lambda}{2 \sin(\theta/2)}$$

where d is the distance between fringes, λ is the wavelength of the light source, and θ is the angle between the object and reference ray at the plate.

A simple holographic setup consists of the laser source, beam splitter, reflecting surfaces, filters, and the recording plate. A possible arrangement is depicted in Fig. 5.2.79. Some arrangement for loading the specimen must also be provided. Additional auxiliary and refining hardware becomes necessary as the analysis assumes greater complexity. Thus the system layout is limited only by test requirements and the experimenter's imagination. However, only a thorough understanding of the laws of optics and interferometry will make possible a reliable investigation and interpretation of results.

Stability of setup must be assured via a rigid optical bench and supporting brackets. Component instruments must be spaced upon the

bench so that beam coherence is assured, required coherence depth satisfied, and the object/reference angle θ consistent with the fringe spacing desired. The film must also possess adequate sensitivity in the spectral range of the laser beam used. It is important to recognize the inherent hazards of the high-intensity radiation in laser beams and to practice every precaution in the use of lasers.

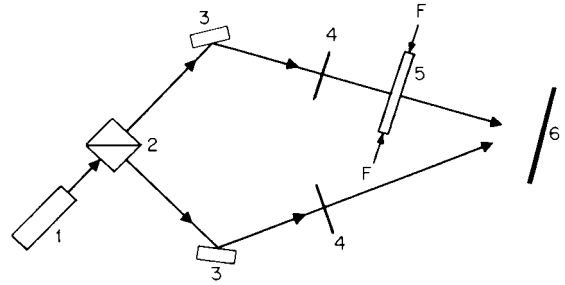


Fig. 5.2.79 Simple holographic setup. (1) Laser source; (2) beam splitter; (3) reflecting surfaces; (4) circular polarizers; (5) loaded specimen (birefringent); (6) photographic plate.

Holography, using pulsed lasers, can be used to measure transient disturbances. Thus vibration studies are possible. Fatigue detection using holographic techniques has also been undertaken. Holography has been used in acoustical studies and in automatic gaging as well. It is a versatile engineering tool.

5.3 PIPELINE FLEXURE STRESSES

by Harold V. Hawkins

EDITOR'S NOTE: The almost universal availability and utilization of personal computers in engineering practice has led to the development of many competing and complementary forms of piping stress analysis software. Their use is widespread, and individual packaged software allows analysis and design to take into account static and dynamic conditions, restraint conditions, aboveground and buried configurations, etc. The reader is referred to the technical literature for the most suitable and current software available for use in solving the immediate problems at hand.

The brief discussion in this section addresses the fundamental concepts entailed and sets forth the solution of simple systems as an exercise in application of the principles.

REFERENCES: Shipman, Design of Steam Piping to Care for Expansion, *Trans. ASME*, 1929. Wahl, Stresses and Reactions in Expansion Pipe Bends, *Trans. ASME*, 1927. Hoygaard, The Elastic Deformation of Pipe Bends, *Jour. Math. Phys.*, Nov. 1926, Oct. 1928, and Dec. 1929. M. W. Kellogg Co., "The Design of Piping Systems," Wiley.

For details of pipe and pipe fittings see Sec. 8.7.

Nomenclature (see Figs. 5.3.1 and 5.3.2)

- M_0 = end moment at origin, in · lb (N · m)
- M = max moment, in · lb (N · m)
- F_x = end reaction at origin in x direction, lb (N)
- F_y = end reaction at origin in y direction, lb (N)
- $S_l = (Mr/I)\alpha$ = max unit longitudinal flexure stress, lb/in² (N/m²)
- $S_t = (Mr/I)\beta$ = max unit transverse flexure stress, lb/in² (N/m²)
- $S_s = (Mr/I)\gamma$ = max unit shearing stress, lb/in² (N/m²)
- Δx = relative deflection of ends of pipe parallel to x direction caused by either temperature change or support movement, or both, in (m)

Δy = same as Δx but parallel to y direction, in. Note that Δx and Δy are positive if under the change in temperature the end opposite the origin tends to move in a positive x or y direction, respectively.

- t = wall thickness of pipe, in (m)
- r = mean radius of pipe cross section, in (m)
- λ = constant = tR/r^2
- I = moment of inertia of pipe cross section about pipe centerline, in⁴ (m⁴)
- E = modulus of elasticity of pipe at actual working temperature, lb/in² (N/m²)
- K = flexibility index of pipe. $K = 1$ for all straight pipe sections, $K = (10 + 12\lambda^2)/(1 + 12\lambda^2)$ for all curved pipe sections where $\lambda > 0.335$ (see Fig. 5.3.3)

α, β, γ = ratios of actual max longitudinal flexure, transverse flexure, and shearing stresses to M/I for curved sections of pipe (see Fig. 5.3.3)

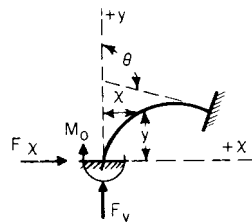


Fig. 5.3.1

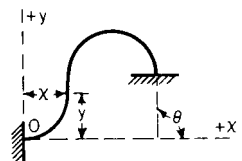


Fig. 5.3.2

- A, B, C, F, G, H = constants given by Table 5.3.2
- θ = angle of intersection between tangents to direction of pipe at reactions
- $\Delta\theta$ = change in θ caused by movements of supports, or by temperature change, or both, rad
- ds = an infinitesimal element of length of pipe
- s = length of a particular curved section of pipe, in (m)
- R = radius of curvature of pipe centerline, in (m)

General Discussion

Under the effect of changes in temperature of the pipeline, or of movement of support reactions (either translation or rotation), or both, the determination of stress distribution in a pipe becomes a statically indeterminate problem. In general the problem may be solved by a slight modification of the standard arch theory: $\Delta x = -K \int M y ds / (EI)$, $\Delta y = K \int M x ds / (EI)$, and $\Delta\theta = K \int M ds / (EI)$ where the constant K is introduced to correct for the increased flexibility of a curved pipe, and where the integration is over the entire length of pipe between supports. In Table 5.3.1 are given equations derived by this method for moment and thrust at one reaction point for pipes in one plane that are fully fixed, hinged at both ends, hinged at one end and fixed at the other, or partly fixed. If the reactions at one end of the pipe are known, the moment distribution in the entire pipe then can be obtained by simple statics.

Since an initially curved pipe is more flexible than indicated by its moment of inertia, the constant K is introduced. Its value may be taken from Fig. 5.3.3, or computed from the equation given below. $K = 1$ for all straight pipe sections, since they act according to the simple flexure theory.

In Fig. 5.3.3 are given the flexure constants K , α , β , and γ for initially curved pipes as functions of the quantity $\lambda = tR/r^2$. The flexure constants are derived from the equations.

$$\begin{aligned}
 K &= (10 + 12\lambda^2)/(1 + 2\lambda^2) && \text{when } \lambda > 0.335 \\
 \alpha &= \frac{2}{3}K\sqrt{(5 + 6\lambda^2)/18} && \lambda \leq 1.472 \\
 \alpha &= K(6\lambda^2 - 1)/(6\lambda^2 + 5) && \lambda > 1.472 \\
 \beta &= 18\lambda / (1 + 12\lambda^2) \\
 \gamma &= [8\lambda - 36\lambda^3 + (32\lambda^2 + 20/3) \\
 &\quad \times \sqrt{(4/3)\lambda^2 + 5/18}] \div (1 + 12\lambda^2) && \text{when } \lambda < 0.58 \\
 &= (12\lambda^2 + 18\lambda - 2) / (1 + 12\lambda^2) && \text{when } \lambda > 0.58
 \end{aligned}$$

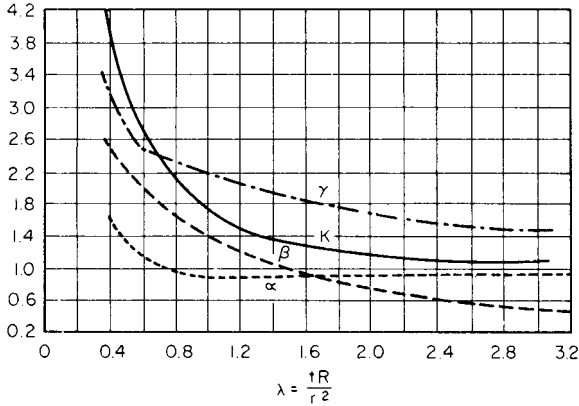


Fig. 5.3.3 Flexure constants of initially curved pipes.

Table 5.3.1 General Equations for Pipelines in One Plane (See Figs. 5.3.1 and 5.3.2)

Type of supports	Unsymmetric	Symmetric about y-axis
Both ends fully fixed	$M_0 = \frac{EI \Delta x(CF - AB) + EI \Delta y(BF - AG)}{2ABF + CGH - B^2H - A^2G - CF^2}$ $F_x = \frac{EI \Delta x(CH - A^2) + EI \Delta y(BH - AF)}{2ABF + CGH - B^2H - A^2G - CF^2}$ $F_y = \frac{EI \Delta x(BH - AF) + EI \Delta y(GH - F^2)}{2ABF + CGH - B^2H - A^2G - CF^2}$ $\Delta\theta = 0$	$M_0 = \frac{EI \Delta x F}{GH - F^2}$ $F_x = \frac{EI \Delta x H}{GH - F^2}$ $F_y = 0$ $\Delta\theta = 0$
Both ends hinged	$M_0 = 0$ $F_x = \frac{EI \Delta x C + EI \Delta y B}{CG - B^2}$ $F_y = \frac{EI \Delta x B + EI \Delta y G}{CG - B^2}$ $\Delta\theta = \frac{\Delta x(AB - CF) + \Delta y(AG - BF)}{CG - B^2}$	$M_0 = 0$ $F_x = \frac{EI \Delta x}{G}$ $F_y = 0$ $\Delta\theta = \frac{-\Delta x F}{G}$
Origin end only hinged, other end fully fixed	$M_0 = 0$ $F_x = \frac{EI \Delta x C + EI \Delta y B}{CG - B^2}$ $F_y = \frac{EI \Delta x B + EI \Delta y G}{CG + B^2}$ $\Delta\theta = \frac{\theta_x(AB - CF) + \Delta y(AG - BF)}{CG - B^2}$	
In general for any specific rotation $\Delta\theta$ and movement Δx and Δy . . .	$M_0 = \frac{EI \Delta x(CF - AB) + EI \Delta y(BF - AG) + EI \Delta\theta(CG - B^2)}{2ABF + CGH - A^2G - CF^2 - B^2H}$ $F_x = \frac{EI \Delta x(CH - A^2) + EI \Delta y(BH - AF) + EI \Delta\theta(CF - AB)}{2ABF + CGH - A^2G - CF^2 - B^2H}$ $F_y = \frac{EI \Delta x(BH - AF) + EI \Delta y(GH - F^2) + EI \Delta\theta(BF - AG)}{2ABF + CGH - A^2G - CF^2 - B^2H}$	

The increased flexibility of the curved pipe is brought about by the tendency of its cross section to flatten. This flattening causes a transverse flexure stress whose maximum is S_r . Because the maximum longitudinal and maximum transverse stresses do not occur at the same point in the pipe's cross section, the resulting maximum shear is not one-half the difference of S_l and S_r ; it is S_s . In the straight sections of the pipe, $\alpha = 1$, the transverse stress disappears, and $\lambda = 1/2$. This discussion of S_s does not include the uniform transverse or longitudinal tension stresses induced by the internal pressure in the pipe; their effects should be added if appreciable.

Table 5.3.2 gives values of the constants $A, B, C, F, G,$ and H for use in equations listed in Table 5.3.1. The values may be used (1) for the solution of any pipeline or (2) for the derivation of equations for standard shapes composed of straight sections and arcs of circles as of Fig. 5.3.5. Equations for shapes not given may be obtained by algebraic addition of those given. All measurements are from the left-hand end of the pipeline. Reactions and stresses are greatly influenced by end conditions. Formulas are given to cover the extreme conditions. The following suggestions and comments should be considered when laying out a pipeline:

Avoid expansion bends, and design the entire pipeline to take care of its own expansion.

The movement of the equipment to which the ends of the pipeline are attached must be included in the Δx and Δy of the equations.

Maximum flexibility is obtained by placing **supports** and **anchors** so that they will not interfere with the natural movement of the pipe.

That shape is most efficient in which the **maximum length of pipe is working** at the maximum safe stress.

Excessive **bending moment at joints** is more likely to cause trouble than excessive stresses in pipe walls. Hence, keep pipe joints away from points of high moment.

Reactions and stresses are greatly influenced by **flattening of the cross section** of the curved portions of the pipeline.

It is recommended that **cold springing** allowances be discounted in stress calculations.

Application to Two- and Three-Plane Pipelines Pipelines in more than one plane may be solved by the successive application of the preceding data, dividing the pipeline into two or more one-plane lines.

EXAMPLE 1. The unsymmetric pipeline of Fig. 5.3.4 has fully fixed ends. From Table 5.3.2 use $K = 1$ for all sections, since only straight segments are involved.

Upon introduction of $a = 120$ in (3.05 m), $b = 60$ in (1.52 m), and $c = 180$ in (4.57 m), into the preceding relations (Table 5.3.3) for $A, B, C, F, G, H,$ the equations for the reactions at 0 from Table 5.3.1 become

$$M_0 = EI \Delta x (-7.1608 \times 10^{-5}) + EI \Delta y (-8.3681 \times 10^{-5})$$

$$F_x = EI \Delta x (+1.0993 \times 10^{-5}) + EI \Delta y (+3.1488 \times 10^{-6})$$

$$F_y = EI \Delta x (+3.1488 \times 10^{-6}) + EI \Delta y (+1.33717 \times 10^{-6})$$

Also it follows that

$$M_1 = M_0 + F_y a = EI \Delta x (+3.0625 \times 10^{-4}) + EI \Delta y (+7.6779 \times 10^{-5})$$

$$M_2 = M_1 - F_x b = EI \Delta x (-3.5333 \times 10^{-4}) + EI \Delta y (-1.1215 \times 10^{-4})$$

$$M_3 = M_2 + F_y c = EI \Delta x (+2.1345 \times 10^{-4}) + EI \Delta y (+1.2854 \times 10^{-4})$$

Thus the maximum moment M occurs at 3.

The total maximum longitudinal fiber stress ($\alpha = 1$ for straight pipe)

$$S_l = \frac{F_x}{2\pi r t} \pm \frac{M_3 r}{I}$$

There is no transverse flexure stress since all sections are straight. The maximum shearing stress is either (1) one-half of the maximum longitudinal fiber stress as given above, (2) one-half of the hoop-tension stress caused by an internal radial pressure that might exist in the pipe, or (3) one-half the difference of the maximum longitudinal fiber stress and hoop-tension stress, whichever of these three possibilities is numerically greatest.

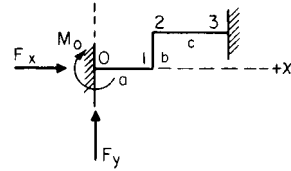


Fig. 5.3.4

EXAMPLE 2. The equations of Table 5.3.1 may be employed to develop the solution of generalized types of pipe configurations for which Fig. 5.3.5 is a typical example. If only temperature changes are considered, the reactions for the right-angle pipeline (Fig. 5.3.5) may be determined from the following equations:

$$M_0 = C_1 EI \Delta x / R^2$$

$$F_x = C_2 EI \Delta x / R^3$$

$$F_y = C_3 EI \Delta x / R^3$$

In these equations, Δx is the x component of the deflection between reaction points caused by temperature change only. The values of $C_1, C_2,$ and C_3 are given in Fig. 5.3.6 for $K = 1$ and $K = 2$. For other values of K , interpolation may be employed.

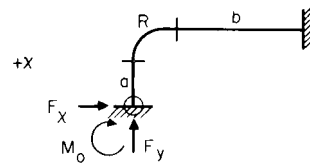
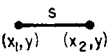
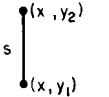
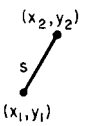
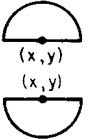

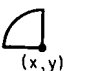


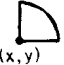
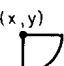
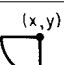
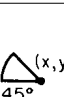
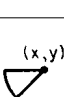

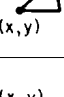
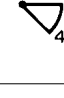
Fig. 5.3.5 Right angle pipeline.

EXAMPLE 3. With $a/R = 20$ and $b/R = 3$, the value of C_1 is 0.185 for $K = 1$ and 0.165 for $K = 2$. If $K = 1.75$, the interpolated value of C_1 is 0.175.

Elimination of Flexure Stresses Pipeline flexure stresses that normally would result from movement of supports or from the tendency of the pipes to expand under temperature change often may be avoided entirely through the use of expansion joints (Sec. 8.7). Their use may simplify both the design of the pipeline and the support structure. When using expansion joints, the following suggestions should be considered: (1) select expansion joint carefully for maximum temperature range (and deflection) expected so as to prevent damage to expansion fitting; (2) provide guides to limit movement at expansion joint to direction permitted by joint; (3) provide adequate anchors at one end of each straight section or along their midlength, forcing movement to occur at expansion joint yet providing adequate support for pipeline; (4) mount expansion joints adjacent to an anchor point to prevent sagging of the pipeline under its own weight and do not depend upon the expansion joint for stiffness—it is intended to be flexible; (5) give consideration to effects of corrosion, since corrugated character of expansion joints makes cleaning difficult.

Table 5.3.2 Values of A, B, C, F, G, and H for Various Piping Elements

	$A = K \int x \, ds$	$B = K \int xy \, ds$	$C = K \int x^2 \, ds$	$F = K \int y \, ds$	$G = K \int y^2 \, ds$	$H = K \int ds$
	$\frac{s}{2}(x_1 + x_2)$	Ay	$s \left(\frac{s^2}{3} + x_1 x_2 \right)$	sy	Fy	s
	sx	$\frac{A}{2}(y_1 + y_2)$	Ax	$\frac{s}{2}(y_1 + y_2)$	$s \left(\frac{s^2}{3} + y_1 y_2 \right)$	s
	$\frac{s}{2}(x_1 + x_2)$	$\frac{A}{3}(y_1 + y_2) + \frac{s}{6}(x_1 y_1 + x_2 y_2)$	$\frac{s}{3}(x_1^2 + x_1 x_2 + x_2^2)$	$\frac{s}{2}(y_1 + y_2)$	$\frac{s}{3}(y_1^2 + y_1 y_2 + y_2^2)$	s
	πKRx	$A \left(y + \frac{2R}{\pi} \right)$	$A \left(x + \frac{R^2}{2x} \right)$	$(\pi y + 2R)KR$	$Fy + \left(2y + \frac{\pi}{2} R \right) KR^2$	πKR
		$A \left(y - \frac{2R}{\pi} \right)$		$(\pi y - 2R)KR$	$Fy - \left(2y - \frac{\pi}{2} R \right) KR^2$	
	$\left(\frac{\pi x}{2} - R \right) KR$	$Ay + \left(x - \frac{R}{2} \right) KR^2$	$Ax + \left(\frac{\pi R}{4} - x \right) KR^2$	$\left(\frac{\pi y}{2} + R \right) KR$	$Fy + \left(\frac{\pi R}{4} + y \right) KR^2$	$\frac{\pi KR}{2}$

	$\left(\frac{\pi x}{2} + R\right) KR$	$Ay + \left(x + \frac{R}{2}\right) KR^2$	$Ax + \left(\frac{\pi R}{4} + x\right) KR^2$	$\left(\frac{\pi y}{2} + R\right) KR$	$Fy + \left(\frac{\pi R}{4} + y\right) KR^2$	$\frac{\pi KR}{2}$
		$Ay - \left(x + \frac{R}{2}\right) KR^2$		$\left(\frac{\pi y}{2} - R\right) KR$	$Fy + \left(\frac{\pi R}{4} - y\right) KR^2$	
	$\left(\frac{\pi x}{2} - R\right) KR$	$Ay - \left(x - \frac{R}{2}\right) KR^2$	$Ax + \left(\frac{\pi R}{4} - x\right) KR^2$	$\left(\frac{\pi y}{2} - R\right) KR$	$Fy + \left(\frac{\pi R}{4} - y\right) KR^2$	
	$\left(\frac{\pi x}{4} - \frac{R}{\sqrt{2}}\right) KR$	$Ay + \left[\left(1 - \frac{\sqrt{2}}{2}\right) x - \frac{R}{4} \right] KR^2$	$Ax + \left[\left(\frac{\pi}{8} + \frac{1}{4}\right) R - \frac{x\sqrt{2}}{2} \right] KR^2$	$\left[\frac{\pi y}{4} + \left(1 - \frac{\sqrt{2}}{2}\right) R \right] KR$	$Fy + \left[\left(1 - \frac{\sqrt{2}}{2}\right) y + \left(\frac{\pi}{8} - \frac{1}{4}\right) R \right] KR^2$	$\frac{\pi KR}{4}$
		$Ay - \left[\left(1 - \frac{\sqrt{2}}{2}\right) x - \frac{R}{4} \right] KR^2$		$\left[\frac{\pi y}{4} - \left(1 - \frac{\sqrt{2}}{2}\right) R \right] KR$	$Fy - \left[\left(1 - \frac{\sqrt{2}}{2}\right) y - \left(\frac{\pi}{8} - \frac{1}{4}\right) R \right] KR^2$	
	$\left(\frac{\pi x}{4} + \frac{R}{\sqrt{2}}\right) KR$	$Ay + \left[\left(1 - \frac{\sqrt{2}}{2}\right) x + \frac{R}{4} \right] KR^2$	$Ax + \left[\left(\frac{\pi}{8} + \frac{1}{4}\right) R + \frac{x\sqrt{2}}{2} \right] KR^2$	$\left[\frac{\pi y}{4} + \left(1 - \frac{\sqrt{2}}{2}\right) R \right] KR$	$Fy + \left[\left(1 - \frac{\sqrt{2}}{2}\right) y + \left(\frac{\pi}{8} - \frac{1}{4}\right) R \right] KR^2$	$\frac{\pi KR}{4}$
		$Ay - \left[\left(1 - \frac{\sqrt{2}}{2}\right) x + \frac{R}{4} \right] KR^2$		$\left[\frac{\pi y}{4} - \left(1 - \frac{\sqrt{2}}{2}\right) R \right] KR$	$Fy - \left[\left(1 - \frac{\sqrt{2}}{2}\right) y - \left(\frac{\pi}{8} - \frac{1}{4}\right) R \right] KR^2$	
	$[r(\theta_2 - \theta_1 - R(\sin \theta_2 - \sin \theta_1))] KR$	$Ay - \left[x(\cos \theta_2 - \cos \theta_1) + \frac{R}{2}(\sin^2 \theta_2 - \sin^2 \theta_1) \right] KR^2$	$Ax - \left[x(\sin \theta_2 - \sin \theta_1) - \frac{R}{4}(\sin 2\theta_2 - \sin 2\theta_1) - \frac{R}{2}(\theta_2 - \theta_1) \right] KR^2$	$[y(\theta_2 - \theta_1) - R(\cos \theta_2 - \cos \theta_1)] KR$	$Fy - \left[y(\cos \theta_2 - \cos \theta_1) + \frac{R}{4}(\sin 2\theta_2 - \sin 2\theta_1) - \frac{R}{2}(\theta_2 - \theta_1) \right] KR^2$	$(\theta_2 - \theta_1) KR$

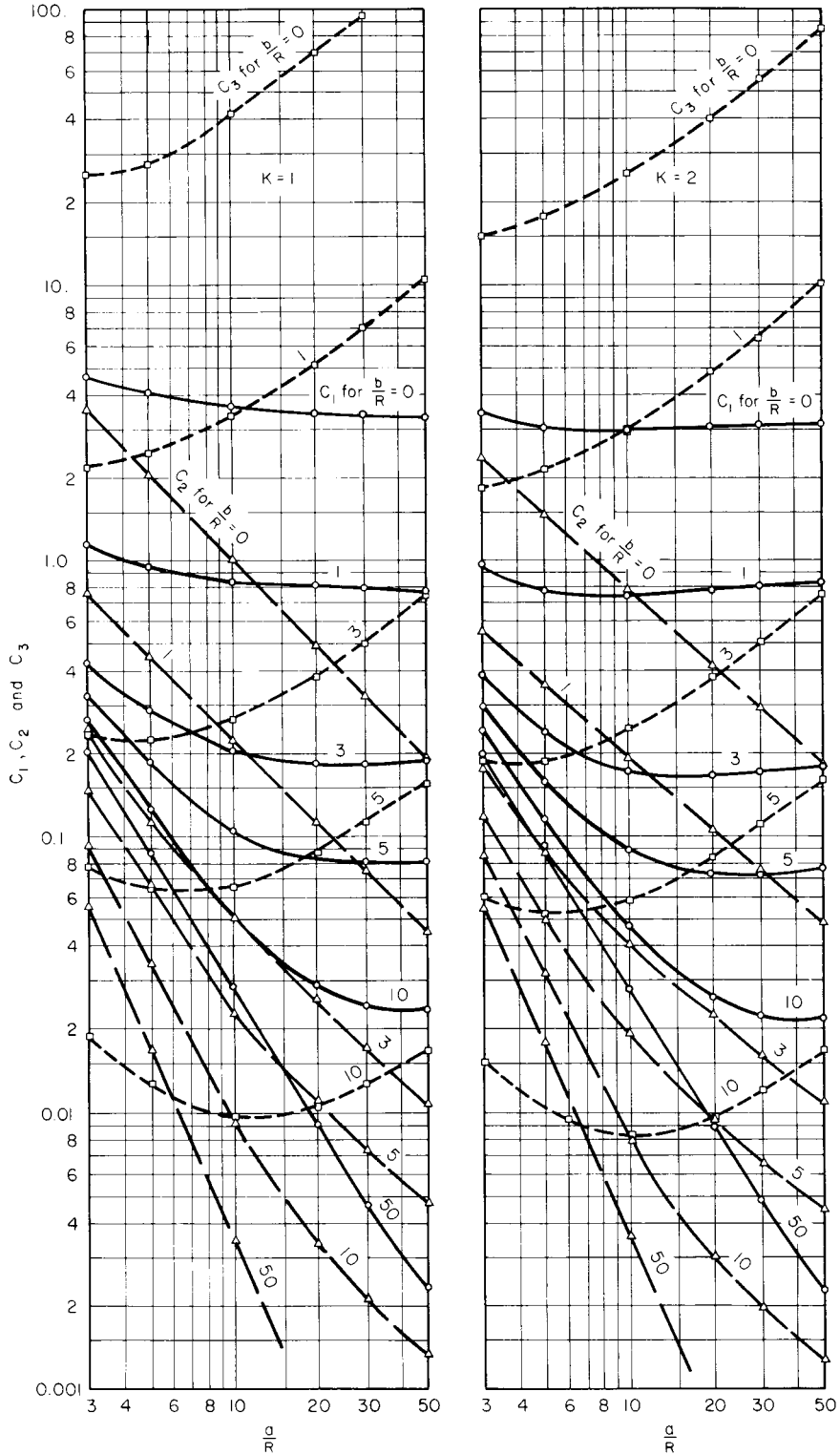


Fig. 5.3.6 Reactions for right-angle pipelines.

Table 5.3.3 Example 1 Showing Determination of Integrals

Part of pipe	Values of integrals					
	A	B	C	F	G	H
0-1	$\frac{a^2}{2}$	0	$\frac{a^3}{3}$	0	0	a
1-2	ab	$\frac{ab^2}{2}$	a^2b	$\frac{b^2}{2}$	$\frac{b^3}{3}$	b
2-3	$\frac{c}{2}(2a+c)$	$\frac{bc}{2}(2a+c)$	$\frac{c^3}{3}+ac(a+c)$	bc	b^2c	c
Total 0-3	$\frac{a^2}{2}+ab$ $+\frac{c}{2}(2a+c)$	$\frac{ab^2}{2}+\frac{bc}{2}(2a+c)$	$\frac{a^3}{3}+a^2b+\frac{c^3}{3}$ $+ac(a+c)$	$\frac{b^2}{2}+bc$	$\frac{b^3}{3}+b^2c$	$a+b+c$

5.4 NONDESTRUCTIVE TESTING

by Donald D. Dodge

REFERENCES: Various authors, "Nondestructive Testing Handbook," 8 vols., American Society for Nondestructive Testing. Boyer, "Metals Handbook," vol. 11, American Society for Metals. Heuter and Bolt, "Sonic," Wiley. Krautkramer, "Ultrasonic Testing of Materials," Springer-Verlag. Spanner, "Acoustic Emission: Techniques and Applications," Intex, American Society for Nondestructive Testing. Crowther, "Handbook of Industrial Radiography," Arnold. Wiltshire, "A Further Handbook of Industrial Radiography," Arnold. "Standards," vol. 03.03, ASTM, Boiler and Pressure Vessel Code, Secs. III, V, XI, ASME. ASME Handbook, "Metals Engineering—Design," McGraw-Hill. SAE Handbook, Secs. J358, J359, J420, J425–J428, J1242, J1267, SAE. Materials Evaluation, *Jour. Am. Soc. Nondestructive Testing*.

Nondestructive tests are those tests that determine the usefulness, serviceability, or quality of a part or material without limiting its usefulness. Nondestructive tests are used in machinery maintenance to avoid costly unscheduled loss of service due to fatigue or wear; they are used in manufacturing to ensure product quality and minimize costs. Consideration of test requirements early in the design of a product may facilitate testing and minimize testing cost. Nearly every form of energy is used in nondestructive tests, including all wavelengths of the electromagnetic spectrum as well as vibrational mechanical energy. Physical properties, composition, and structure are determined; flaws are detected; and thickness is measured. These tests are here divided into the following basic methods: **magnetic particle, penetrant, radiographic, ultrasonic, eddy current, acoustic emission, microwave, and infrared**. Numerous techniques are utilized in the application of each test method. Table 5.4.1 gives a summary of many nondestructive test methods.

MAGNETIC PARTICLE METHODS

Magnetic particle testing is a nondestructive method for detecting discontinuities at or near the surface in **ferromagnetic materials**. After the test object is properly magnetized, finely divided magnetic particles are applied to its surface. When the object is properly oriented to the induced magnetic field, a discontinuity creates a leakage flux which attracts and holds the particles, forming a visible indication. Magnetic-field direction and character are dependent upon how the magnetizing force is applied and upon the type of current used. For best sensitivity, the **magnetizing current** must flow in a direction parallel to the principal direction of the expected defect. Circular fields, produced by passing current through the object, are almost completely contained within the test object. Longitudinal fields, produced by coils or yokes, create external poles and a general-leakage field. Alternating, direct, or half-

wave direct current may be used for the location of surface defects. Half-wave direct current is most effective for locating subsurface defects. Magnetic particles may be applied dry or as a wet suspension in a liquid such as kerosene or water. Colored **dry powders** are advantageous when testing for subsurface defects and when testing objects that have rough surfaces, such as castings, forgings, and weldments. **Wet particles** are preferred for detection of very fine cracks, such as fatigue, stress corrosion, or grinding cracks. Fluorescent wet particles are used to inspect objects with the aid of ultraviolet light. Fluorescent inspection is widely used because of its greater sensitivity. Application of particles while magnetizing current is on (continuous method) produces stronger indications than those obtained if the particles are applied after the current is shut off (residual method). Interpretation of subsurface-defect indications requires experience. Demagnetization of the test object after inspection is advisable.

Magnetic flux leakage is a variation whereby leakage flux due to flaws is detected electronically via a Hall-effect sensor. Computerized signal interpretation and data imaging techniques are employed.

Electrified particle testing indicates minute cracks in nonconducting materials. Particles of calcium carbonate are positively charged as they are blown through a spray gun at the test object. If the object is metal-backed, such as porcelain enamel, no preparation other than cleaning is necessary. When it is not metal-backed, the object must be dipped in an aqueous penetrant solution and dried. The penetrant remaining in cracks provides a mobile electron supply for the test. A readily visible powder indication forms at a crack owing to the attraction of the positively charged particles.

PENETRANT METHODS

Liquid penetrant testing is used to locate flaws open to the surface of **nonporous materials**. The test object must be thoroughly cleaned before testing. Penetrating liquid is applied to the surface of a test object by a brush, spray, flow, or dip method. A time allowance (1 to 30 min) is required for liquid penetration of surface flaws. Excess penetrant is then carefully removed from the surface, and an absorptive coating, known as developer, is applied to the object to draw penetrant out of flaws, thus showing their location, shape, and approximate size. The developer is typically a fine powder, such as talc usually in suspension in a liquid. Penetrating-liquid types are (1) for test in visible light, and (2) for test under ultraviolet light (3,650 Å). Sensitivity of penetrant testing is greatest when a fluorescent penetrant is used and the object is observed

Table 5.4.1 Nondestructive Test Methods*

Method	Measures or detects	Applications	Advantages	Limitations
Acoustic emission	Crack initiation and growth rate Internal cracking in welds during cooling Boiling or cavitation Friction or wear Plastic deformation Phase transformations	Pressure vessels Stressed structures Turbine or gearboxes Fracture mechanics research Weldments Sonic-signature analysis	Remote and continuous surveillance Permanent record Dynamic (rather than static) detection of cracks Portable Triangulation techniques to locate flaws	Transducers must be placed on part surface Highly ductile materials yield low-amplitude emissions Part must be stressed or operating Interfering noise needs to be filtered out
Acoustic-impact (tapping)	Debonded areas or delaminations in metal or nonmetal composites or laminates Cracks under bolt or fastener heads Cracks in turbine wheels or turbine blades Loose rivets or fastener heads Crushed core	Brazed or adhesive-bonded structures Bolted or riveted assemblies Turbine blades Turbine wheels Composite structures Honeycomb assemblies	Portable Easy to operate May be automated Permanent record or positive meter readout No couplant required	Part geometry and mass influences test results Impactor and probe must be repositioned to fit geometry of part Reference standards required Pulser impact rate is critical for repeatability
D-Sight (Diffrauto)	Enhances visual inspection for surface abnormalities such as dents protrusions, or waviness' Crushed core Lap joint corrosion Cold-worked holes Cracks	Detect impact damage to composites or honeycomb corrosion in aircraft lap joints Automotive bodies for waviness	Portable Fast, flexible Noncontact Easy to use Documentable	Part surface must reflect light or be wetted with a fluid
Eddy current	Surface and subsurface cracks and seams Alloy content Heat-treatment variations Wall thickness, coating thickness Crack depth Conductivity Permeability	Tubing Wire Ball bearings "Spot checks" on all types of surfaces Proximity gage Metal detector Metal sorting Measure conductivity in % IACS	No special operator skills required High speed, low cost Automation possible for symmetric parts Permanent-record capability for symmetric parts No couplant or probe contact required	Conductive materials Shallow depth of penetration (thin walls only) Masked or false indications caused by sensitivity to variations such as part geometry Reference standards required Permeability variations
Magneto-optic eddy-current imager	Cracks Corrosion thinning in aluminum	Aluminum aircraft Structure	Real-time imaging Approximately 4-in area coverage	Frequency range of 1.6 to 100 kHz Surface contour Temperature range of 32 to 90°F Directional sensitivity to cracks
Eddy-sonic	Debonded areas in metal-core or metal-faced honeycomb structures Delaminations in metal laminates or composites Crushed core	Metal-core honeycomb Metal-faced honeycomb Conductive laminates such as boron or graphite-fiber composites Bonded-metal panels	Portable Simple to operate No couplant required Locates far-side debonded areas Access to only one surface required May be automated	Specimen or part must contain conductive materials to establish eddy-current field Reference standards required Part geometry
Electric current	Cracks Crack depth Resistivity Wall thickness Corrosion-induced wall thinning	Metallic materials Electrically conductive materials Train rails Nuclear fuel elements Bars, plates other shapes	Access to only one surface required Battery or dc source Portable	Edge effect Surface contamination Good surface contact required Difficult to automate Electrode spacing Reference standards required
Electrified particle	Surface flaws in nonconducting material Through-to-metal pinholes on metal-backed material Tension, compression, cyclic cracks Brittle-coating stress cracks	Glass Porcelain enamel Nonhomogeneous materials such as plastic or asphalt coatings Glass-to-metal seals	Portable Useful on materials not practical for penetrant inspection	Poor resolution on thin coatings False indications from moisture streaks or lint Atmospheric conditions High-voltage discharge

Table 5.4.1 Nondestructive Test Methods* (Continued)

Method	Measures or detects	Applications	Advantages	Limitations
Filtered particle	Cracks Porosity Differential absorption	Porous materials such as clay, carbon, powdered metals, concrete Grinding wheels High-tension insulators Sanitary ware	Colored or fluorescent particles Leaves no residue after baking part over 400°F Quickly and easily applied Portable	Size and shape of particles must be selected before use Penetrating power of suspension medium is critical Particle concentration must be controlled Skin irritation
Infrared (radiometry) (thermography)	Hot spots Lack of bond Heat transfer Isotherms Temperature ranges	Brazed joints Adhesive-bonded joints Metallic platings or coatings; debonded areas or thickness Electrical assemblies Temperature monitoring	Sensitive to 0.1°F temperature variation Permanent record or thermal picture Quantitative Remote sensing; need not contact part Portable	Emissivity Liquid-nitrogen-cooled detector Critical time-temperature relationship Poor resolution for thick specimens Reference standards required
Leak testing	Leaks: Helium Ammonia Smoke Water Air bubbles Radioactive gas Halogens	Joints: Welded Brazed Adhesive-bonded Sealed assemblies Pressure or vacuum chambers Fuel or gas tanks	High sensitivity to extremely small, light separations not detectable by other NDT methods Sensitivity related to method selected	Accessibility to both surfaces of part required Smear metal or contaminants may prevent detection Cost related to sensitivity
Magnetic particle	Surface and slightly subsurface flaws; cracks, seams, porosity, inclusions Permeability variations Extremely sensitive for locating small tight cracks	Ferromagnetic materials; bar, plate, forgings, weldments, extrusions, etc.	Advantage over penetrant is that it indicates subsurface flaws, particularly inclusions Relatively fast and low-cost May be portable	Alignment of magnetic field is critical Demagnetization of parts required after tests Parts must be cleaned before and after inspection Masking by surface coatings
Magnetic field (also magnetic flux leakage)	Cracks Wall thickness Hardness Coercive force Magnetic anisotropy Magnetic field Nonmagnetic coating thickness on steel	Ferromagnetic materials Ship degaussing Liquid-level control Treasure hunting Wall thickness of nonmetallic materials Material sorting	Measurement of magnetic material properties May be automated Easily detects magnetic objects in nonmagnetic material Portable	Permeability Reference standards required Edge effect Probe lift-off
Microwave (300 MHz–300 GHz)	Cracks, holes, debonded areas, etc., in nonmetallic parts Changes in composition, degree of cure, moisture content Thickness measurement Dielectric constant Loss tangent	Reinforced plastics Chemical products Ceramics Resins Rubber Wood Liquids Polyurethane foam Radomes	Between radio waves and infrared in electromagnetic spectrum Portable Contact with part surface not normally required Can be automated	Will not penetrate metals Reference standards required Horn-to-part spacing critical Part geometry Wave interference Vibration
Liquid penetrants (dye or fluorescent)	Flaws open to surface of parts; cracks, porosity, seams, laps, etc. Through-wall leaks	All parts with nonabsorbing surfaces (forgings, weldments, castings, etc.). Note: Bleed-out from porous surfaces can mask indications of flaws	Low cost Portable Indications may be further examined visually Results easily interpreted	Surface films such as coatings, scale, and smeared metal may prevent detection of flaws Parts must be cleaned before and after inspection Flaws must be open to surface
Fluoroscopy (cinefluorography) (kinefluorography)	Level of fill in containers Foreign objects Internal components Density variations Voids, thickness Spacing or position	Flow of liquids Presence of cavitation Operation of valves and switches Burning in small solid-propellant rocket motors	High-brightness images Real-time viewing Image magnification Permanent record Moving subject can be observed	Costly equipment Geometric unsharpness Thick specimens Speed of event to be studied Viewing area Radiation hazard

Table 5.4.1 Nondestructive Test Methods* (Continued)

Method	Measures or detects	Applications	Advantages	Limitations
Neutron radiology (thermal neutrons from reactor, accelerator, or Californium 252)	Hydrogen contamination of titanium or zirconium alloys Defective or improperly loaded pyrotechnic devices Improper assembly of metal, nonmetal parts Corrosion products	Pyrotechnic devices Metallic, nonmetallic assemblies Biological specimens Nuclear reactor fuel elements and control rods Adhesive-bonded structures	High neutron absorption by hydrogen, boron, lithium, cadmium, uranium, plutonium Low neutron absorption by most metals Complement to X-ray or gamma-ray radiography	Very costly equipment Nuclear reactor or accelerator required Trained physicists required Radiation hazard Nonportable Indium or gadolinium screens required
Gamma radiology (cobalt 60, iridium 192)	Internal flaws and variations, porosity, inclusions, cracks, lack of fusion, geometry variations, corrosion thinning Density variations Thickness, gap, and position	Usually where X-ray machines are not suitable because source cannot be placed in part with small openings and/or power source not available Panoramic imaging	Low initial cost Permanent records; film Small sources can be placed in parts with small openings Portable Low contrast	One energy level per source Source decay Radiation hazard Trained operators needed Lower image resolution Cost related to source size
X-ray radiology	Internal flaws and variations; porosity, inclusions, cracks, lack of fusion, geometry variations, corrosion Density variations Thickness, gap, and position Misassembly Misalignment	Castings Electrical assemblies Weldments Small, thin, complex wrought products Nonmetallics Solid-propellant rocket motors Composites Container contents	Permanent records; film Adjustable energy levels (5 kV–25 meV) High sensitivity to density changes No couplant required Geometry variations do not affect direction of X-ray beam	High initial costs Orientation of linear flaws in part may not be favorable Radiation hazard Depth of flaw not indicated Sensitivity decreases with increase in scattered radiation
Radiometry X-ray, gamma ray, beta ray) (transmission or backscatter)	Wall thickness Plating thickness Variations in density or composition Fill level in cans or containers Inclusions or voids	Sheet, plate, strip, tubing Nuclear reactor fuel rods Cans or containers Plated parts Composites	Fully automatic Fast Extremely accurate In-line process control Portable	Radiation hazard Beta ray useful for ultrathin coatings only Source decay Reference standards required
Reverse-geometry digital X-ray	Cracks Corrosion Water in honeycomb Carbon epoxy honeycomb Foreign objects	Aircraft structure	High-resolution 10 ⁶ pixel image with high contrast	Access to both sides of object Radiation hazard
X-ray computed tomography (CT)	Small density changes Cracks Voids Foreign objects	Solid-propellant rocket motors Rocket nozzles Jet-engine parts Turbine blades	Measures X-ray opacity of object along many paths	Very expensive Trained operator Radiation hazard
Shearography electronic	Lack of bond Delaminations Plastic deformation Strain Crushed core Impact damage Corrosion in Al honeycomb	Composite-metal honeycomb Bonded structures Composite structures	Large area coverage Rapid setup and operation Noncontacting Video image easy to store	Requires vacuum thermal, ultrasonic, or microwave stressing of structure to cause surface strain
Thermal (thermochromic paint, liquid crystals)	Lack of bond Hot spots Heat transfer Isotherms Temperature ranges Blockage in coolant passages	Brazed joints Adhesive-bonded joints Metallic platings or coatings Electrical assemblies Temperature monitoring	Very low initial cost Can be readily applied to surfaces which may be difficult to inspect by other methods No special operator skills	Thin-walled surfaces only Critical time-temperature relationship Image retentivity affected by humidity Reference standards required
Sonic (less than 0.1 MHz)	Debonded areas or delaminations in metal or nonmetal composites or laminates Cohesive bond strength under controlled conditions Crushed or fractured core Bond integrity of metal insert fasteners	Metal or nonmetal composite or laminates brazed or adhesive-bonded Plywood Rocket-motor nozzles Honeycomb	Portable Easy to operate Locates far-side debonded areas May be automated Access to only one surface required	Surface geometry influences test results Reference standards required Adhesive or core-thickness variations influence results

Table 5.4.1 Nondestructive Test Methods* (Continued)

Method	Measures or detects	Applications	Advantages	Limitations
Ultrasonic (0.1–25 MHz)	Internal flaws and variations; cracks, lack of fusion, porosity, inclusions, delaminations, lack of bond, texturing Thickness or velocity Poisson's ratio, elastic modulus	Metals Welds Brazed joints Adhesive-bonded joints Nonmetallics In-service parts	Most sensitive to cracks Test results known immediately Automating and permanent-record capability Portable High penetration capability	Couplant required Small, thin, or complex parts may be difficult to inspect Reference standards required Trained operators for manual inspection Special probes
Thermoelectric probe	Thermoelectric potential Coating thickness Physical properties Thompson effect <i>P-N</i> junctions in semiconductors	Metal sorting Ceramic coating thickness on metals Semiconductors	Portable Simple to operate Access to only one surface required	Hot probe Difficult to automate Reference standards required Surface contaminants Conductive coatings

* From Donald J. Hagemair, "Metal Progress Databook," Douglas Aircraft Co., McDonnell-Douglas Corp., Long Beach, CA.

in a semidarkened location. After testing, the penetrant and developer are removed by washing with water, sometimes aided by an emulsifier, or with a solvent.

In **filtered particle** testing, cracks in **porous objects** (100 mesh or smaller) are indicated by the difference in absorption between a cracked and a flaw-free surface. A liquid containing suspended particles is sprayed on a test object. If a crack exists, particles are filtered out and concentrate at the surface as liquid flows into the additional absorbent area created by the crack. Fluorescent or colored particles are used to locate flaws in unfired dried clay, certain fired ceramics, concrete, some powdered metals, carbon, and partially sintered tungsten and titanium carbides.

RADIOGRAPHIC METHODS

Radiographic test methods employ X-rays, gamma rays, or similar penetrating radiation to reveal flaws, voids, inclusions, thickness, or structure of objects. Electromagnetic energy wavelengths in the range of 0.01 to 10 Å ($1 \text{ Å} = 10^{-8} \text{ cm}$) are used to examine the interior of opaque materials. Penetrating radiation proceeds from its source in straight lines to the test object. Rays are differentially absorbed by the object, depending upon the energy of the radiation and the nature and thickness of the material.

X-rays of a variety of wavelengths result when high-speed electrons in a vacuum tube are suddenly stopped. An X-ray tube contains a heated filament (cathode) and a target (anode); radiation intensity is almost directly proportional to filament current (mA); tube voltage (kV) determines the penetration capability of the rays. As tube voltage increases, shorter wavelengths and more intense X-rays are produced. When the energy of penetrating radiation increases, shorter wavelengths and more intense X-rays are produced. Also, when the energy of penetrating radiation increases, the difference in attenuation between materials decreases. Consequently, more film-image contrast is obtained at lower voltage, and a greater range of thickness can be radiographed at one time at higher voltage.

Gamma rays of a specific wavelength are emitted from the disintegrating nuclei of natural radioactive elements, such as radium, and from a variety of artificial radioactive isotopes produced in nuclear reactors. Cobalt 60 and iridium 192 are commonly used for industrial radiography. The half-life of an isotope is the time required for half of the radioactive material to decay. This time ranges from a few hours to many years.

Radiographs are photographic records produced by the passage of penetrating radiation onto a film. A void or reduced mass appears as a darker image on the film because of the lesser absorption of energy and the resulting additional exposure of the film. The quantity of X-rays absorbed by a material generally increases as the atomic number increases.

A radiograph is a shadow picture, since X-rays and gamma rays follow the laws of light in shadow formation. Four factors determine the best geometric sharpness of a picture: (1) The effective focal-spot size of the radiation source should be as small as possible. (2) The source-to-object distance should be adequate for proper definition of the area of the object farthest from the film. (3) The film should be as close as possible to the object. (4) The area of interest should be in the center of and perpendicular to the X-ray beams and parallel to the X-ray film.

Radiographic films vary in speed, contrast, and grain size. Slow films generally have smaller grain size and produce more contrast. Slow films are used where optimum sharpness and maximum contrast are desired. Fast films are used where objects with large differences in thickness are to be radiographed or where sharpness and contrast can be sacrificed to shorten exposure time. Exposure of a radiographic film comes from direct radiation and scattered radiation. **Direct radiation** is desirable, image-forming radiation; **scattered radiation**, which occurs in the object being X-rayed or in neighboring objects, produces undesirable images on the film and loss of contrast. **Intensifying screens** made of 0.005- or 0.010-in. (0.13-mm or 0.25-mm) thick lead are often used for radiography at voltages above 100 kV. The lead filters out much of the low-energy scatter radiation. Under action of X-rays or gamma rays above 88 kV, a lead screen also emits electrons which, when in intimate contact with the film, produce additional coherent darkening of the film. Exposure time can be materially reduced by use of intensifying screens above and below the film.

Penetrameters are used to indicate the contrast and definition which exist in a radiograph. The type generally used in the United States is a small rectangular plate of the same material as the object being X-rayed. It is uniform in thickness (usually 2 percent of the object thickness) and has holes drilled through it. ASTM specifies hole diameters 1, 2, and 4 times the thickness of the penetrometer. Step, wire, and bead penetrameters are also used. (See ASTM Materials Specification E94.)

Because of the variety of factors that affect the production and measurements of an X-ray image, operating factors are generally selected from reference tables or graphs which have been prepared from test data obtained for a range of operating conditions.

All materials may be inspected by radiographic means, but there are limitations to the configurations of materials. With optimum techniques, wires 0.0001 in. (0.003 mm) in diameter can be resolved in small electrical components. At the other extreme, welded steel pressure vessels with 20-in. (500-mm) wall thickness can be routinely inspected by use of high-energy accelerators as a source of radiation. **Neutron radiation** penetrates extremely dense materials such as lead more readily than X-rays or gamma rays but is attenuated by lighter-atomic-weight materials such as plastics, usually because of their hydrogen content.

Radiographic standards are published by ASTM, ASME, AWS, and API, primarily for detecting lack of penetration or lack of fusion in welded objects. Cast-metal objects are radiographed to detect condi-

tions such as shrink, porosity, hot tears, cold shuts, inclusions, coarse structure, and cracks.

The usual method of utilizing penetrating radiation employs film. However, Geiger counters, semiconductors, phosphors (fluoroscopy), photoconductors (xeroradiography), scintillation crystals, and vidicon tubes (image intensifiers) are also used. Computerized digital radiography is an expanding technology.

The **dangers** connected with exposure of the human body to X-rays and gamma rays should be fully understood by any person responsible for the use of radiation equipment. NIST is a prime source of information concerning radiation safety. NRC specifies maximum permissible exposure to be a 1.25 R/¼ year.

ULTRASONIC METHODS

Ultrasonic nondestructive test methods employ high-frequency mechanical vibrational energy to detect and locate structural discontinuities or differences and to measure thickness of a variety of materials. An electric pulse is generated in a test instrument and transmitted to a transducer, which converts the electric pulse into mechanical vibrations. These low-energy-level vibrations are transmitted through a coupling liquid into the test object, where the ultrasonic energy is attenuated, scattered, reflected, or resonated to indicate conditions within material. Reflected, transmitted, or resonant sound energy is reconverted to electrical energy by a transducer and returned to the test instrument, where it is amplified. The received energy is then usually displayed on a cathode-ray tube. The presence, position, and amplitude of echoes indicate conditions of the test-object material.

Materials capable of being tested by ultrasonic energy are those which transmit vibrational energy. Metals are tested in dimensions of up to 30 ft (9.14 m). Noncellular plastics, ceramics, glass, new concrete, organic materials, and rubber can be tested. Each material has a characteristic sound velocity, which is a function of its density and modulus (elastic or shear).

Material characteristics determinable through ultrasonics include structural discontinuities, such as flaws and unbonds, physical constants and metallurgical differences, and thickness (measured from one side). A common application of ultrasonics is the inspection of welds for inclusions, porosity, lack of penetration, and lack of fusion. Other applications include location of unbond in laminated materials, location of fatigue cracks in machinery, and medical applications. Automatic testing is frequently performed in manufacturing applications.

Ultrasonic systems are classified as either **pulse-echo**, in which a single transducer is used, or **through-transmission**, in which separate sending and receiving transducers are used. Pulse-echo systems are more common. In either system, ultrasonic energy must be transmitted into, and received from, the test object through a **coupling medium**, since air will not efficiently transmit ultrasound of these frequencies. Water, oil, grease, and glycerin are commonly used couplants. Two types of testing are used: contact and immersion. In contact testing, the transducer is placed directly on the test object. In immersion testing, the transducer and test object are separated from one another in a tank filled with water or by a column of water or by a liquid-filled wheel. Immersion testing eliminates transducer wear and facilitates scanning of the test object. Scanning systems have paper-printing or computerized video equipment for readout of test information.

Ultrasonic transducers are piezoelectric units which convert electric energy into acoustic energy and convert acoustic energy into electric energy of the same frequency. Quartz, barium titanate, lithium sulfate, lead metaniobate, and lead zirconate titanate are commonly used transducer crystals, which are generally mounted with a damping backing in a housing. Transducers range in size from ¼ to 5 in (0.15 to 12.7 cm) and are circular or rectangular. Ultrasonic beams can be focused to improve resolution and definition. Transducer characteristics and beam patterns are dependent upon frequency, size, crystal material, and construction.

Test frequencies used range from 40 kHz to 200 MHz. Flaw-detection and thickness-measurement applications use frequencies between

500 kHz and 25 MHz, with 2.25 and 5 MHz being most commonly employed for flaw detection. Low frequencies (40 kHz to 1.0 MHz) are used on materials of low elastic modulus or large grain size. High frequencies (2.25 to 25 MHz) provide better resolution of smaller defects and are used on fine-grain materials and thin sections. Frequencies above 25 MHz are employed for investigation and measurement of physical properties related to acoustic attenuation.

Wave-vibrational modes other than longitudinal are effective in detecting flaws that do not present a reflecting surface to the ultrasonic beam, or other characteristics not detectable by the longitudinal mode. They are useful also when large areas of plates must be examined. Wedges of plastic, water, or other material are inserted between the transducer face and the test object to convert, by refraction, to shear, transverse, surface, or Lamb vibrational modes. As in optics, Snell's law expresses the relationship between incident and refracted beam angles; i.e., the ratio of the sines of the angle from the normal, of the incident and refracted beams in two mediums, is equal to the ratio of the mode acoustic velocities in the two mediums.

Limiting conditions for ultrasonic testing may be the test-object shape, surface roughness, grain size, material structure, flaw orientation, selectivity of discontinuities, and the skill of the operator. Test sensitivity is less for cast metals than for wrought metals because of grain size and surface differences.

Standards for acceptance are published in many government, national society, and company specifications (see references above). Evaluation is made by comparing (visually or by automated electronic means) received signals with signals obtained from reference blocks containing flat bottom holes between ¼ and ⅝ in (0.40 and 0.325 cm) in diameter, or from parts containing known flaws, drilled holes, or machined notches.

EDDY CURRENT METHODS

Eddy current nondestructive tests are based upon correlation between electromagnetic properties and physical or structural properties of a test object. Eddy currents are induced in metals whenever they are brought into an ac magnetic field. These eddy currents create a secondary magnetic field, which opposes the inducing magnetic field. The presence of discontinuities or material variations alters eddy currents, thus changing the apparent impedance of the inducing coil or of a detection coil. Coil impedance indicates the magnitude and phase relationship of the eddy currents to their inducing magnetic-field current. This relationship is dependent upon the mass, conductivity, permeability, and structure of the metal and upon the frequency, intensity, and distribution of the alternating magnetic field. Conditions such as heat treatment, composition, hardness, phase transformation, case depth, cold working, strength, size, thickness, cracks, seams, and inhomogeneities are indicated by eddy current tests. Correlation data must usually be obtained to determine whether test conditions for desired characteristics of a particular test object can be established. Because of the many factors which cause variation in electromagnetic properties of metals, care must be taken that the instrument response to the condition of interest is not nullified or duplicated by variations due to other conditions.

Alternating-current **frequencies** between 1 and 5,000,000 Hz are used for eddy current testing. Test frequency determines the depth of current penetration into the test object, owing to the ac phenomenon of "skin effect." One "standard depth of penetration" is the depth at which the eddy currents are equal to 37 percent of their value at the surface. In a plane conductor, depth of penetration varies inversely as the square root of the product of conductivity, permeability, and frequency. High-frequency eddy currents are more sensitive to surface flaws or conditions while low-frequency eddy currents are sensitive also to deeper internal flaws or conditions.

Test coils are of three general types: the **circular coil**, which surrounds an object; the **bobbin coil**, which is inserted within an object; and the **probe coil**, which is placed on the surface of an object. Coils are further classified as **absolute**, when testing is conducted without direct comparison with a reference object in another coil; or **differential**, when compar-

ison is made through use of two coils connected in series opposition. Many variations of these coil types are utilized. Axial length of a circular test coil should not be more than 4 in (10.2 cm), and its shape should correspond closely to the shape of the test object for best results. Coil diameter should be only slightly larger than the test-object diameter for consistent and useful results. Coils may be of the air-core or magnetic-core type.

Instrumentation for the analysis and presentation of electric signals resulting from eddy current testing includes a variety of means, ranging from meters to oscilloscopes to computers. Instrument meter or alarm circuits are adjusted to be sensitive only to signals of a certain electrical phase or amplitude, so that selected conditions are indicated while others are ignored. Automatic and automated testing is one of the principal advantages of the method.

Thickness measurement of metallic and nonmetallic coatings on metals is performed using eddy current principles. Coating thicknesses measured typically range from 0.0001 to 0.100 in (0.00025 to 0.25 cm). For measurement to be possible, coating conductivity must differ from that of the base metal.

MICROWAVE METHODS

Microwave test methods utilize electromagnetic energy to determine characteristics of nonmetallic substances, either solid or liquid. Frequencies used range from 1 to 3,000 GHz. Microwaves generated in a test instrument are transmitted by a waveguide through air to the test object. Analysis of reflected or transmitted energy indicates certain material characteristics, such as moisture content, composition, structure, density, degree of cure, aging, and presence of flaws. Other applications include thickness and displacement measurement in the range of 0.001 in (0.0025 cm) to more than 12 in (30.4 cm). Materials that can be tested include most solid and liquid nonmetals, such as chemicals, minerals, plastics, wood, ceramics, glass, and rubber.

INFRARED METHODS

Infrared nondestructive tests involve the detection of infrared electromagnetic energy emitted by a test object. Infrared radiation is produced naturally by all matter at all temperatures above absolute zero. Materials

emit radiation at varying intensities, depending upon their temperature and surface characteristics. A **passive** infrared system detects the natural radiation of an unheated test object, while an **active** system employs a source to heat the test object, which then radiates infrared energy to a detector. Sensitive indication of temperature or temperature distribution through infrared detection is useful in locating irregularities in materials, in processing, or in the functioning of parts. Emission in the infrared range of 0.8 to 15 μm is collected optically, filtered, detected, and amplified by a test instrument which is designed around the characteristics of the detector material. Temperature variations on the order of 0.1°F can be indicated by meter or graphic means. Infrared theory and instrumentation are based upon radiation from a blackbody; therefore, **emissivity correction** must be made electrically in the test instrument or arithmetically from instrument readings.

ACOUSTIC SIGNATURE ANALYSIS

Acoustic signature analysis involves the analysis of sound energy emitted from an object to determine characteristics of the object. The object may be a simple casting or a complex manufacturing system. A passive test is one in which **sonic** energy is transmitted into the object. In this case, a mode of resonance is usually detected to correlate with cracks or structure variations, which cause a change in effective modulus of the object, such as a nodular iron casting. An active test is one in which the object emits sound as a result of being struck or as a result of being in operation. In this case, characteristics of the object may be correlated to damping time of the sound energy or to the presence or absence of a certain frequency of sound energy. Bearing wear in rotating machinery can often be detected prior to actual failure, for example. More complex analytical systems can monitor and control manufacturing processes, based upon analysis of emitted sound energy.

Acoustic emission is a technology distinctly separate from acoustic signature analysis and is one in which strain produces bursts of energy in an object. These are detected by **ultrasonic** transducers coupled to the object. Growth of microcracks, and other flaws, as well as incipient failure, is monitored by counting the pulses of energy from the object or recording the time rate of the pulses of energy in the ultrasonic range (usually a discrete frequency between 1 kHz and 1 MHz).